FINITE ELEMENT INVESTIGATION ON THE CAPACITY OF SLENDER HSS STEEL COLUMNS STRENGTHENED WITH MULTILAYER CFRP STRIPS

URMI DEVI

DEPARTMENT OF CIVIL ENGINEERING

BANGLADESH UNIVERSITY OF ENGINEERING AND TECHNOLOGY (BUET), DHAKA

FINITE ELEMENT INVESTIGATION ON THE CAPACITY OF SLENDER HSS STEEL COLUMNS STRENGTHENED WITH MULTILAYER CFRP STRIPS
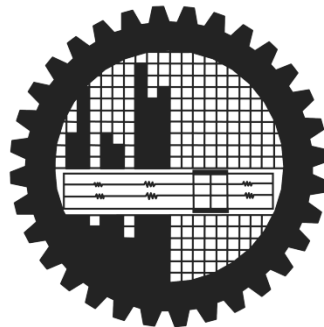
Submitted by

URMI DEVI

Student ID: 0413042319

A thesis submitted to the Department of Civil Engineering, Bangladesh University of Engineering and Technology in partial fulfillment of the requirements for the degree of

Master of Science in Civil Engineering (Structural).

Department of Civil Engineering

BANGLADESH UNIVERSITY OF ENGINEERING AND TECHNOLOGY (BUET)

Dhaka, Bangladesh

July, 2016

DEDICATED

TO

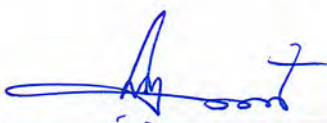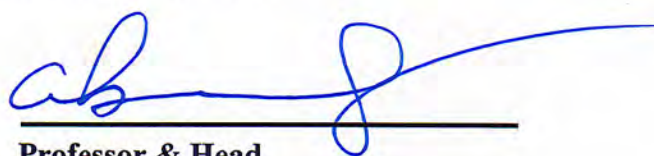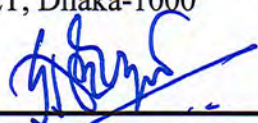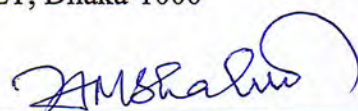*My Beloved Parents*

Sushil Kumar Nath

and

Lakshmi Priya Devi

CERTIFICATE OF APPROVAL

The thesis titled **"Finite Element Investigation on the Capacity of Slender HSS Steel Columns Strengthened with Multilayer CFRP Strips"** submitted by Urmi Devi, Student Number: 0413042319, Session: April, 2013 has been accepted as satisfactory in partial fulfillment of the requirement for the degree of Master of Science in Civil Engineering (Structural) on Saturday, 23rd July 2016.

BOARD OF EXAMINERS

1. **Dr. Khan Mahmud Amanat**
   Professor
   Department of Civil Engineering
   BUET, Dhaka-1000

   Chairman
   (Supervisor)

2. **Professor & Head**
   Department of Civil Engineering
   BUET, Dhaka-1000

   Member

3. **Dr. Raquib Ahsan**
   Professor
   Department of Civil Engineering
   BUET, Dhaka-1000

   Member

4. **Dr. A.F.M. Saiful Amin**
   Professor
   Department of Civil Engineering
   BUET, Dhaka-1000

   Member

5. **Dr. Md. Shahin Hossain**
   Professor
   Department of Civil Engineering
   Islamic University of Technology (IUT)
   Gazipur, Dhaka

   Member
   (External)

DECLARATION

Except for the contents where specific references have been made to the work of others, the studies embodied in this dissertation are the outcome of the research conducted by the author.

It is hereby declared that, this thesis or any part of it has not been submitted elsewhere for the award of any degree or diploma or other qualifications (except for publication).

Urmi Devi

ACKNOWLEDGEMENTS

ABSTRACT

This thesis presents a numerical finite element (FE) investigation on the behavior of steel square hollow structural section (HSS) columns (mild steel) strengthened with CFRP materials. Three dimensional finite element (FE) models of square HSS sections were developed using shell elements considering both material and geometric nonlinearities whereas CFRP strengthening was incorporated with additional layers of both conventional and continuum shell elements. Damage properties of CFRP and GFRP materials were incorporated in the FE model. The developed FE models were used to simulate experimental studies done by past researchers. Good agreement was found in between present analysis and past experimental results, which validated the acceptability of the FE model to carry out further investigation. Study was then focused on some selected non-compact AISC square HSS columns and the effects of number of CFRP layers, slenderness ratio and cross-sectional geometry on the increase in axial load capacity of those columns were studied. From the parametric study it was found that the axial strength of column specimens can be possible to increase by up to two-thirds to that of unstrengthened specimens. For columns of short and intermediate lengths, variation in strength is less significant. When column length increases, strength decreases significantly as expected. The capacity generally increases with the increase in the number of CFRP layers. In some cases, the strength gains, however, do not correlate directly to the number of CFRP layers. Medium sized HSS sections benefit most from CFRP strengthening compared to larger or smaller sized sections. This is because addition of CFRP layers decreases the b/t ratio more for medium sized sections and hence brings the section closer to compactness and delays local buckling which contributes to significant increase in capacity.

TABLE OF CONTENTS

Chapter 3: Methodology for Finite Element Analysis

LIST OF FIGURES

xv

LIST OF TABLES

LIST OF SYMBOLS

F_y Yield stress

ε_y Strain corresponding to yield stress

E_s Modulus of elasticity up to yield point

E_t Tangent Modulus

e'   Out of Straightness

Nu_{12} Poisson's Ratio

X^T Longitudinal Tensile Strength

X^C Longitudinal Compressive Strength

Y^T Transverse Tensile Strength

Y^C Transverse Compressive Strength

S^L Longitudinal Shear Strength

S^T Transverse Shear Strength

G_{ft}^C Longitudinal Tensile Fracture Energy

G_{fc}^C Longitudinal Compressive Fracture Energy

G_{mt}^C Transverse Tensile Fracture Energy

G_{mc}^C Transverse Compressive Fracture Energy

Chapter 1

INTRODUCTION

1.1 GENERAL

A large part of infrastructure today consists of steel structures that remained in service are increasingly becoming in urgent need of retrofitting and strengthening. This is attributed to a number of reasons; including deterioration due to corrosion, fatigue cracking, increased loading, design errors and lack of maintenance over the years. Moreover, aging and overburdened structures need retrofitting to get satisfied with the modified and more stringent design codes and specifications of the recent years. For most cases, retrofitting a structure costs less than replacing it entirely and takes less time to implement, therefore, reducing the service interruption time.

Conventional methods of strengthening steel structures involve welding or bolting additional steel plates. These techniques have a number of shortcomings, including the long installation time, difficulty of shaping and fitting complex profiles and the need for an elaborate and expensive shoring system. Adding plates also increases the area of the column as well as the dead weight, which could cause issues for some projects. Naturally, steel has high strength and stiffness, which makes it harder to strengthen compared to materials such as concrete and wood. When steel is strengthened with a material whose Young's modulus is lower, the strengthening should only be effective after the steel yields. Also, welding is not desired in many cases due to fatigue problems associated with weld defects, while bolted connections are costly and time consuming. The continuous process of corrosion and the reduced fatigue life associated with the welded steel plates may reduce the durability and limit the effectiveness of conventional repair methods.

In such applications, the need for adopting durable materials and cost-effective retrofit techniques is evident. A possible solution is the use of Fiber Reinforced Polymers

(FRPs). Though they originally may have a larger material cost than steel, the material cost alone is normally small compared to the total cost of the project. This is demonstrated by strengthening the London underground railway. The option of using steel and FRPs were both examined. The FRP strengthening scheme gave a comparable overall cost with the steel strengthening and was used because of the time restraints of the project. FRPs provide many advantages such as being lightweight, corrosive resistant and having high-strength capabilities (Karbhari and Shulley 1995). There are different types of FRPs but among them two mostly used FRP's are carbon fibers and glass fibers. Due to wanting a higher modulus, carbon fibers are generally used when strengthening steel. They are available in strips or flexible sheets allowing for easy application to any project, even when the member is already in use. FRP flexible sheets in particular offer a unique advantage of being able to conform to complex and curved surfaces.

By applying CFRP in practical field, satisfactory results have been obtained in strengthening problems along with many other problematic situations. For example, the Tickford Bridge, Newport Pagnell, Buckinghamshire, UK, was built in 1810 and is the oldest cast iron bridge in service. The bridge was strengthened by bonding wet lay-up CFRP sheets instead of plates, in order to conform to the curved surfaces. Many other metallic bridges in the UK were also strengthened with CFRP plates. The Hythe Bridge had eight inverted Tee sections (cast iron beams) of 7800 mm span. Four prestressed high modulus CFRP plates were bonded to each beam using epoxy adhesive, in addition to the mechanical end anchorages. In order to overcome fatigue problems in the Acton Bridge of the London Underground, prefabricated high modulus CFRP plates were epoxy bonded to the underside of the girders supporting the track and were capable of reducing the live load stresses by 25 percent.

Most researchers have investigated the properties of steel beams strengthened with plates or sheets (Dawood *et al.* 2006; Peiris and Harik 2014; Narmashiri and Jumaat 2011; Narmashiri *et al.* 2012). These researchers studied optimum fiber to resin ratios and different modulus types on I-beams or wide flange beams. The increase in ultimate loads were measured and studied along with the failure modes experienced. This research has shown that strengthening beams is promising and does get a significant increase in strength of the beam without sacrificing too much space or adding more weight.

The next step was to apply the method to steel columns and see if the axial capacity can also experience a significant increase. Because through strengthening of steel columns using CFRP the whole structure may perform better than that of rebuilding them. By only retrofitting the columns vertical extension of floor, design fault removal, damage reduction due to lateral loads may be possible. Research has been done by several people on various sections of steel varying from T-sections to hollow sections (Harries *et al.* 2006; Kalavagunta *et al.* 2014; Bambach *et al.* 2009_1; Bambach *et al.* 2009_2; Bambach and Elchalakani 2007; Shaat and Fam 2006; Shaat and Fam 2009). This research has shown that applying Carbon Fiber Reinforced Polymers (CFRP) in sheets or plates has helped to increase the capacity of the columns tested, whether short or slender.

In recent days steel HSS (hollow structural section) columns of medium to high slenderness ratios have gained much popularity in steel construction industry because of their greater strength-to-weight ratios and more load bearing capacity. But the capacity of such columns are generally governed by overall buckling before developing their full plastic capacity and the strength of column may be significantly reduced by lateral deflections. In such cases, strengthening of such columns with Carbon Fiber Reinforced Polymer (CFRP) materials has earned much attention in increasing their axial load capacity (Shaat and Fam 2006; Shaat and Fam 2009). But, very few studies have been conducted in this field due to relatively expensive experimental procedure. Therefore the present study is emphasized on the numerical simulation of steel AISC hollow structural section (HSS) columns strengthened using CFRP materials to predict their behavior to avoid the costly experimental work. It is expected that this investigation can be used as a better reference for the structural engineers to strengthen HSS column sections using CFRP materials.

1.2   OBJECTIVES OF THE PRESENT STUDY

The main objectives addressed by this study are to:
1. To study the behavior of axially loaded Steel Square Hollow Structural Section (HSS) Columns strengthened using Carbon Fiber Reinforced Polymer (CFRP) multilayer strips to see whether any improvement in axial load

carrying capacity can be achieved considering both geometric and material nonlinearities.

2. The whole study will be performed through finite element investigation so that experimental procedure of costly CFRP materials can be avoided for future study.

1.3   METHODOLOGY OF THE PRESENT STUDY

The numerical simulation of axially loaded CFRP strengthened steel HSS column has been performed using Abaqus 6.14-4, a finite element software package. A 3D finite element model incorporating both the geometric and material nonlinearities has been developed. Damage properties of both the CFRP and GFRP materials have been incorporated using Hashin Damage Model (Abaqus 2013) available in Abaqus 6.14-4. A perfect bond surface interaction model has been assumed to define the contact behavior of the steel-CFRP interface and in between FRP layers interface.

The performance of the developed model has been studied by simulating test columns strengthened using CFRP available in the published literature and it has shown good agreement. These columns had various geometric shapes as well as various CFRP configurations. The proposed model is then used for performing the parametric study on some of the non-compact HSS column sections from AISC Manual (13th edition, 2005) with varying number of CFRP layers, slenderness ratios and cross sectional geometry. And the effect of variables on the increase of axial load capacity of different CFRP strengthened HSS sections compared to that of the unstrengthened specimen has been presented graphically and also in tabular form.

1.4   ORGANIZATION OF THE THESIS

The report of the analysis is organized in this paper to represent and discuss the problem and findings that come out from the studies performed by FEM in most convenient way.

Chapter 1 introduces the topic, in which an overall idea is presented before entering into the main studies and discussion.

Chapter 2 is Literature Review, which represents the work performed so far in connection with it and is collected from different references. It also describes the strategy of advancement for the present problem to a success.

Chapter 3 is all about the finite element modeling exclusively used in this problem and it also shows some figures associated with this study for proper presentation and understanding.

Chapter 4 is concerned with the verification of the model developed in Chapter 3 with reference to an experimental study carried out by Shaat and Fam (2007).

Chapter 5 is based on the parametric study on some selected AISC HSS (Hollow Structural Section) sections with presentation by many tables and figures followed by some discussions on the obtained results.

Chapter 6, the concluding chapter, summarizes the whole study as well as points out its outcome with some further scope and directions.

Chapter 2

LITERATURE REVIEW

2.1   INTRODUCTION

The development of metallic structures has evolved significantly over the years, from the 19th century era of construction using cast or wrought iron, to modern steel construction. In general, the steel construction industry involves two types of steel structural members. The first includes the hot-rolled shapes and members built-up of plates, and the second includes cold-formed sections fabricated using steel sheets, strips or plates.

Many of the old cast iron and steel structures and bridges that remained in service are increasingly becoming in urgent need of retrofitting and strengthening. This is attributed to a number of reasons; including deterioration due to corrosion, fatigue cracking, increased loading, and change in design loads over the years. In most cases, maintaining this infrastructure through retrofit to extend their service life may be far more economical than replacing them.

The conventional strengthening method for a steel member includes bolting or welding additional steel plates onto the member or cutting out the deteriorated section and replacing it with a steel plate. These techniques have a number of shortcomings, such as the plates require heavy equipment or possibly shoring to lift them in place during installation. Adding plates also increases the area of the column as well as the dead weight of the structure, which could cause issues for some projects. The plates are susceptible to corrosion. Fastening plates to a steel structure produces stress concentrations and welding can generate thermally induced stresses or heat affected areas (Grabovac *et al*. 1991). Also, welding is not desired in many cases due to fatigue problems associated with weld defects, while bolted connections are costly

and time consuming. The continuous process of corrosion and the reduced fatigue life associated with the welded steel plates may reduce the durability and limit the effectiveness of conventional repair methods.

In such applications, the need for adopting durable materials and cost-effective retrofit techniques is evident. A possible solution is the use of Fiber Reinforced Polymers (FRPs). Though they originally may have a larger material cost than steel, the material cost alone is normally small compared to the total cost of the project. This is demonstrated for strengthening the London underground railway. The option of using steel and FRPs were both examined. The FRP strengthening scheme gave a comparable overall cost with the steel strengthening and was used because of the time restraints of the project.

FRPs provide many advantages such as being lightweight, having excellent corrosion resistance (Raj and Nirmalkumar 2014) along with fatigue properties (Al-Hammoud *et al.* 2011; Badawi and Soudki 2010) and having high-strength capabilities (Karbhari and Shulley 1995) and also having high stiffness-to-weight ratios. They have minimal impact visually, and have minimal effect on clearance. Implementation of repair strategies using CFRP is faster and easier than other repair techniques (Shaat and Fam 2007). There are many different types of FRPs with the main two using carbon or glass fibers. But due to wanting a higher modulus, the use of Carbon Fiber Reinforced Polymer (CFRP) materials is gaining popularity day by day for repairing and strengthening of steel structures (Zhao 2013; Teng and Fernando 2012; Zhao and Zhang 2007) compared to other retrofitting techniques (Di Sarno and Elnashai 2005). They are available in strips or flexible sheets allowing for easy application to any project, even when the member is already in use. FRP flexible sheets in particular offer a unique advantage of being able to conform to complex and curved surfaces.

This section first presents an overview of metallic structural materials, followed by a brief summary of conventional methods currently used in retrofitting steel structures. This section presents the background and describes applications of externally bonded Fiber Reinforced Polymer (FRP) plates or sheets used as a method to strengthen or rehabilitate structural steel. A more detailed discussion on Carbon Fiber Reinforced Polymer (CFRP) materials and their use in retrofitting metallic structures, along with recent research advances in this field will follow.

2.2   METALLIC MATERIALS

A wide range of metallic materials has been used in construction. This section briefly describes two of the most commonly used structural metals, namely, cast iron and steel.

2.2.1   CAST IRON

Structural cast iron was developed at the end of the 18th century and the first cast iron bridge was built in 1779. Cast iron typically has non-linear stress-strain relationship with low values of secant modulus ranging between 100 GPa and 145 GPa. It also has a higher compressive strength than its tensile strength. The maximum compressive strength can reach 772 MPa while the maximum tensile strength is limited to 280 MPa.

2.2.2   STEEL

Steel is one of the most abundantly used structural materials, owing to its strength, scrap value and ease of transport. Commercial steel has been produced since 1860; however, it is rare to find steel structures built before 1890. Steel has become the backbone of the structural engineering infrastructure and has remained the material of choice for various projects by engineers due to its light weight, and favorable strength and ductility. Steel is also an ideal material because of its durability, ease of maintenance and ease of use in construction. Typically, steel has similar mechanical properties in tension and compression, including an elastic modulus of 200 to 210 GPa and a yield strength ranging between 230 MPa and 700 MPa.

2.2.3   BUCKLING STRENGTH OF STEEL MEMBERS

An important phenomenon to be considered by designers is the buckling strength of steel. Two types of buckling may occur to compression steel elements, namely, local buckling, which occurs within the thin elements comprising the cross section of a member, and overall buckling that takes place in slender compression members. Although there are no definite boundaries between short and long columns, it is believed that columns with slenderness ratio values less than 20 (F_y= 300 MPa) may be considered as short columns and will not undergo the overall buckling type of failure. Local buckling of the walls of a cross section depends on the width-to-

thickness ratio and the type of support provided to the wall. For example, in short columns consisting of rectangular Hollow Structural Sections (HSS), two opposite sides would typically buckle outwards and the other two sides would buckle inwards. In thin-walled sections, this type of buckling occurs before reaching the cross-sectional yielding capacity, whereas in thick-walled sections, it occurs after yielding. Steel columns of medium to high slenderness ratios are rather susceptible to overall buckling failure, before developing their full plastic capacity. Due to some unavoidable disturbances during the rolling and cooling processes, the steel sections produced can never be perfectly straight. As such, when these sections with their imperfect shapes (also known as out-of-straightness) are used as columns, overall buckling will be introduced.

2.2.4   POSSIBLE BUCKLING MODES

The general buckling modes comprise

1) Overall or Global Buckling and
2) Local Buckling

Again overall buckling include the following sub modes such as

a) Flexural buckling
b) Torsional buckling
c) Flexural torsional buckling

A brief description for each of the buckling modes is provided below.

2.2.4.1   Flexural Buckling

It is the primary type of buckling and is also referred as Euler buckling. Members are subjected to flexure or bending when they become unstable (Figure 2.1).

2.2.4.2   Torsional Buckling

Column may buckle in a twisting manner rather than in the bending mode. This is called torsional buckling (Figure 2.2). Torsional buckling is generally applicable for

- Short lengths usually *kL/r* less than approximate 50.
- Doubly symmetric sections such as wide flange sections, cruciform sections, double channels, point symmetric sections etc.
- Not for closed sections such as HSS since they are very strong in torsion.
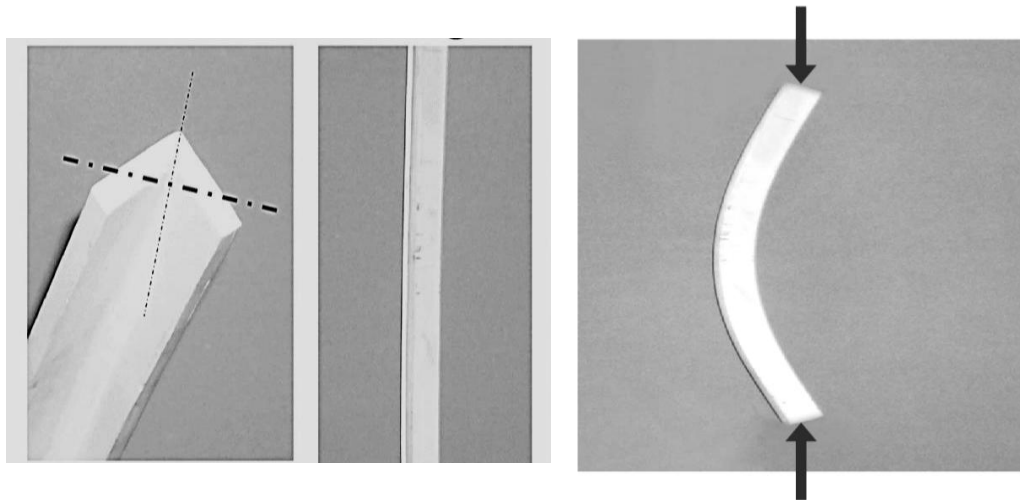
Figure 2.1: Flexural buckling.
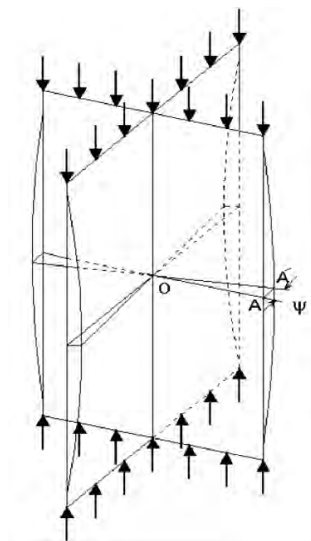
Figure 2.2: Torsional buckling of a cruciform section.

2.2.4.3 Flexural-Torsional Buckling

Buckling combined with flexure and torsion will eventually result in flexural-torsional Buckling (Figure 2.3).
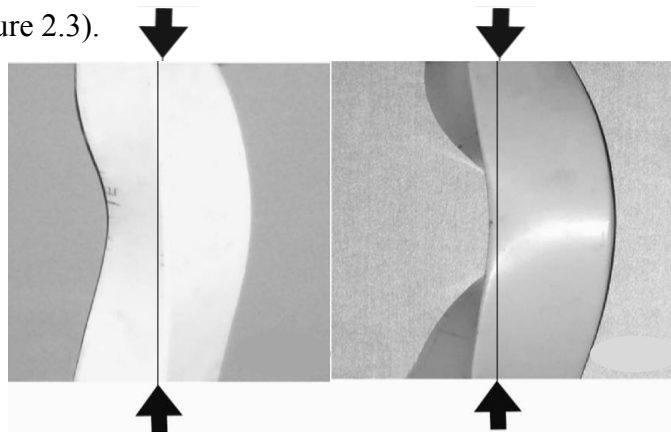
Figure 2.3: Flexural-Torsional Buckling.

2.2.4.4   Local Buckling

Local Buckling is the wave formation developed in flanges, webs and other plate elements of a steel member (column, beam) when they are compressed. Local buckling of a plate element can cause premature failure of the entire section of member. It can be prevented by keeping the width-thickness ratio within certain limits (Figure 2.4).
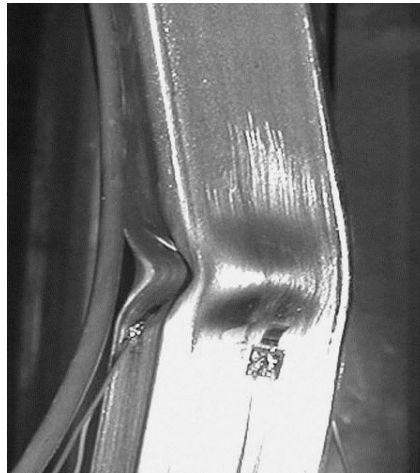
Figure 2.4: Local Buckling (https://nees.org/warehouse/experiment/1112/project/605). The limiting values of width to thickness ratios to avoid local buckling for plates in compression are shown in the following table.

Table 2.1: Typical limiting values of width-to-thickness ratio (*b/t*) for plates in compression.

Type of Element	Specification		
	AISC F_y, ksi	AREA F_y, psi	AASHTO f_a, psi
Supported on one unloaded edge:			
Single Angle	$\dfrac{76}{\sqrt{F_y}}$	...	$\dfrac{1625}{\sqrt{f_a}}$
Projecting element	$\dfrac{95}{\sqrt{F_y}}$	$\dfrac{2300}{\sqrt{F_y}}$	$\dfrac{1625}{\sqrt{f_a}}$
Stem of T	$\dfrac{127}{\sqrt{F_y}}$	$\dfrac{3000}{\sqrt{F_y}}$	...

Type of Element	Specification		
	AISC F_y, ksi	AREA F_y, psi	AASHTO f_a, psi
Supported on both unloaded edges:			
Webs	$\dfrac{253}{\sqrt{F*}}$	$\dfrac{6000}{\sqrt{F_y}}$	$\dfrac{4000}{\sqrt{f_a}}$
Cover plates	$\dfrac{238}{\sqrt{F*}}$	$\dfrac{7500}{\sqrt{F_y}}$	$\dfrac{5000}{\sqrt{f_a}}$
Perforated cover plates	$\dfrac{317}{\sqrt{F*}}$	$\dfrac{7500}{\sqrt{F_y}}$	$\dfrac{6000}{\sqrt{f_a}}$

* ASD : $F = F_y$; LRFD : $F = F_y = F_r$, where $F_r = 10$ ksi for rolled shapes, 16.5 ksi for welded shapes.

2.3 CONVENTIONAL RETROFIT TECHNIQUES OF STEEL STRUCTURES

Retrofit of existing structures is typically needed when live loads increase beyond those the structures were originally designed for. It may also be required because of an inadequate design, damage, fatigue cracking, or deterioration such as corrosion. The methods of retrofitting steel structures typically involve bolting or welding additional steel plates to the structure. These methods, however, have a number of constructability and durability drawbacks including the added dead load, installation time, difficulty of shaping and fitting complex profiles, and the need for an elaborate and expensive shoring system (Figure 2.5).

Figure 2.5: Bolted Steel plates to the affected areas.

In many cases, welding is not a desirable solution due to fatigue problems associated with weld defects. On the other hand, mechanical (bolted) connections, which have better fatigue life, are time consuming and costly. Drilling holes for bolted connections also results in a cross sectional loss as well as the introduction of stress raisers. Additionally, steel plates require heavy lifting equipment and may add considerable dead loads to the structure, which reduces their strengthening effectiveness (Figure 2.6 and 2.7). The added steel plates are also susceptible to corrosion, which could lead to an increase in future maintenance costs.
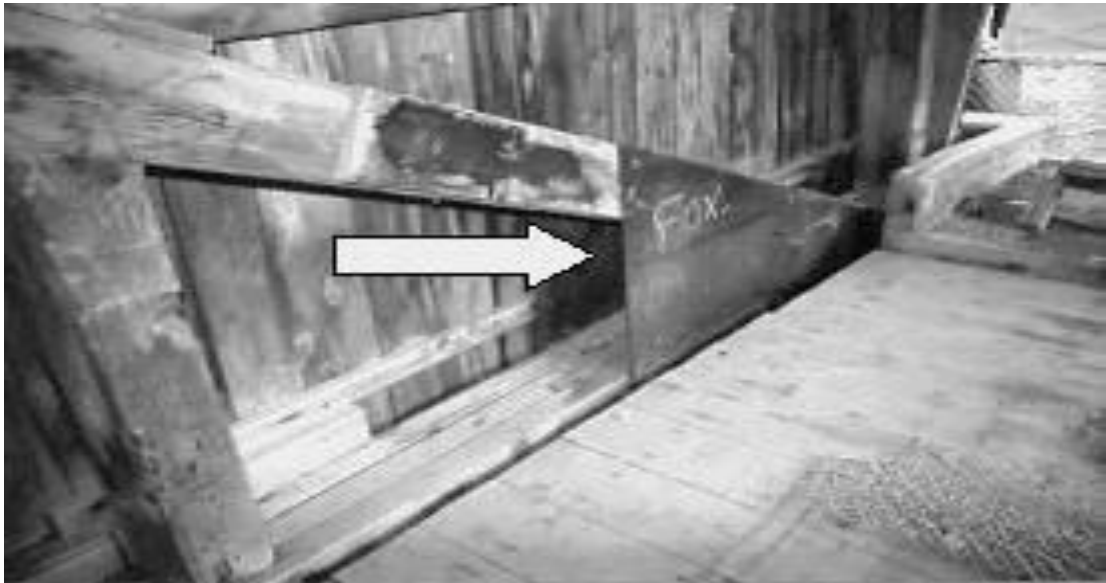
Figure 2.6: Steel plates at heel connection of queenpost truss.
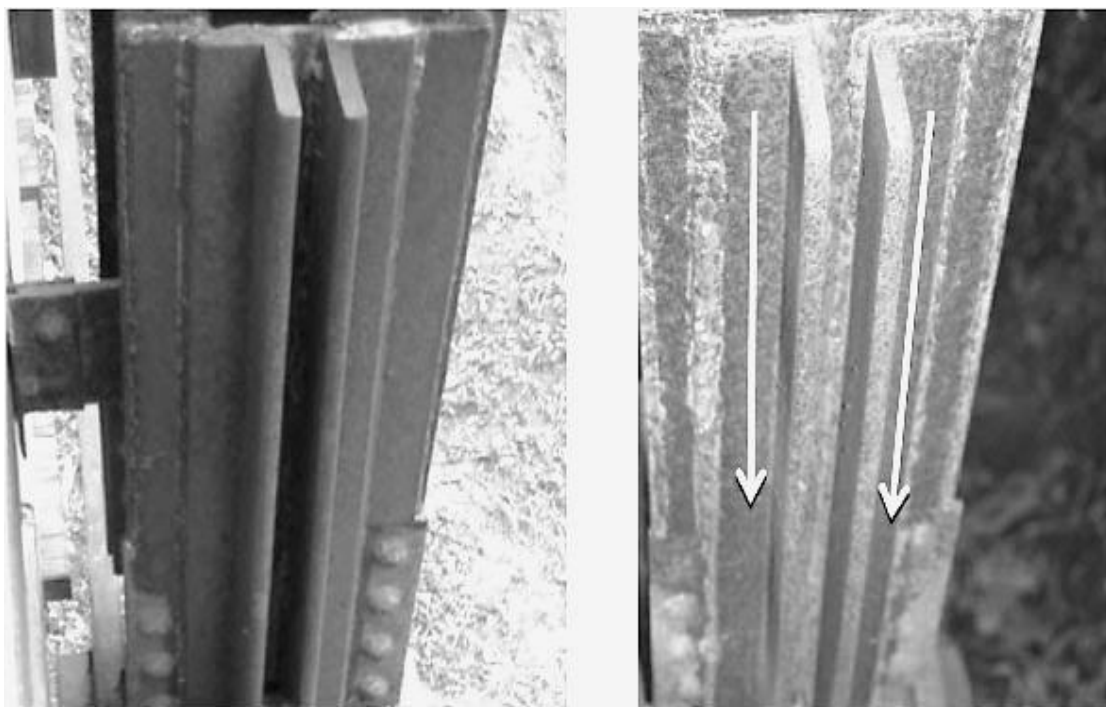
Figure 2.7: Retrofitted Steel plates (left) and Rusting of Steel plates (right).

2.4 RETROFITTING OF STEEL STRUCTURES USING FIBER REINFORCED POLYMER (FRP) MATERIALS

There is a need for adopting durable materials and cost-effective retrofit techniques to overcome some of the drawbacks of conventional techniques stated earlier. One of the possible solutions is to use high performance non-metallic materials such as FRPs. In general, FRP materials provide superior strength-to-weight ratios for retrofit of structures. FRP rigid plates and flexible sheets are available and can easily be applied to the metallic surface. FRP flexible sheets in particular offer a unique advantage of being able to conform to complex and curved surfaces.

2.4.1 TYPES OF FRP FIBERS AND RESINS

Fiber-reinforced polymer (FRP) is a composite material made of a polymer matrix reinforced with fibers. The fibers are usually glass, carbon or aramid, although other fibers such as paper or wood or asbestos have been sometimes used. The polymer is usually an epoxy, vinylester or polyester thermosetting plastic and phenol formaldehyde resins are still in use. FRPs are commonly used in the aerospace, automotive, marine and construction industries. A brief description of these types is stated below.

2.4.1.1 Carbon Fibers

CFRP (Carbon Fiber Reinforced Polymer) is a composite material, consisting of various carbon fibers and thermosetting resins. Carbon fiber's main attraction is its strength-to-weight ratio, which is 20 percent the mass of steel yet equally stiff and strong. They have low density, excellent damping properties and a high resistance to impacting combined with exactly modifiable thermal expansion to complement the complex characteristics profile. Glass reinforced plastic is lightweight and has good thermal insulation properties. It has a high strength to weight ratio, making it useful for the production of products such as water tanks, surfboards, canoes, small boat hulls and similar products (Figure 2.8 and Figure 2.9).
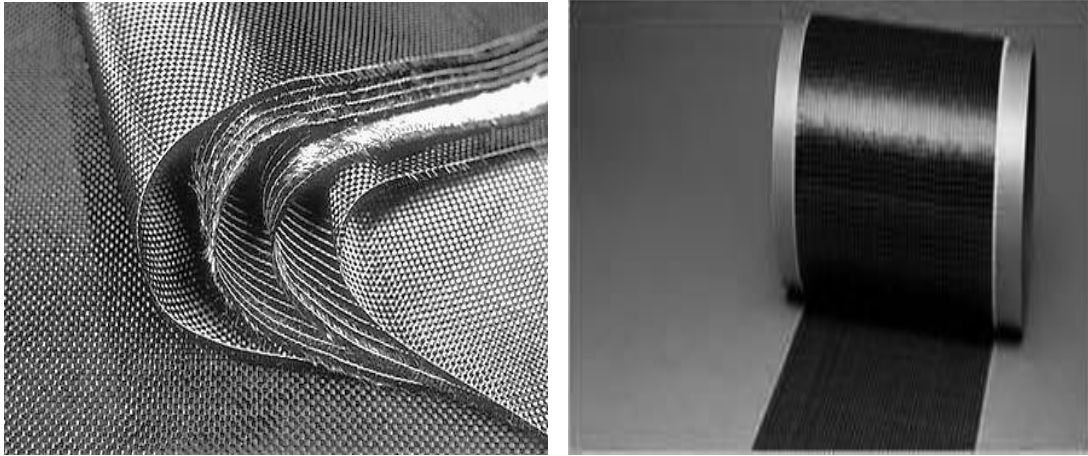
Figure 2.8: Carbon Fiber Reinforced Polymer (CFRP) Sheets (https://www.build-on-
prince.com).
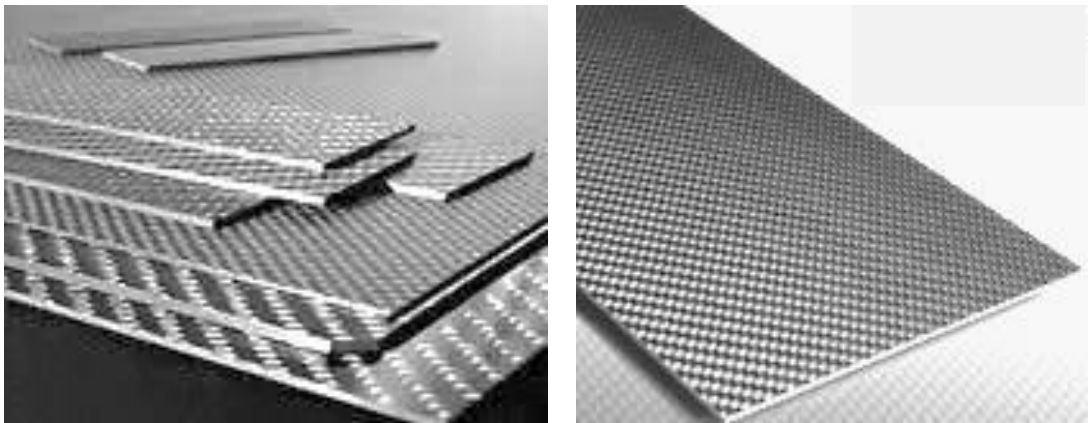
Figure 2.9: Carbon Fiber Reinforced Polymer (CFRP) Plates (https://www.build-on-
prince.com).

2.4.1.2   Glass Fibers

Glass Fiber Reinforced Polymer (GFRP) is composed of strands of glass. Each individual glass fiber is very fine with a small diameter and they are woven to form a flexible fabric. The fabric is normally placed in a mould, for instance a mould for a canoe and polyester resin is added, followed by a catalyst (to speed up the reaction). The process is repeated so that there are many layers of fiber glass and resin and allowed to dry/cure. The resulting material is strong and light. Glass Reinforced Plastic can be sanded for a smooth finish and painted. Glass reinforced plastic has good thermal insulation properties. It has resistance against salt water, chemicals, and the environment unaffected by acid rain, salts, and most chemicals. It has a high strength to weight ratio, making it useful for the production of products such as water tanks, surfboards, canoes, small boat hulls and similar products (Figure 2.10).
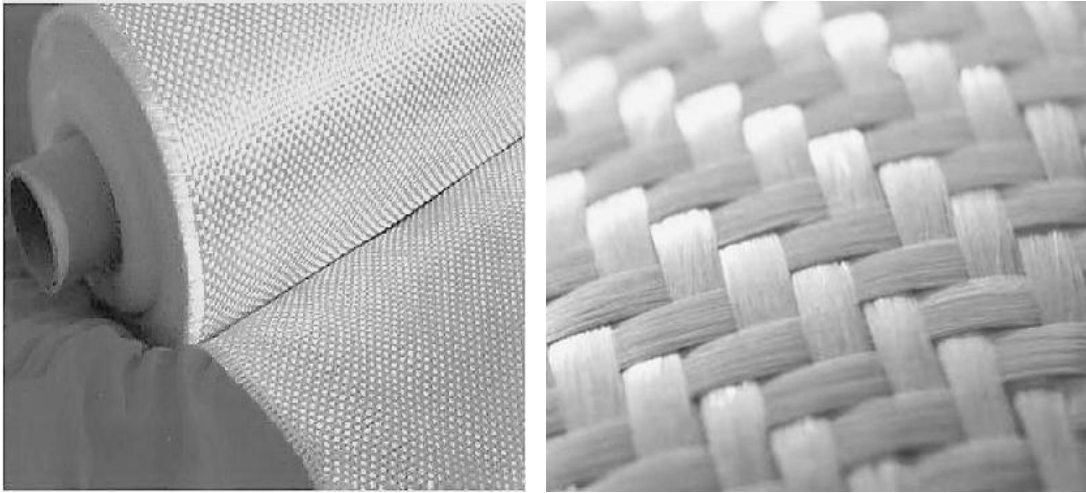
Figure 2.10: Glass Fiber Reinforced Polymer (GFRP) (https://www.build-on-prince.com).

2.4.1.3   Aramid Fibers

Aramid fibers are long-chain synthetic polyamides. Aramid fibers have extremely high tensile strength, which is why they are commonly used in armor and ballistic protection applications (Figure 2.11).
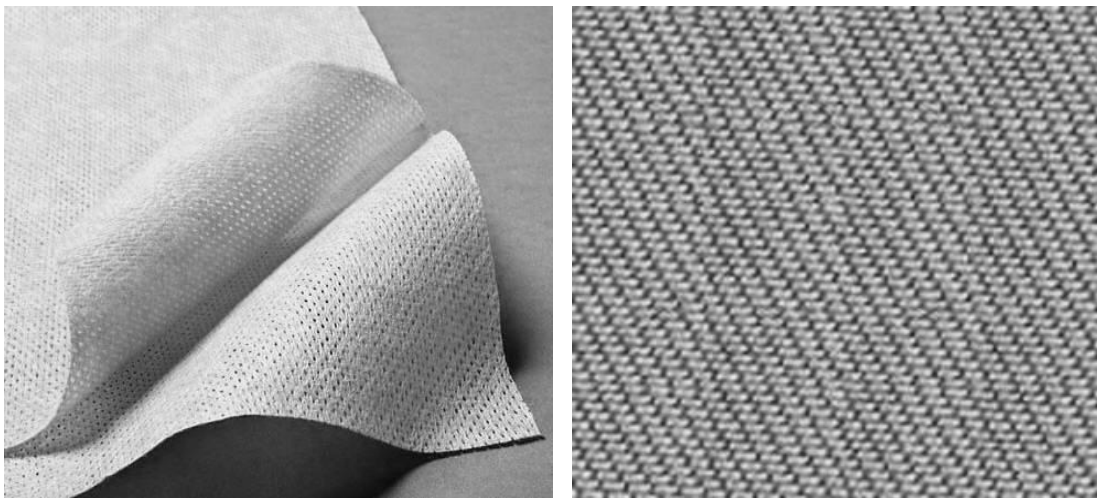
Figure 2.11: Aramid Fibers (https://www.build-on-prince.com).

With a distinctive yellow color, aramid fibers are frequently used in advanced composite products which require high-strength and light-weight properties. Products made with aramid fibers include: bulletproof vests, space craft components, fire suits, football pads, boats, and more.

2.4.1.4   Epoxy Resins

Epoxy resins are advanced thermosetting resins used in FRP composites. They are made of tightly linked adhesive polymer structures that are often used in surface adhesives and coatings (Figure 2.13).
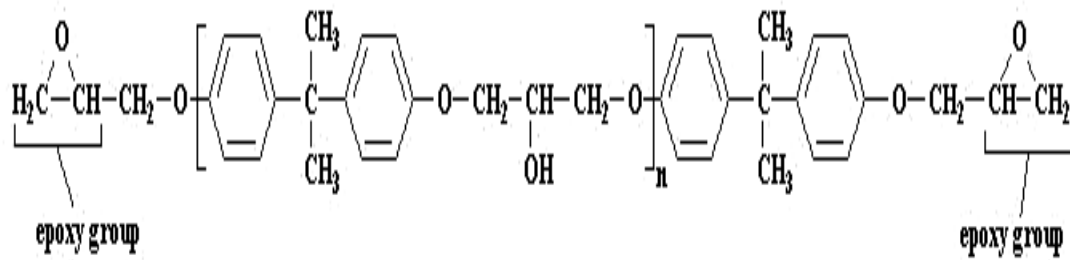
Figure 2.12: Chemical structure of Epoxy Resin (https://www.build-on-prince.com).

(a)   (b)
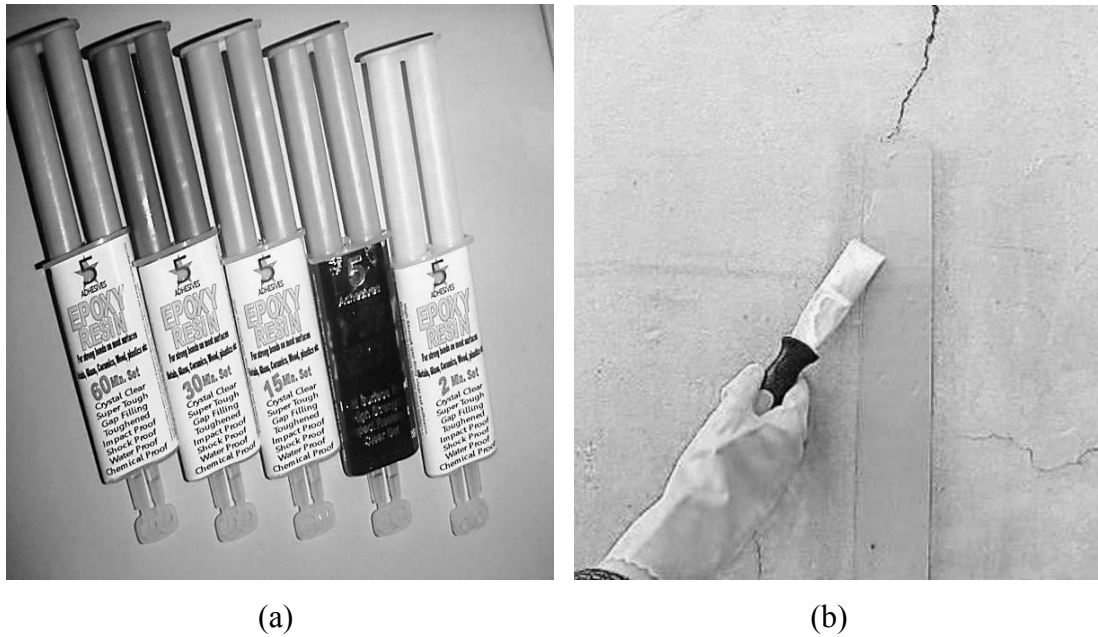
Figure 2.13: (a) Epoxy Resin Tube and (b) Application of HM-180C3P Modified
            Epoxy Resin Carbon Fiber Impregnation Adhesive (https://www.build-
            on-prince.com).

Epoxy resins are capable of forming tight cross-linked polymer structures characterized by toughness, strong adhesion, and low shrinkage. Epoxy adhesives are nearly unmatched in heat and chemical resistance. Epoxy resin has various uses such as; the resins that are cured through exposure with ultra violet light are normally used in optoelectronics, fiber optic and dentistry. Industrial tooling applications normally use resin to make laminates, fixtures, castings and moulds. In the electronic world, epoxy resin is used to make transformer, insulator, switch gear and generators. Epoxy resins are tough, chemically resistant, rigid materials that cure at room temperature. They are typically used as structural adhesives. Chemical structure of epoxy resins are shown in Figure 2.12.

2.4.1.5 Polyester Resins

Polyester resin is an unsaturated, thermosetting resin produced by a reaction between several organic acids and polyhydric alcohols. It is most commonly used in the construction of molded reinforced fiber and composite products. Although these products have several distinct disadvantages when compared to other commonly used composite resins, they still offer an attractive balance of ease of use, low cost, and positive physical characteristics. When working around large amounts of polyester resins, it is a good idea to use a chemical respirator and also wear gloves since polyester resin fumes could be harmful.

2.4.1.6 Vinylester Resins

Vinylester resins are similar in their molecular structure to polyesters, but differ primarily in the location of their reactive sites, these being positioned only at the ends of the molecular chains (Figure 2.14). As the whole length of the molecular chain is available to absorb shock loadings, this makes vinylester resins tougher and more resilient than polyesters. The vinylester molecule also features fewer ester groups. These ester groups are susceptible to water degradation by hydrolysis which means that vinylesters exhibit better resistance to water and many other chemicals than their polyester counterparts and are frequently found in applications such as pipelines and chemical storage tanks.
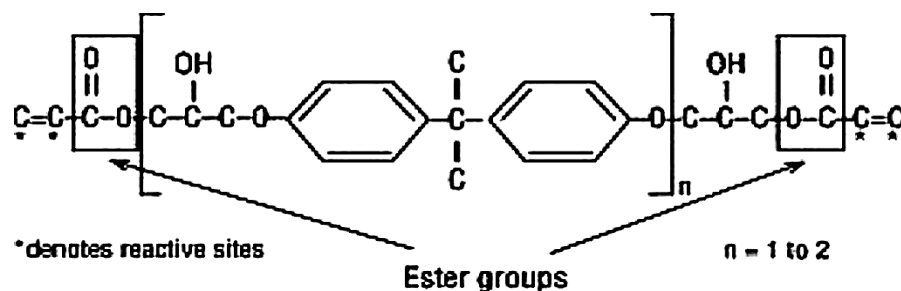
Figure 2.14: Idealized chemical structure of a typical vinylester (https://www.build-on-prince.com).

2.4.2 PROPERTIES AND BEHAVIOR OF FRP MATERIALS

2.4.2.1 Tensile Behavior of FRP

The tensile strength and stiffness of FRP material is dependent on several factors. As the fibers of FRP are the main load carrying constituents, so the type of fibers, the orientation of fibers and the quantity of fibers govern the tensile behavior mostly.

When this FRP is loaded under direct tension it does not exhibit any plastic behavior (yielding) before rupture. Most of the time, CFRP shows a linearly elastic stress-strain relationship until failure. Table 2.2 represents the tensile properties of commercially available FRP system.

Table 2.2: The tensile properties of some of the commercially available FRP systems.

Fiber Type	Elastic Modulus		Ultimate Strength		Rupture Strain, min
	10^3 ksi	GPa	ksi	MPa	%
Carbon					
General Purpose	32-34	220-240	300-550	2050-3790	1.2
High Strength	32-34	220-240	550-700	3790-4820	1.4
Ultra-High Strength	32-34	220-240	700-900	4820-6200	1.5
High Modulus	50-75	340-520	250-450	1720-3100	0.5
Ultra-High Modulus	75-100	520-690	200-350	1380-2400	0.2
Glass					
E-Glass	10-10.5	69-72	270-390	1860-2680	4.5
S-Glass	12.5-13	86-90	500-700	3440-4140	5.4
Aramid					
General Purpose	10-12	69-83	500-600	3440-4140	2.5
High Performance	16-18	110-124	500-600	3440-4140	1.6

(Italian National Research Council, 2004)

The typical tensile strengths and stress-strain relationship of FRP and steel reinforcements are shown in Figure 2.15.
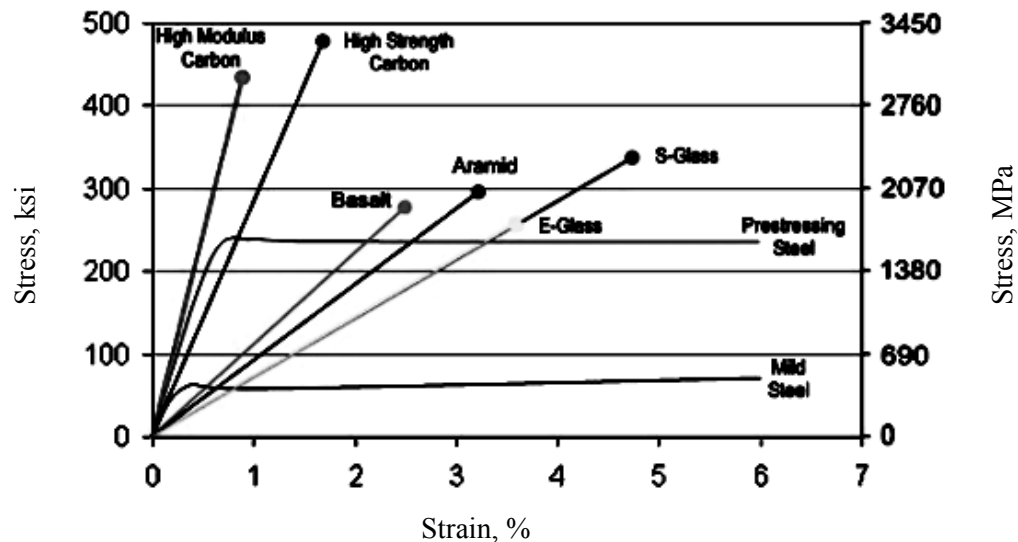
Figure 2.15: The typical tensile strengths and stress-strain relationship of FRP and steel reinforcements (https://www.build-on-prince.com).

2.4.2.2   Compressive Behavior of FRP

The tests for predicting compressive strength of externally bonded FRP systems are insufficient, so it should not be used as compressive reinforcement. For this reason it is not recommended to rely on FRP systems to resist compressive stress. Shear failure, fiber micro buckling transverse tensile failure is some modes of failure of FRP laminates subjected to longitudinal compression. The methods of failure depends on i) the type of fiber, ii) the fiber-volume fraction and iii) the type of resin.

In general, compressive strengths are higher for materials with higher tensile strengths, except in the case of a FRP. It is reported that GFRP, CFRP and AFRP exhibit compressive strength of 55%, 78% and 20% of the tensile strength respectively (Ehsani and Saadatmanesh 1990).

The modulus of elasticity of compressive stress is generally lower than the tensile modulus of elasticity. The compressive modulus of elasticity is approximately 80% for GFRP, 85% for CFRP and 100% for AFRP of the tensile modulus of elasticity (Ehsani and Saadatmanesh 1990).

2.5   ENGINEERING PROPERTIES OF CFRP MATERIALS

Carbon-fiber-reinforced polymers are composite materials. In this case the composite consists of two parts; a matrix and reinforcement. In CFRP the

reinforcement is carbon fiber, which provides the strength. The matrix is usually a polymer resin, such as epoxy, to bind the reinforcements together. Since CFRP consists of two distinct elements, the properties depend on these two elements.

2.5.1 PHYSICAL PROPERTIES OF CFRP

Physical properties of CFRP materials are listed below.

1. High strength to weight ratio, specific toughness, light weight.
2. Good vibration damping, strength, and toughness.
3. High dimensional stability, low coefficient of thermal expansion, and low abrasion.
4. Electrical conductivity.
5. Biological inertness and x-ray permeability.
6. Fatigue resistance, self-lubrication, high damping.
7. Electromagnetic properties.
8. Chemical inertness, high corrosion resistance.

2.5.2 MATERIAL PROPERTIES OF CFRP

Carbon-FRP (CFRP) materials are available in a variety of grades, according to the process by which they are manufactured. In the context of this thesis, CFRP material will be referred to according to its elastic modulus.
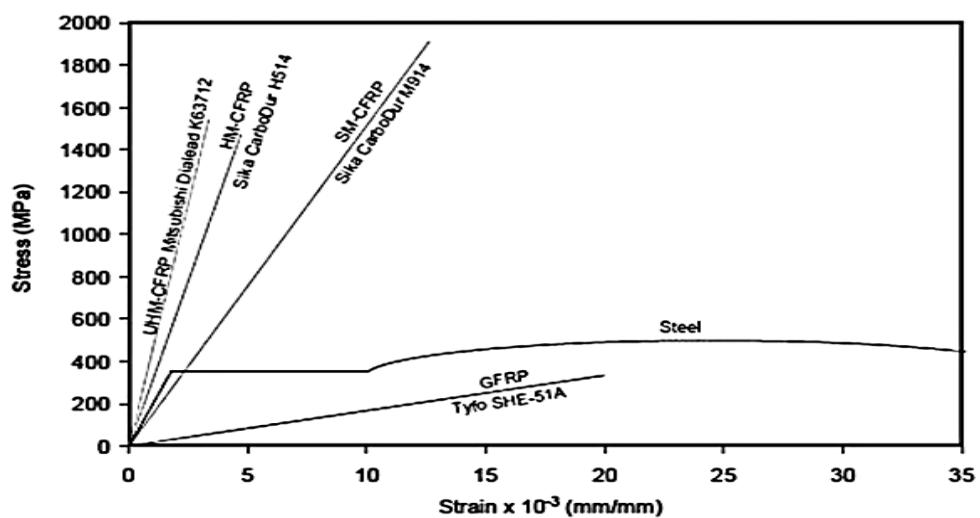
Figure 2.16: Typical stress-strain curves of SM-, HM-, and UHM-CFRP, compared to mild steel and GFRP.

CFRP material with an elastic modulus value less than that of steel (i.e. *ECFRP* < 200 GPa) will be referred to as Standard Modulus-CFRP (SM-CFRP), whereas CFRP having elastic modulus ranging between 200 GPa and 400 GPa will be referred to as High Modulus-CFRP (HM-CFRP). CFRP material with high value of elastic modulus larger than 400 GPa will be referred to as Ultra High Modulus-CFRP (UHM-CFRP).

2.5.3   MECHANICAL PROPERTIES OF CFRP

Mechanical properties of CFRP material are shown in the following Table 2.3.

Table 2.3: Mechanical Properties of CFRP.

Fibres @ 0° (UD), 0/90° (fabric) to loading axis, Dry, Room Temperature (UD = Unidirectional)					
	Units	Std. Carbon Fiber (CF) Fabric	High Modulus Carbon Fiber (HM-CF) Fabric	Std. Carbon Fiber (CF) UD	High Modulus Carbon Fiber (HM-CF) UD
Young's Modulus 0°	GPa	70	85	135	175
Young's Modulus 90°	GPa	70	85	10	8
In-plane Shear Modulus	GPa	5	5	5	5
Major Poisson's Ratio		0.10	0.10	0.30	0.30
Ult. Tensile Strength 0°	MPa	600	350	1500	1000
Ult. Comp. Strength 0°	MPa	570	150	1200	850
Ult. Tensile Strength 90°	MPa	600	350	50	40
Ult. Comp. Strength 90°	MPa	570	150	250	200
Ult. In-plane Shear Strength	MPa	90	35	70	60
Ult. Tensile Strain 0°	%	0.85	0.40	1.05	0.55
Ult. Comp. Strain 0°	%	0.80	0.15	0.85	0.45
Ult. Tensile Strain 90°	%	0.85	0.40	0.50	0.50
Ult. Comp. Strain 90°	%	0.80	0.15	2.50	2.50
Ult. In-plane shear strain	%	1.80	0.70	1.40	1.20
Density	g/cc	1.60	1.60	1.60	1.60

Fibres @ +/-45 Deg. to loading axis, Dry, Room Temperature					
	Units	Std. CF	HM CF	Std. CF fabric	Steel
Longitudinal Modulus	GPa	17	17	19.1	207
Transverse Modulus	GPa	17	17	19.1	207
In Plane Shear Modulus	GPa	33	47	30	80
Poisson's Ratio		0.77	0.83	0.74	
Tensile Strength	MPa	110	110	120	990
Compressive Strength	MPa	110	110	120	990
In Plane Shear Strength	MPa	260	210	310	
Thermal Expansion Co-efficient	Strain /K	2.15×10^{-6}	0.9×10^{-6}	4.9×10^{-6}	11×10^{-6}
Moisture Co-efficient	Strain /K	3.22×10^{-4}	2.49×10^{-4}	-	-

This table relates to only two of the many fiber orientations possible.

2.5.4   CHEMICAL PROPERTIES OF CFRP

Carbon fiber is a long, thin strand of material about 0.0002-0.0004 in (0.005-0.010 mm) in diameter and composed mostly of carbon atoms. The carbon atoms are bonded together in microscopic crystals that are more or less aligned parallel to the long axis of the fiber. The crystal alignment makes the fiber incredibly strong for its size. Several thousand carbon fibers are twisted together to form a yarn, which may be used by itself or woven into a fabric. The yarn or fabric is combined with epoxy and wound or molded into shape to form various composite materials. Carbon fiber-reinforced composite materials are used to make aircraft and spacecraft parts, racing car bodies, golf club shafts, bicycle frames, fishing rods, automobile springs, sailboat masts, and many other components where light weight and high strength are needed.

2.5.5   BOND STRENGTH AND FORCE TRANSFER

Force transfer between FRP and steel is controlled by bond at the interface between the two materials. Bond performance is influenced by several factors such as the bonded length and width, type of fibers and adhesive (resin), surface preparation, thickness of adhesive, and thickness of FRP laminate. One of the simplest test configurations for investigating bond strength and behavior between either similar or dissimilar materials is the single- or double-lap shear joint test (ASTM, D5868-01).

Various investigations showed that the low value of ultimate strain of the HM-CFRP resulted in joints with lower strength compared to using the SM-CFRP plates, which have a higher ultimate strain. Moreover, inserting a layer of GFRP with a low value of elastic modulus (softer) between steel and HM-CFRP resulted in a more gradual load transfer (i.e. better shear stress distribution) and increased the joint capacity by approximately 20 percent.

2.6   APPLICATION OF FRP IN STRUCTURAL REHABILITATION

In the last ten to fifteen years, FRP materials have emerged as promising alternative repair materials for steel structures along with the reinforced concrete structures (Carolin *et al.* 2015; Garcia *et al.* 2014; Gajdosova and Bilcik 2013; Zilch *et al.* 2014; Wu et al. 2014; Sadeghian *et al.* 2010; Oehlers *et al.* 2004; Darwish 2000; El-Saikaly *et al.* 2014; Balaguru *et al.* 2009) and they are rapidly becoming materials of choice for strengthening and rehabilitation of steel infrastructure.

2.6.1   STRENGTHENING OF STEEL BEAMS WITH FRP

FRP systems have a wide range of uses including rehabilitating existing structural elements, retrofitting or strengthening a structurally sound member or correcting construction errors. Retrofitting of steel structures using FRPs has been somewhat limited compared to concrete structures; however it has shown great success (Miller *et al.* 2004; Schnerch *et al.* 2008; Illig and White 2010; Hollaway and Cadei 2002). Shaat *et al*. (2004) performed an overall review of research done in the field of strengthening and repairing steel structures with FRPs. Further review study relating FRP strengthened steel structures has also been provided by Zhao and Zhang (2007) and Zhao (2013).

Strengthening or retrofitting steel beams has been the subject of most research with FRP systems and steel. Rui *et al*. (2010) focused on strengthening I-beams by using a hybrid FRP with carbon/glass fibers and a vinyl-ester resin. They conducted four-point bending tests and found an optimal carbon volume content of 25-30% (Rui *et al*. 2010). Dawood *et al*. (2006) used carbon fiber reinforced polymers (CFRP) in the form of strips with different moduli applied to steel-concrete composite beams located in bridges. They concluded that high and intermediate modulus of CFRP increased the

elastic stiffness, yield load and ultimate capacity of the beams. When testing the beams for fatigue resistance, comparable results to the unstrengthened beams were obtained (Dawood *et al.* 2006). Peiris and Harik (2014) looked at the bond characteristics and flexural behaviour of normal and ultra-high modulus CFRP applied to wide flange steel beams. Peiris noted that the normal modulus had a load carrying capacity of 22% higher than the ultra-high modulus (Peiris and Harik 2014).

Narmashiri *et al.* (2012) performed flexural strengthening experiments for steel I-beams using CFRP strips and studied the effects of varying the thickness and type of CFRP. The authors noted that a thicker plate increased the load bearing capacity but the specimens experienced a brittle failure and premature debonding at the ends (Narmashiri *et al.* 2012).

Gillespie *et al.* (1996) strengthened a steel girder on a bridge in the field with CFRP plates and monitored the effect. Load tests in the field observed 11% reduction in the tension flange strains (Gillespie *et al.* 1996). Tavakkolizadeh, and Saadatmanesh (2001) repaired steel-concrete composite girders with CFRP sheets and showed that the ultimate load capacities and stiffness could be regained. Three large tests were done with one, three or five layers of CFRP applied to repair specimens with 25, 50 or 100% loss in cross-sectional area (Tavakkolizadeh and Saadatmanesh 2001). Shaat and Fam (2008) performed similar tests on artificially damaged steel-concrete composite beams. Varied lengths and number of layers were applied on the cracked flange and strengths of 46-116% of the original undamaged specimens were observed (Shaat and Fam 2008).

These studies, among many others, validate the use of strengthening steel beams with CFRP. The focus of this thesis is on strengthening steel columns with CFRP strips and the research done so far on this subject is discussed in the following section.

2.6.2   STRENGTHENING OF STEEL COLUMNS WITH FRP

FRP systems have also had success when used to strengthen steel columns. The FRP has proven to increase the axial capacity and stiffness of the columns. Research has been done on a variety of steel sections ranging from T-sections, C channels, square hollow sections, steel tubes and S-sections. Each study has also used a range of FRP types. This section presents a summary of their findings.

Harries *et al.* (2006) tried to enhance web or flange capacity of T-sections against local buckling by using high strength CFRP strips or ultra-high modulus GFRP strips. The FRP was applied on both sides of the web with either one or two layers. Testing the specimens in loading cycles showed that the axial capacities did not improve significantly. The GFRP specimen capacity increased 6 and 9% and the CFRP specimens showed a minor decrease in capacity. The specimens did exhibit greater resistance to weak-axis lateral displacement. It was shown that decreasing the slenderness of a member increases the cyclic loading lifespan and capacity (Harries *et al.* 2009).

Kalavagunta *et al.* (2014) studied the effect of using CFRP to control the local buckling of cold formed lipped steel channels. These tests showed an increase in the load-carrying capacity of up to 16.75% (Kalavagunta *et al.* 2014). Silvestre *et al.* (2008) also investigated CFRP strengthened cold formed lipped steel channel columns. The parameters involved were seven different strengthening configurations, a constant CFRP modulus of 235GPa, and two different lengths of columns, 600mm and 2200mm. The largest increase in ultimate strength of 19.8% was obtained for a column strengthened with CFRP wrapped around the entire column. Just strengthening the web and flange increased the load by 15.7-18.4%. The columns that demonstrated higher ultimate loads also had brittle failures (Silvestre *et al.* 2008).

Teng and Hu (2007) studied the effect of adding GFRP to steel tubes assuming that due to GFRP possessing a larger ultimate tensile strain it would increase the ductility of the tubes. The GFRP strengthened load-axial curve showed a slow lengthy ascending branch before finally reaching the peak, indicating ductility. The ultimate load increased 5-10% proving that the number of layers of GFRP applied had a minimal impact on the ultimate load (Teng and Hu 2007).

Haedir and Zhao (2011) studied the effect of adding CFRP sheets to circular steel tubular short columns to investigate the effects of the yield strength, modulus of elasticity of the hoop fibre and the amount and direction of the fibre reinforcement. The columns, with slenderness values ranging from 67-142, were tested in a concentric compression test. The axial load-shortening of each of the columns were observed with an increase of 15-36% in the peak load. With this information, Haedir

and Zhao (2011) proposed a set of design curves to be used for CFRP-reinforced steel short columns (Haedir and Zhao 2011).

Liu *et al.* (2005) looked at retrofitting steel-notched S-sections with an open GFRP jacket and then filling the jacket with expansive lightweight concrete to provide active confinement. Of the seven specimens, there were three different lengths of jackets tested in the Y-Y axis. Buckling in these specimens occurred at the end of the GFRP jacket as opposed to in the middle like the bare steel column. It was noticed that the longer retrofit lengths reached a higher ultimate load capacity. Liu *et al.* used their data to develop a model to predict the capacities and design guidelines (Liu *et al.* 2005).

Ritchie *et al.* (2014) investigated CFRP strengthening of a different type of slender steel columns against global buckling around weak axis using CFRP plates of various moduli. In this study, twelve 2.6 m long S75×8 steel columns of 197 slenderness ratio that represents the upper limit permitted by code were tested under concentric axial loading using pin-ended conditions. CFRP plates were adhesively bonded to the flanges of the steel I-shape sections in nine of the columns and buckling was studied about the weak axis. The main parameters studied were the level of initial out-of-straightness [length (L)/8,387 to L/1,020], CFRP modulus (168-430 GPa), CFRP reinforcement ratio (13-34%) and the length of CFRP plate (33-95% of L). The gain in axial strength due to CFRP strengthening ranged from 11 to 29%, depending on the various parameters. The gain generally increased as CFRP modulus, initial out-of-straightness or CFRP reinforcement ratio increased.

2.6.3   STRENGTHENING OF STEEL HSS COLUMNS WITH FRP

Now-a-days steel hollow structural section (HSS) columns are gaining much popularity due to the number of advantages they offer over their shapes.

1. Steel HSS (hollow structural section) columns are very efficient in resisting compression loads and are used in the construction of framed structures in office and industrial buildings.

2. With HSS column, less steel by weight and more load bearing capacity can be ensured.

3. They provide a significant cost savings over wide flange structural shapes.

4. They also provide greater strength-to-weight ratios than structural wide flange shapes.

For the purpose of strengthening the steel HSS columns in field condition several experimental research works have been performed over the years (Bambach 2014; Gardner and Nethercot 2004[1]; Gardner and Nethercot 2004[2]; Law and Gardner 2013). A pioneering study was conducted by Shaat and Fam (2006) on strengthening slender hollow square section (HSS) steel columns against global buckling using longitudinally oriented carbon-FRP laminates and also short HSS columns against local buckling using combined transverse and longitudinal CFRP sheets. Shaat and Fam (2006) performed multiple studies on hollow steel square columns of many different slenderness ratios, ranging from 5 to 93. A layer of GFRP was installed on the steel surface between the carbon fibres and the steel as a measure to prevent galvanic corrosion (West 2001). The short columns had a slenderness ratio of five with varying number of layers, fibre orientation and CFRP types. The maximum gain in capacity for the short columns, 18%, came from two transverse layers of the lower modulus fibre. The long columns had a slenderness ratio of 68 with the number of layers varying and the CFRP applied to opposite sides or on all four sides. The long columns strengthened with three layers on all sides produced the maximum 23% gain in ultimate capacity. It was noticed that the increase in capacity did not correlate with the number of layers added to the long columns. After examining the strain data, the existence of imperfections of various magnitudes were discovered, possibly from out-of-straightness in the specimens or misalignment within the setup. The specimens that had similar imperfections were compared and shown to have higher strengths with CFRP added and enhanced stability against lateral deflections (Shaat and Fam 2006).

Bambach *et al*. (2009)[1] tested short square hollow sections with CFRP applied using the wet layup method. The sections had FRP applied in two different fiber layouts and the steel sections varied in slenderness (*kL/r*) ratio. The axial capacities of the FRP reinforced sections generally increased up to two times the capacity of the plain steel. The increase could have arisen from the CFRP confining the short column, therefore allowing fewer deformations. Bambach *et al*. (2009)[1] noted that there was a plateau in the gain beyond plate slenderness ratios of 2.5.

Bambach and Elchalakani (2007) extended the research to examine the effect of slenderness ratios and the number of layers applied. Increasing the number of layers

proved to provide a larger increase in strength with the largest increase occurring in the slender columns. Since slender columns experience larger elastic deformations before reaching the ultimate load, a greater increase in strength was observed due to the presence of the CFRP. Bambach and Elchalakani also measured energy absorption increases. More layers increased the absorption, with the highest increase occurring in short columns (Bambach and Elchalakani 2007).

An experimental study was carried out by Shaat and Fam (2007) to investigate the effect of adhesively bonded CFRP sheets on the behavior of axially loaded hollow structural section (HSS) slender columns. The study was conducted using five slender 89×89×3.2 mm HSS column specimens, including a control (unstrengthened) specimen and three specimens strengthened with one, three and five layers of CFRP, applied to two opposite side in the plane of overall buckling. The fifth specimen was strengthened with three layers, applied to all four sides. The length of the pin-ended columns was 2380 mm, giving a slenderness ratio (kL/r) of 68. High-modulus unidirectional carbon fiber sheets were bonded to the columns in the longitudinal direction using a wet lay-up procedure. A layer of glass-FRP (GFRP) sheet was first installed directly on the steel surface before applying the CFRP layers to prevent galvanic corrosion. Tyfo S epoxy resin was used to bond the fibers together and to the steel surface. The steel surface was sand blasted and then cleaned using acetone, immediately before applying the FRP sheets. Care was taken to ensure longitudinal alignment of FRP sheets. Specimens were given identification codes. For example, 3L-2S indicates three CFRP layers applied on two opposite sides. Details of materials used for experiment are listed below. It was shown experimentally that CFRP sheets have increased the columns strengths by up to 23%.

The study was then extended to include high modulus CFRP of 313 GPa and showed that effectiveness of the CFRP increases as slenderness ratio (kL/r) of slender columns increase (Shaat and Fam 2009). Shaat and Fam (2009) performed tests on slender sections strengthened with CFRP strips and saw an increase in ultimate load ranging from 6 to 71% and an increase in stiffness ranging from 10 to 17%. The CFRP plates were less effective at low slenderness ratios, changing the failure mode of the plates to debonding prior to buckling rather than crushing afterwards. The focus of the slender column study was on using high modulus CFRP plates with the

reinforcement ratio held constant and the length of the columns varied. The columns with similar out-of-straightness values were grouped together. Shaat and Fam (2009) also mentioned that these values may differ once the epoxy and CFRP are applied and that in real life applications the out-of-straightness would not be an issue due to the fact that two columns that are compared would actually be the exact same column. For the application of the plates, they were cut 25mm shorter on each end to simulate the case where it would not be feasible to access the ends. When applying more than one layer the second layer was also cut 25mm shorter to allow for a gradual termination of CFRP, then two layers of GFRP were wrapped around the ends. The data indicated that the effectiveness of the CFRP is larger at higher slenderness ratios (Shaat and Fam 2009). Shaat and Fam (2009) also developed an analytical model that predicted the axial load capacity of hollow square steel sections.

A numerical finite element investigation to study the behavior of steel hollow structural section (HSS) columns strengthened with CFRP (Carbon Fiber Reinforced Polymer) materials was also conducted by Devi and Amanat (2015)[2]. A three dimensional finite element model of steel HSS column was developed using shell element considering both material and geometric nonlinearities whereas CFRP strengthening was incorporated in the model with additional layers of shell elements. The developed finite element model was then used to simulate experimental studies done by Shaat and Fam (2007). It has been found that good agreement exists between numerical analysis and experimental results, which has established the acceptability and validity of the proposed finite element model to carry out further investigation.

A further numerical investigation was also carried out by Devi and Amanat (2015)[1] where study was focused on some selected non-compact AISC square HSS columns and the effects of number of CFRP layers, slenderness ratio and cross-sectional geometry on the strength gain of those columns had been observed. It was observed that CFRP strengthening is comparatively effective for higher slenderness ratios. For smaller sections strengthening tends to be effective at smaller slenderness ratios as well. For relatively large AISC square HSS columns, with increasing number of CFRP layers (from 1 to 5 layers) the axial strength gain is only approximately by about 1 to 20%. For medium and small square HSS sections, effectiveness of CFRP strengthening increases approximately by about 10 to 90%.

2.7   FAILURE MODES OF FRP ON STEEL STRUCTURES

Four main failure modes have been observed when testing steel beams strengthened with FRP. These modes are the flange buckling in compression, the web buckling in shear, the FRP strips rupturing or the FRP strips debonding, and are shown below in Figure 2.17 (Buyukozturk *et al*. 2004).
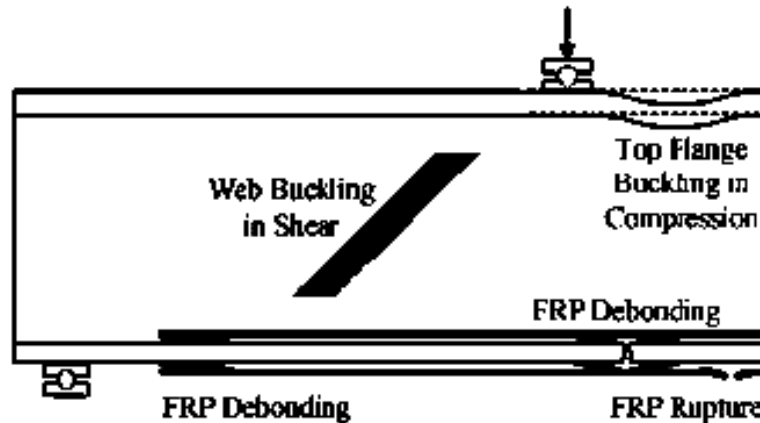
Figure. 2.17: Common Failure Modes (Buyukozturk *et al*. 2004).
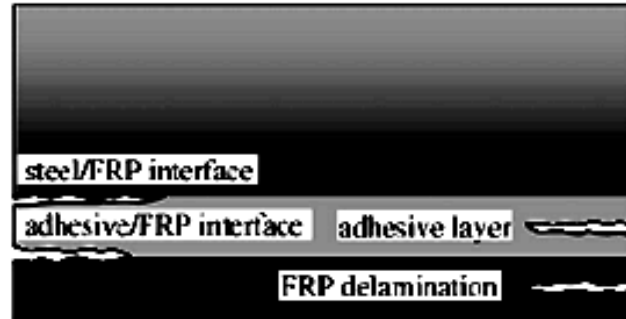
Figure. 2.18: Forms of debonding (Buyukozturk *et al*. 2004).

When a debonding failure happens, it commonly occurs in areas where high stress concentrations occur, which are generally where there are material discontinuities or cracks. Debonding can take place at different boundaries such as the steel and FRP interface, the adhesive and FRP interface, in the adhesive itself or a delamination of the FRP (Buyukozturk *et al*. 2004). These areas of debonding are shown in Figure 2.18.

Narmashiri *et al*. (2012) found that for different thicknesses of CFRP there were various failure modes observed. For a thickness of 1.2 mm there was splitting and

debonding below the load points, as well as delamination and debonding in the tips. For thickness values of 1.4 and 2mm, again debonding happened below the point load with debonding and delamination at the ends. For the largest thickness of 4mm, there was no delamination at the ends (Narmashiri et al. 2012). Peiris noted that the ultra-high modulus laminates used in their study debonded before the steel plate yielded while the normal modulus laminates debonded afterwards (Peiris and Harik 2014).

The failure modes normally observed for unstrengthened S-section columns include lateral torsional buckling, global buckling and local buckling. The purpose of many of the studies discussed in the previous section was to delay the onset of these failure modes. Most of the experiments performed by previous researchers have noticed that less displacement was observed at each load with the addition of FRP. Harries *et al.* (2006) found that for the WT sections, the control sample failures occurred with large lateral translations of the stem tip and twisting about the centroid and nominal strong axis. For slender stems, plastic "kinking" was seen with increases in axial displacement. Adding FRP to these columns helped diminish the post-buckling crippling and resulted in a more ductile failure, controlling the plastic buckling. It was noted that debonding was always observed for these tests after the peak load was reached and was driven based on the degree of curvature in the stem (Harries et al., 2006).

Cold formed lipped steel channel columns commonly fail due to local-plate or distortional buckling with collapse always taking place in a distortional mechanism. When Silvestre et al. attached carbon fibres to these columns, the fibres debonded after reaching the maximum load, similar to the Harries et al. observations. Cracking sounds were heard as the CFRP sheets detached from the steel surface near the yield line zone (Silvestre *et al.* 2008). For square hollow sections, Bambach and Elchalakani (2007) observed no delamination before reaching the ultimate load. Once large deformations occurred, the CFRP typically delaminated from the ends and ruptured at the corners and exterior folds. The CFRP was tending to delaminate across some folds rather than rupturing under large deformations for the slender specimens. As the width over thickness (b/t) ratio increased, the folding mechanisms changed. The folds become more noticeable for higher b/t ratios and Bambach and Elchalakani found that the CFRP would delaminate across the fold rather than maintain the bond and rupture as for lower b/t ratios (Bambach and Elchalakani 2007).

Shaat and Fam (2006) also looked at the failure modes in hollow square sections. For the short specimens strengthened with longitudinal and transverse sheets, delamination occurred in all specimens. Specimens with a higher modulus of CFRP in the transverse direction underwent rupture of the fibres near the corners. It was noted that none of the specimens failed at the CFRP joint overlap. The long specimens failed mostly due to overall buckling with subsequent local buckling in the compression side, near mid-length. This local buckling caused delamination and crushing of the FRP sheets. For the column with CFRP on all four faces, the CFRP fractured due to the local bending from the buckling (Shaat and Fam 2006).

For the tests done using CFRP strips, Shaat and Fam (2009) found that there were two different failure modes, along with overall buckling. For lower slenderness ratios, the CFRP debonded on the inner side and the GFRP transverse wraps located at the ends partially ruptured. At the lowest slenderness (46) value, debonding happened before overall buckling, exhibited as a load drop followed by an increase in load up to the peak value. The middle slenderness (70) specimens underwent debonding on one side, increasing the lateral deflection because of the eccentricity from the now asymmetric column. The load suddenly dropped and then did not increase again. At the highest slenderness ratio (93), the CFRP layers on the inner side crushed at mid height, after buckling, without debonding. This occurred a long time after reaching the peak load. The strains occurring at this time were 58% of the tensile rupture strain. The outer side of the column did not observe any debonding or CFRP rupture (Shaat and Fam 2009).

Ritchie *et al*. (2014) examined the effect of using three different moduli of CFRP to strengthen S-sections of a constant length. The length and number of layers of CFRP applied to each column had been varied between full, two-third and one-third of the column length and one, two and three layers. Ritchie *et al*. (2014) observed failure modes in long columns and found that all unstrengthened and CFRP strengthened column specimens with various levels of out-of-straightness failed due to the classical global buckling of the pin-ended slender column. However, in strengthened column, after the peak load was reached, this was also followed by local failure of CFRP plates, with cracking sounds that were heard, in the specimens with 430 GPa CFRP plates. Some specimens experienced CFRP crushing on the compression side followed by CFRP rupture on the tension side. Specimens with the shortest length of

430 GPa CFRP plate and also specimens with the 212 and 168 GPa CFRP full length plates, all experienced just global buckling with no observed CFRP material failure. Deformed shape of specimen with short CFRP plate was interesting with a distinct change in curvature (kink) appeared in the buckled column, right where the CFRP plate terminates, due to the sudden change in stiffness of the column. In this specimen, acoustic emission was noticed after the peak load but no CFRP material failure was observed.

Based on the research presented, it is clear that there are still gaps of knowledge for steel columns strengthened with FRP. Again such experimental studies provide useful results regarding strengthening, however more research is still required in this field. Though laboratory experiments provide firsthand experience and knowledge, cost of such lab procedures sometimes prohibits conducting extensive testing scheme. A reliable numerical finite element analysis is often regarded as an alternative to costly experimental procedures (Jama *et al.* 2009; Patton and Singh 2012).

This study is focused on developing a three dimensional finite element model to investigate the behavior and axial strength of steel square column of Hollow Structural Section (HSS) strengthened using Carbon Fiber Reinforced Polymer (CFRP) multilayer strips considering both the geometric and material nonlinearities. Verification of this finite element model has been demonstrated with reference to the experiment of Shaat and Fam (2007). The proposed model is then used to examine the effects of number of CFRP layers, CFRP thickness, slenderness ratios, cross sectional geometry of non-compact HSS column sections from AISC Manual, 13th edition (2005) and also to examine the different potential failure modes of CFRP strengthened square HSS columns of different slenderness ratios and CFRP configurations.

2.8   REMARKS

From the review of literature presented in this chapter it is clear that extensive experimental investigations have been performed on strengthening of steel columns using carbon fiber reinforced polymers. The performance of CFRP steel columns is now relatively well understood from the experimental point of view. But there are still gaps of knowledge for steel HSS columns strengthened with CFRP strips. Since laboratory experiments are expensive and time-consuming, reliable numerical or

analytical procedures should be developed for predicting the structural response of steel columns strenghthened with carbon-FRP multilayer strips. To fully simulate their behavior up to failure, numerical models which are capable of predicting the complexities of material nonlinearity, interaction between the steel and FRP surface are required. Therefore, an attempt has been made in current study to address these issues and thereby to develop a full scale 3D finite element model for CFRP strengthened steel HSS columns under axial loading. If it is possible to show that numerical model can adequately simulate the experimental results than it would be really helpful in the era of steel structure strengthening.

Chapter 3

METHODOLOGY FOR FINITE ELEMENT ANALYSIS

3.1 INTRODUCTION

From the very beginning, experimental studies have become popular because of less advancement in the field of numerical analysis. But now-a-days, numerical investigation using finite element method has become more and more popular because of availability of computers on our desk as well as revolutionary advancement in the computer based programs. Again with such computer modeling, huge cost of experimental work, time and effort to accomplish such work can be avoided except with drawback lying in the simplification of assumptions that are almost certainly have to be made in any of such computer model.

Among many computer modeling methods, Finite Element Method (FEM) is the most popular simulation method to predict the physical behavior of systems and structures. Although the method was originally developed to find a solution for problems of structural mechanics it can nowadays be applied to a large number of engineering disciplines in which the physical description results in a mathematical formulation with some typical differential equations which can be solved numerically. Much research work has been done in the field of numerical modeling during the recent years which enables engineers today to perform simulations close to reality. Nonlinear phenomena in structural mechanics such as nonlinear material behavior, large deformations or contact problems have become standard modeling tasks. If experimental or analytical results are available it is easily possible to verify any finite element result.

In this chapter, the actual work regarding the finite element modeling of a slender steel HSS column retrofitted with CFRP strips has been described in detail. The representation of various physical elements with the FEM (Finite Element

Modeling) elements, properties assigned to them, boundary conditions, material behavior and analysis types have also been discussed. The various obstacles faced during modeling, material behavior used and details of finite element meshing have also been discussed in detail.

3.2 A BRIEF HISTORY OF FINITE ELEMENT METHOD (FEM)

The FEM was originated as a method of stress analysis in the design aircrafts. But the engineers, physicists and mathematicians developed the method independently. In 1943, *Courant* made the first effort to use piecewise (finite elements) continuous functions. Later method of analysis based on this concept was developed by *Weinberger, Polya, Agyris* and *Kelsey*. In 1960 *Clough* first introduced the word "Finite Element Method".

During the era of 60's, 70's and 80's, considerable progress was made in the field of FEA. The improvement in speed and memory capacity of computers largely accelerated the advancement of this method. Continuous development induced FEM to handle three dimensional problem, stability and vibration problems, nonlinear analysis etc. quite successfully.

Today the FEM is used not only for the analysis of solid mechanics but even in the analysis of fluid flow, heat transfer, electric and magnetic fields and many others. Civil engineers use this method for analysis of beams, space frames, columns plates, shells, folded plates, foundations, rock mechanics etc. Both static and dynamic problems can be handled by FEA.

3.3 FINITE ELEMENT PACKAGES

The fast improvement of computer hardware technology and slashing of cost of computers have boosted the use of FEM, since computer is the basic need for the application of this method on complex structures. A large number of FEA packages are available at present for analyzing different type of structures. They vary in degree of complexity and versatility. Some of popular packages are shown in Table 3.1.

Table 3.1: Different Finite Element packages.

Abaqus	ANSYS	PROKON	STARDYN
DYNA-3D	ROBOTICS	FEMSKI	ALGOR
MICROFEAP	STRAND 6	MARC	LUSAS
SAP 2000	AMage Catalog	NASTRAN	FELIPE
STAAD-PRO	ETABS	ADINA	SAMTECH
AxisVM	CADRE	GT- STRUDL	SDRC
PATRAN	NISA		

Of all these packages, Abaqus/Standard or Explicit finite element software has been chosen for its versatility, reliability and relative ease of use. Abaqus is capable of modeling and analyzing a vast range of 2D and 3D practical problems. Both linear and nonlinear analysis can be performed by means of this software.

3.4   FINITE ELEMENT MODELING OF STEEL SQUARE HOLLOW STRUCTURAL SECTION (HSS) COLUMNS STRENGTHENED WITH MULTILAYER CFRP STRIPS

Finite element (FE) models of steel HSS columns strengthened with multilayer FRP strips were developed using the commercially available finite element package Abaqus version 6.14-4. An experimental study was carried out by Shaat and Fam (2007) to investigate the effect of adhesively bonded CFRP sheets on the behavior of axially loaded hollow structural section (HSS) slender columns. The models were with the same configurations of the tested columns of Shaat and Fam (2007) which has been described in details in the following chapter. But for understanding the finite element modeling technique, brief cross sectional details of experimental study is shown in Figure 3.1. The model accounts for both material and geometric nonlinearities. The Arc-Length (Riks) (Crisfield 1991) incremental iterative solution method was used to determine the response of the steel HSS columns retrofitted with CFRP multilayer strips.
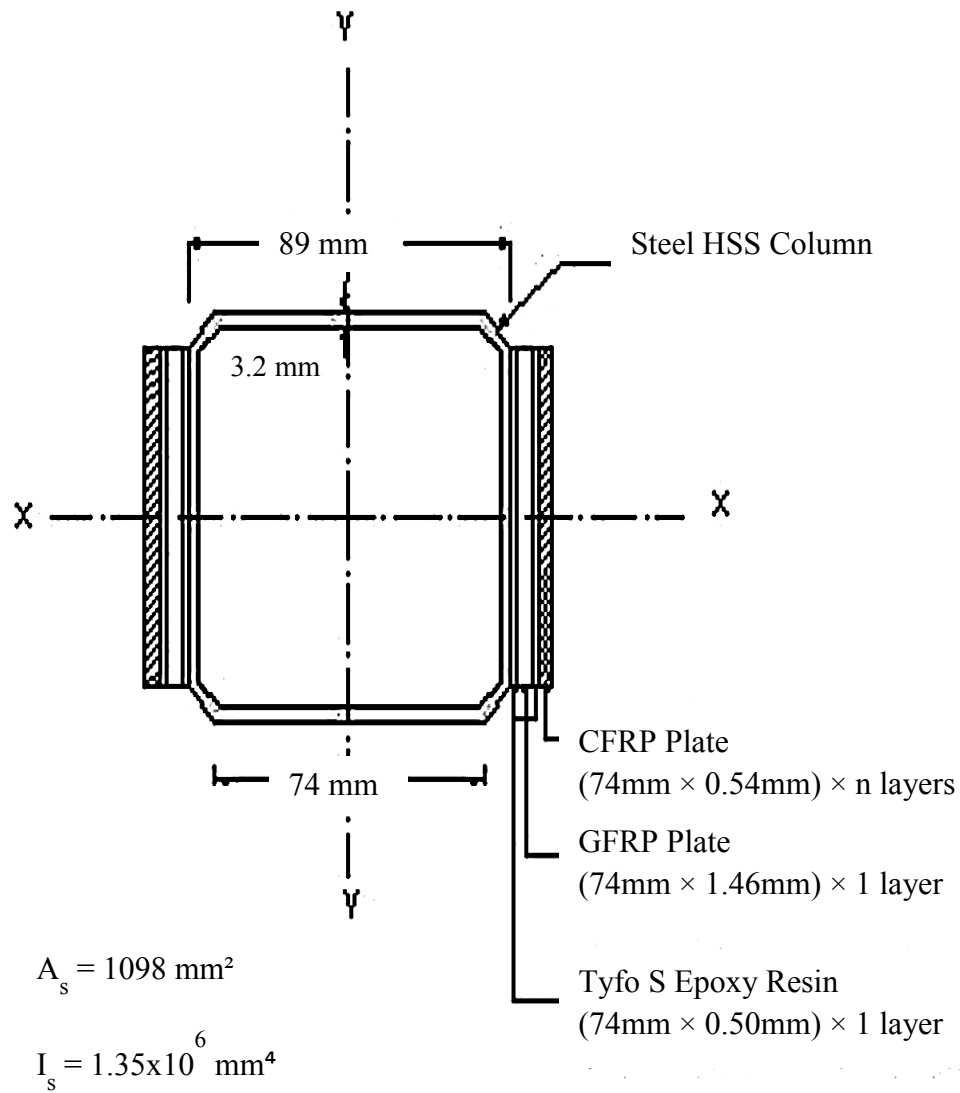
Figure 3.1: Details of Cross-sectional Geometry (Shaat and Fam 2007).

3.4.1 GEOMETRIC PROPERTIES AND FINITE ELEMENT MODEL

Geometry properties of the finite element modeling are incorporated as per the experimental study (Shaat and Fam 2007). To consider the initial curvature of the column specimen, shown in Table 3.2 and Figure 3.3, nodes are carefully defined at each one fourth length division of column. Any of the x coordinate of the curved specimen along the length can be estimated assuming the curve as parabola as ahown in Equation 3.1.

$$x = z\,(1 - x/L) \times Number\ of\ segment/L \times e' \tag{3.1}$$

Force Applied

End Plate

CFRP Sheets along with GFRP and Epoxy Resin

Square Steel HSS Column

(a)

(b)
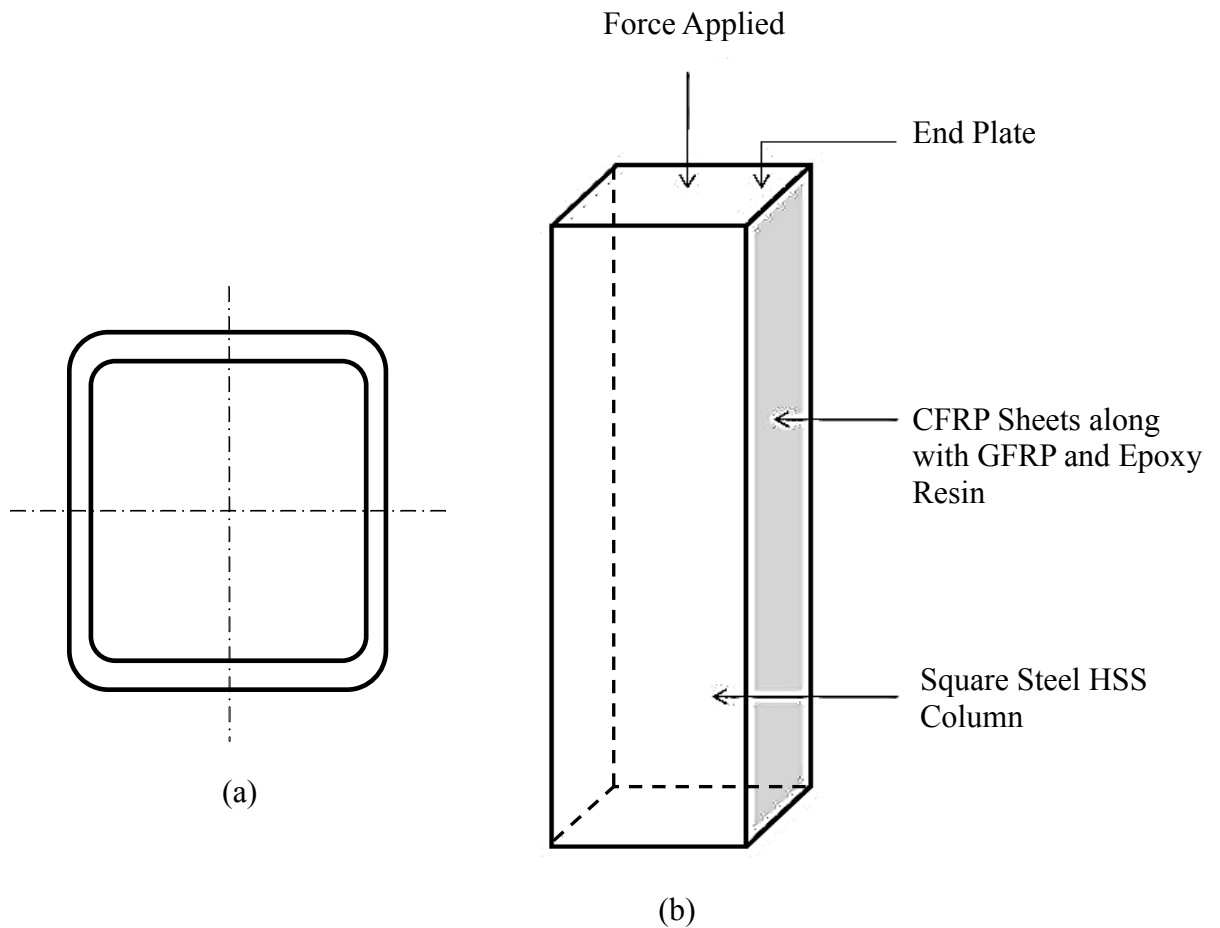
Figure 3.2: (a) Typical Steel Square AISC HSS column cross section (b) Qualitative Sketch of 3D view of HSS column under compression with strengthening materials at the two opposite sides.
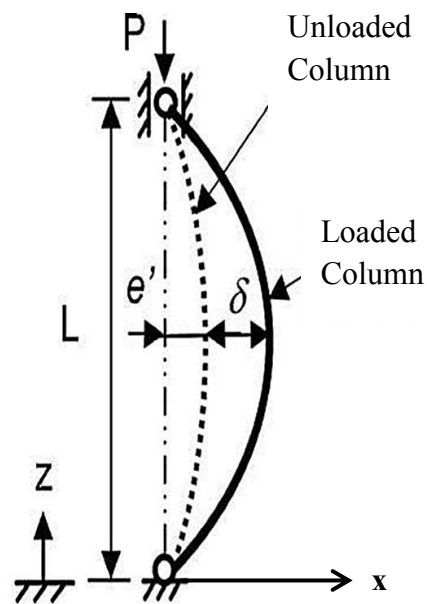
Figure 3.3: Out-of-straightness or initial imperfection (Shaat and Fam 2007).

Table 3.2: Out-of-straightness values for different specimen (Shaat and Fam 2007).

Specimen Identification	Out of Straightness, e' (mm)
89×89×3.2 (Control)	6.60
89×89×3.2 (1L-2S)	0.92
89×89×3.2 (3L-2S)	7.01
89×89×3.2 (5L-2S)	2.04
89×89×3.2 (3L-4S)	5.00

3.4.2   ELEMENT MODELING

Various types of elements are available in the finite element package, Abaqus software. Four materials including steel, CFRP, GFRP strips and epoxy adhesive are modeled as four different part instances. Three different types of elements are used to designate these part instances since CFRP and GFRP strips are considered as similar type of element (continuum shell). The steel HSS column and steel end loading plates are modeled using 4-node, quadrilateral, stress/displacement shell element with reduced integration and a large-strain formulation (S4R) (Abaqus 2013). The CFRP and GFRP strips are meshed with both using a 4-node conventional shell element (S4R) and also using an 8-node quadrilateral in-plane general-purpose continuum shell, reduced integration with hourglass control, finite membrane strains (SC8R) (Abaqus 2013). In defining the damage criteria of FRP materials, SC8R type of element is capable of predicting CFRP failure (Kabir *et al*. 2016; Al-Zubaidy *et al*. 2013; Faggiani and Falzon 2010) the most. In addition, the continuum shell element allow a full three dimensional model and they are more attractive in computation than the standard brick elements because of capturing through the-thickness shear stress without using one element per layer (Falzon and Hitchings 1999; Faggiani and Falzon 2010). Finally, the three dimensional thick shell geometry leads to improve accuracy in resolving contact problems. The adhesive layers i.e. epoxy resin used in this experiment have been modeled in order to capture the actual behavior. Epoxy resin has been modeled using 4-node conventional shell element S4R (Abaqus 2013).

Elements used in this finite element modeling have been listed in the following Table 3.3.

Table 3.3: Possible Elements used for Modeling.

Material Type	Element Type
Steel HSS (Hollow Structural Section) Column	S4R
Steel End Loading Plates	S4R
CFRP (Carbon Fiber Reinforced Polymer) Strips	S4R
	SC8R (For HASHIN Damage Modeling)
GFRP (Glass Fiber Reinforced Polymer) Strips	S4R
	SC8R (For HASHIN Damage Modeling)
Epoxy Resin	S4R

Using the various combinations of above elements the model is generated and the performances of the model are verified. Shell elements are used to model structures in which thickness is significantly smaller than the other dimensions. Conventional shell elements have displacement and rotational degrees of freedom whereas continuum shell elements have only displacement degrees of freedom. From a modeling point of view, continuum shell elements look like three-dimensional continuum solids, but their kinematic and constitutive behavior is similar to the conventional shell elements (Abaqus 2013).

The "top" surface of a conventional shell element is the surface in the positive normal direction and is referred to as the positive (SPOS) face for contact definition. The "bottom" surface is in the negative direction along the normal and is referred to as the negative (SNEG) face for contact definition. Positive and negative are also used to designate top and bottom surfaces when specifying offsets of the reference surface from the shell's mid surface. The positive normal direction defines the convention for pressure load application and output of quantities that vary through the thickness of the shell. A positive pressure load applied to a shell element produces a load that acts

in the direction of the positive normal. For shells in space the positive normal is given by the right-hand rule going around the nodes of the element in the order that they are specified in the element definition.

Displacement and rotation degrees of freedom

Conventional shell model- geometry is specified at the reference surface; thickness is defined by section geometry

Finite Element Model   **Element**

Structural body being modeled

Displacement degrees of freedom only

Continuum shell model-full 3-D geometry is specified; element thickness is defined by nodal geometry

Figure 3.4: Conventional and Continuum shell element (Abaqus 2013).

face SPOS

face SNEG
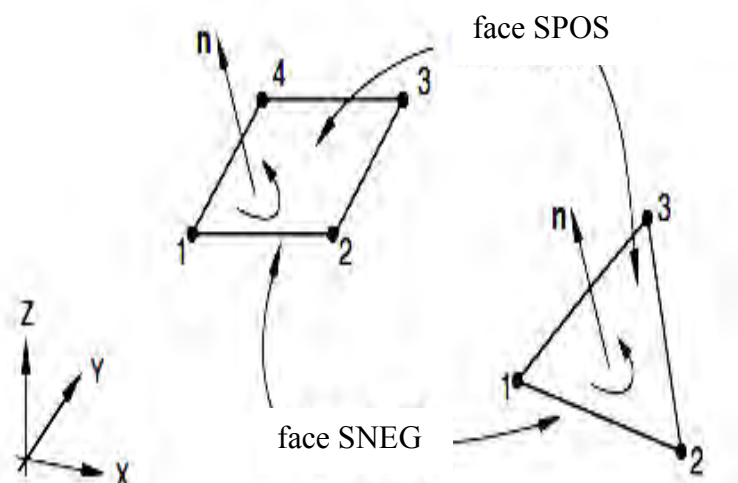
Figure 3.5: Positive Normals for three-dimensional Conventional Shell (Abaqus 2013).
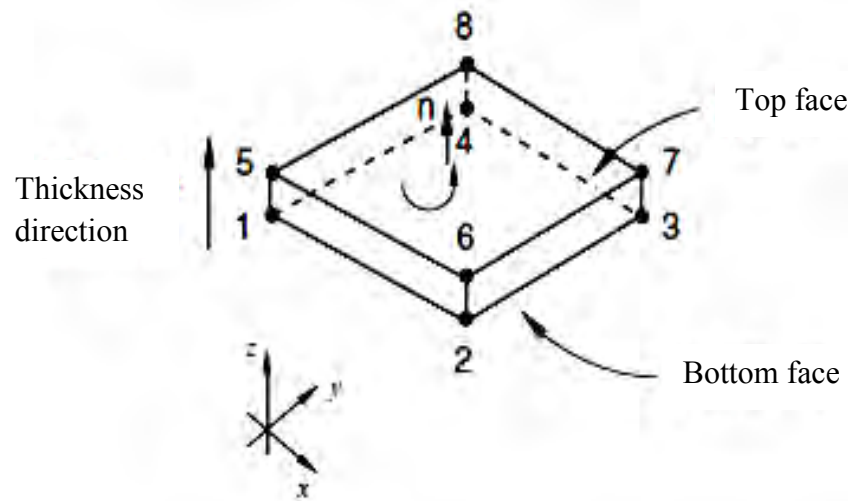
Figure 3.6: Default Normals and thickness direction for Continuum Shell elements (Abaqus 2013).

It is important that the continuum shells are oriented properly, since the behavior in the thickness direction is different from that in the in-plane directions. By default, the element top and bottom faces and, hence, the element normal, stacking direction, and thickness direction are defined by the nodal connectivity. For the quadrilateral continuum shell element (SC8R) the face with corner nodes 1, 2, 3, and 4 is the bottom face; and the face with corner nodes 5, 6, 7, and 8 is the top face (Figure 3.6). The stacking direction and thickness direction are both defined to be the direction from the bottom face to the top face. Additional options for defining the element thickness direction, including one option that is independent of nodal connectivity, are presented below. Surfaces on continuum shells can be defined by specifying the face identifiers S1–S6 identifying the individual faces. Free surface generation can also be used (Abaqus 2013).

3.4.3   MATERIAL PROPERTIES AND FINITE ELEMENT MODEL

3.4.3.1   Steel HSS Tube

The steel tube is modeled as a classical elastic–plastic metal with isotropic hardening. The experimental stress–strain curve of the steel was adopted in FE model to represent the material behavior. Also, multilinear isotropic hardening has been considered to consider the experimental stress-strain curve. In such nonlinear

properties of steel, the uniaxial behavior is described by a piece-wise linear total stress-total strain curve, starting at the origin, with positive stress and strain values. The slope of the first segment of the curve must correspond to the elastic modulus of the material and no segment slope should be larger. No segment can have a slope less than zero. The steel HSS columns are modeled considering such type of nonlinearities which can be better understood from Figure 3.7.

σ

1.3F$_y$

1.2F$_y$

F$_y$

E$_s$

Where,

F_y = Yield stress

ε_y = strain corresponding to yield stress

E_s = Modulus of elasticity up to yield point

ε$_s$ 0.07   1.0   ε
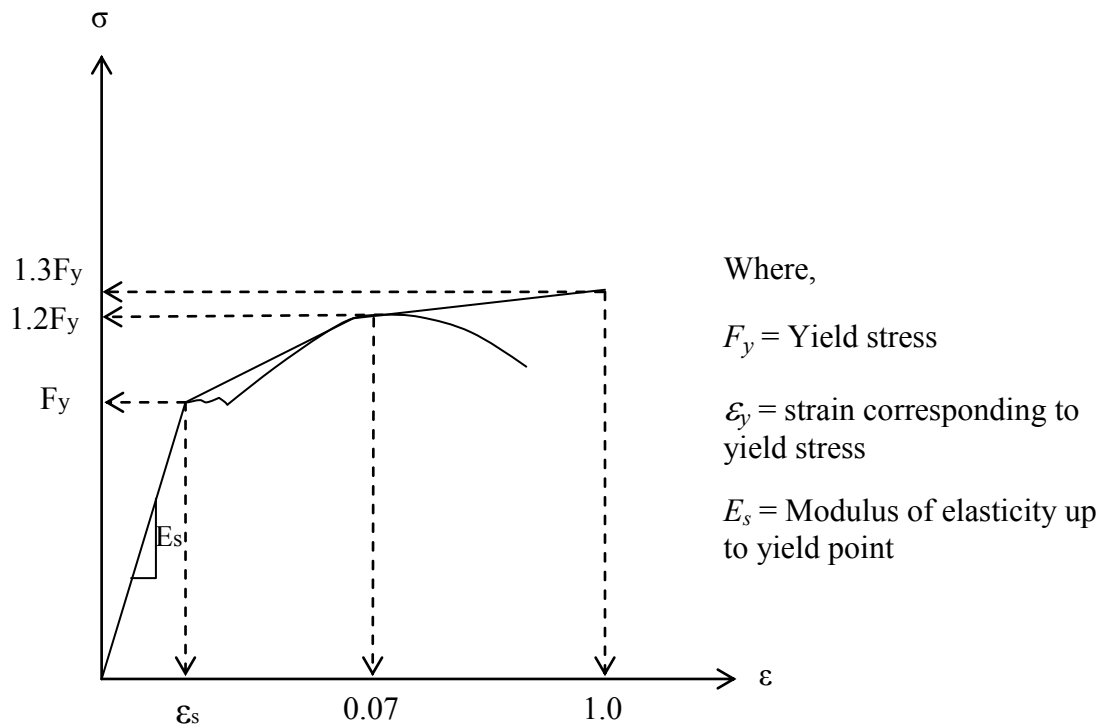
Figure 3.7: Stress Strain Behavior of Steel HSS column in Multilinear Isotropic
Hardening.

3.4.3.2   Steel End Loading Plate

In order to define the linearity of different materials, input of modulus of elasticity and the major Poisson's ratio are quite enough for a certain material type. In the proposed model only the end plates used for loading are modeled considering elastic up to failure. The thickness of the loading plate has not been defined specifically in the experimental study (Shaat and Fam 2007).

Table 3.4: Plate Thickness Variation for Control Specimen 89×89×3.2 mm (Shaat and
Fam 2007).

Plate Thickness (mm)	Maximum Load from Present Analysis (kN)
30	294.418
30.5	295.296
31	296.17
33	299.624
35	302.939
40	309.836
44.5	315

To capture the maximum load of experimental study analysis has been done with
varying loading plate thickness. Analysis has been done for control specimen of
89×89×3.2 mm (Shaat and Fam 2007) and maximum axial load of around 295 kN
(Shaat and Fam 2007) has been used as a target value. From Table 3.4 it has been
seen that for end plate thickness of 30.5 mm the maximum load obtained by finite
element analysis shows close agreement with the experimental maximum load for
control specimen 89×89×3.2 mm. So for further modeling purposes, analysis has been
conducted only by taking the loading plate thickness as a constant value of 30.5 mm.
But in parametric study since various larger sections have been chosen, the plate
thickness have been generalized to the half of the square cross section dimension.

3.4.3.3   Fiber Reinforced Polymer (CFRP and GFRP) Multilayer Strips Model

The Carbon Fiber Reinforced Polymer (CFRP) and Glass Fiber Reinforced Polymer
(GFRP) strips are modeled adopting various strategies. As the fibers of FRP are the
main load carrying constituents, so the type of fibers, the orientation of fibers and the
quantity of fibers govern the tensile behavior mostly. When this FRP is loaded under
direct tension it does not exhibit any plastic behavior (yielding) before rupture. Most
of the time, CFRP and GFRP materials show a linearly elastic stress-strain
relationship until failure. To capture this behavior various finite element
methodologies for material modeling have been adopted available in Abaqus 6.14-4.

3.4.3.3.1   Elasto-plastic material modeling of fibre reinforced materials

In the first approach, CFRP strips as well as GFRP layer have been modeled using as an isotropic homogeneous material using an elasto-plastic stress-strain curve. To define such material property, modulus of elasticity, yield strength and poisson's ratio of individual fiber materials are needed and are taken as per the reference experimental study of Shaat and Fam (2007).

3.4.3.3.2   Hashin Damage modeling of fibre reinforced materials

For more detailed modeling of FRP rupture extensive damage modeling has been adopted for CFRP and GFRP strips modeling. In such composite materials as steel HSS column retrofitted with FRP multilayer strips, the failure generally occurs either in the retrofitting materials or the bonding materials, or both. The Abaqus software is able to capture the damage and failure of the fibre reinforced polymer composites by using the available materials model in it known as "Hashin Damage Model" (Hashin 1980; Hashin and Rotem 1973). By implementing this material model in Abaqus 6.14-4, the damage initiation and propagation of an elastic–brittle material with an isotropic behavior such as unidirectional normal modulus carbon fibre reinforced polymer (CFPR) fabrics can be achieved (Kabir *et al*. 2016; Al-Zubaidy *et al*. 2013).
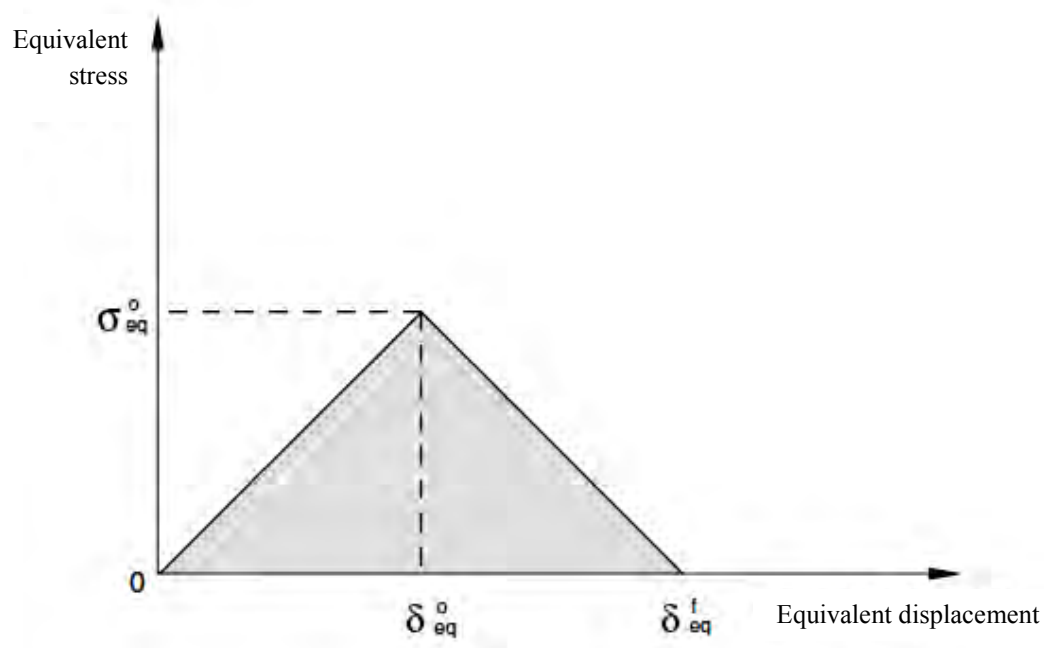
Figure 3.8: Equivalent Stress vs. Equivalent Displacement in Hashin Damage
            Modeling (Hashin 1980; Hashin and Rotem 1973).

The material model for CFRP fabrics depends on continuum damage mechanism and in-built Hashin damage criteria in Abaqus (Kabir *et al*. 2016; Abaqus 2013). In Hashin damage model, the plasticity of the CFRP is always neglected and damage is detected and characterized based on material stiffness reduction. The damage of the CFRP layer initiates due to four main failure criteria, namely: fibre rupture in tension, fibre bucking in compression, matrix cracking under transverse tension and shearing, and matrix crushing under transverse compression (Naghipour *et al*. 2009). Damage propagates when the fracture energy (damage variable) in any of the four mentioned criteria reaches its maximum value ($G_c$max) which can be specified as an input parameter as longitudinal tensile and compressive fracture energy, transverse tensile and compressive fracture energy in Abaqus (2013).

Once damage initiates, three non-negative in-ply parameters, d_f, d_m and d_s reduce the ply stiffness numerically in fibre, transverse and shear direction respectively, until the final failure point is reached (Kabir *et al*. 2016; Naghipour *et al*. 2009). Hence, to provide a more accurate validation of the numerical model with experimental results, the CFRP composite damage is considered in the current study. The parameters used in Abaqus to facilitate Hashin damage criteria are longitudinal tensile and compressive strength which represent ultimate tensile and compressive strength (X^T and X^C) of CFRP in fibre direction, transverse tensile and compressive strength which represent ultimate tensile and compressive strength (Y^T and Y^C) of CFRP in transverse direction (Abaqus 2013; Hashin 1980; Hashin and Rotem 1973). The compressive strength of CFRP patch has been considered a percentage (%) of the average tensile strength. To determine the undetermined damage properties of adhesive and CFRP at structural level, the numerical models were run several times until the best validation were achieved. Then the parameters related to Hashin Damage model are assumed based on the relevant experimental study done by other researchers which are shown in the following Table 3.5 to Table 3.7.

Table 3.5: Elastic Lamina Properties of Fiber Reinforced Polymers.

Fibre Types	E_1 (MPa)	E_2 (MPa) (Assumed)	G_{12} (MPa) (Assumed)	G_{13} (MPa) (Assumed)	G_{23} (MPa) (Assumed)	Nu_{12}
CFRP	230000	$0.5\times E_1$	$0.5\times E_1$	$0.5\times E_1$	$0.5\times G_{12}$	0.3
GFRP	14000	$0.5\times E_1$	$0.5\times E_1$	$0.5\times E_1$	$0.5\times G_{12}$	0.3

Table 3.6: Damage Initiation Properties of Fiber Reinforced Polymers.

Fibre Types	X^T (MPa)	X^C (MPa)	Y^T (MPa)	Y^C (MPa)	S^L (MPa)	S^T (MPa)
CFRP						
Alternate-1	510	$0.1\times X^T$	$0.1\times X^T$	$0.1\times X^T$	$0.6\times X^T$	$0.1\times S^L$
Alternate-2	510	$0.2\times X^T$	$0.2\times X^T$	$0.2\times X^T$	$0.6\times X^T$	$0.2\times S^L$
GFRP						
Alternate-1	269	$0.1\times X^T$	$0.1\times X^T$	$0.1\times X^T$	$0.6\times X^T$	$0.1\times S^L$
Alternate-2	269	$0.2\times X^T$	$0.2\times X^T$	$0.2\times X^T$	$0.6\times X^T$	$0.2\times S^L$

For the interlaminar damage model, the fracture energies associated with the various damage mechanism and all other properties used in FE are also approximated for numerical computations (Lapczyk and Hurtado 2007; Shi *et al*. 2012; Faggiani and Falzon 2010; Naghipour *et al*. 2009; Fawzia 2007).

Table 3.7: In-Plane Fracture Energies for Fiber Reinforced Polymers.

Fibre Types	G_{ft}^C (N/mm) (Assumed)	G_{fc}^C (N/mm) (Assumed)	G_{mt}^C (N/mm) (Assumed)	G_{mc}^C (N/mm) (Assumed)
CFRP				
Alternate-1	$(0.5\times F_y \times E_1)$	$(0.5\times X^C \times 0.1\times E_1)$	$(0.10\times G_{ft}^C)$	$(0.10\times G_{fc}^C)$
Alternate-2	$(0.05\times F_y)$	$(0.80\times G_{ft}^C)$	$(0.20\times G_{ft}^C)$	$(0.80\times G_{fc}^C)$
GFRP				
Alternate-1	$(0.5\times F_y \times E_1)$	$(0.5\times X^C \times 0.1\times E_1)$	$(0.10\times G_{ft}^C)$	$(0.10\times G_{fc}^C)$
Alternate-2	$(0.05\times F_y)$	$(0.80\times G_{ft}^C)$	$(0.20\times G_{ft}^C)$	$(0.80\times G_{fc}^C)$

3.4.4   MODELING OF STEEL-FRP AND FRP-FRP INTERFACE

One of the challenging aspects of this study is to model the connections in between the steel-FRP and FRP-FRP interface. To capture the accurate behavior of modeling perfect bonding approach has been incorporated in the modeling. The connections between steel surface and adhesive surface and between adhesive surface and CFRP composite surface are provided with perfect bonding by using tie constraints. Steel tube and CFRP composite are considered as master surface and adhesive is considered as slave surface for tying purpose.

3.4.5   MESH OPTIMIZATION

Fine meshing will lead to better results at the expense of greater solution time. Coarse meshing will result in lesser solution times but result accuracy may be compromised. The balance is therefore to apply the mesh density for which the solution accuracy is not lost but the computation time is not also that great. An optimal solution is to use a fine mesh in areas of high stress gradient and a coarser mesh in the remaining areas. Different numbers of mesh divisions are considered for analysis in x and y direction respectively such as 4×4, 8×8, 10×10 and 12×12. But with 4×4 number of divisions reasonably close result can be possible to obtain. Increasing the number of mesh divisions does not significantly increase the accuracy of the result. Therefore, for minimizing the computational time of the analysis, number of mesh divisions of 4×4 along x and y directions has been considered.

3.4.6   BOUNDARY CONDITIONS
3.4.6.1   Restraints

Restraints are provided in the model considering the usual test setup of steel column's compression test. One end of the column is kept restrained for translation in all the x, y and z direction at the midpoint while the other end of the column is kept restrained for x and y direction translation only to allow deflection or load along z direction as well as along the length of column. To prevent twisting of column along xy plane a corner point of column is additionally restrained in x and y direction translation. Again to apply bracing against out-of-plane restraints against x and y direction

translation are also provided at the mid length of column to allow buckling about the vertical axis y-y only.

3.4.6.2   Loading

For obtaining the load deflection diagram, we can perform nonlinear analysis either by applying load or deflection. If we want to continue the nonlinear analysis using Arc-Length method both displacement and load application is suitable. But for modeling, displacement controlled loading was applied on the top. Displacement was applied in the negative z direction at the midpoint of the upper end.

3.4.7   SOLUTION STRATEGY

The solution strategy is based on the Arc-Length (Riks) method (Crisfield 1991). In simple cases linear eigen value analysis may be sufficient for design evaluation; but if there is concern about material nonlinearity, geometric nonlinearity prior to buckling, or unstable postbuckling response, a load-deflection (Riks) analysis must be performed to investigate the problem further. The Riks method (Crisfield 1991):

 ➢ Generally is used to predict unstable, geometrically nonlinear collapse of a structure.

 ➢ Can include nonlinear materials and boundary conditions.

 ➢ Often follows an eigen value buckling analysis to provide complete information about a structure's collapse and

 ➢ Can be used to speed convergence of ill-conditioned or snap-through problems that do not exhibit instability.

The arc-length method uses the explicit spherical iterations to maintain the orthogonality between the arc-length radius and orthogonal directions. It is assumed that all load magnitudes are controlled by a single scalar parameter (i.e., the total load factor). As the displacement vectors and the scalar load factor are treated as unknowns, the arc-length method itself is an automatic load step method. For problems with sharp turns in the load-displacement curve or path dependent materials, it is necessary to limit the arc-length radius using the initial arc-length radius. During the solution, the arc-length method will vary the arc-length radius at each arc-length

substep according to the degree of nonlinearities that is involved. To handle zero and negative tangent stiffness, the arc-length multiplies the incremental load by a load factor, λ, where λ is between -1 and +1. Figure 3.9 illustrates this process.
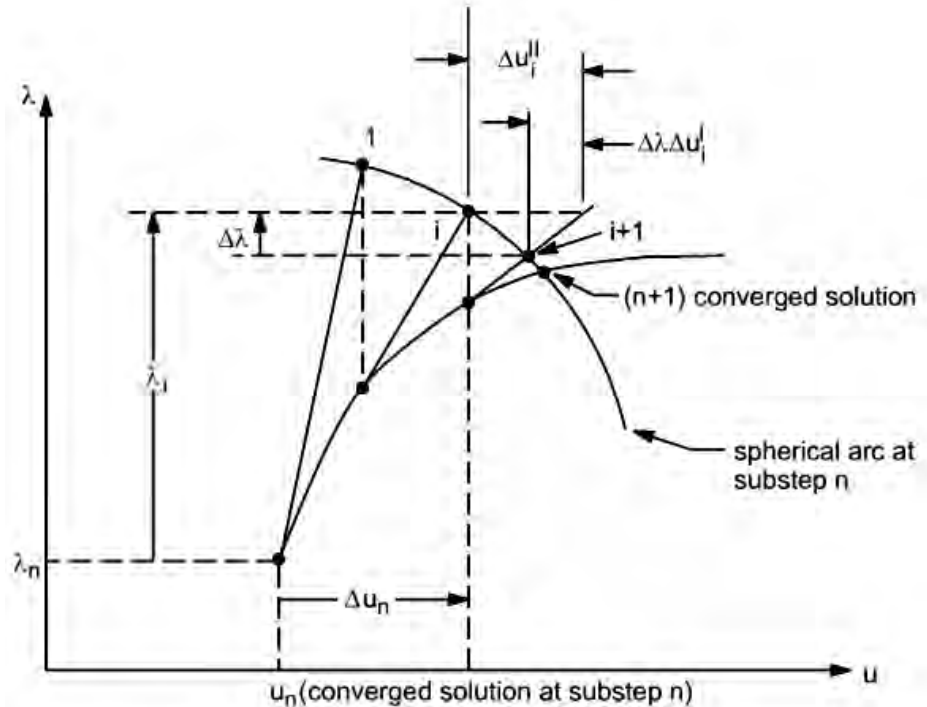
Figure 3.9: Arc Length Method for Nonlinear Solution (Crisfield 1991).

The Riks method (Crisfield 1991) uses the load magnitude as an additional unknown; it solves simultaneously for loads and displacements. Therefore, another quantity must be used to measure the progress of the solution; Abaqus/Standard uses the "arc length", along the static equilibrium path in load-displacement space. This approach provides solutions regardless of whether the response is stable or unstable shown in Figure 3.9 and Figure 3.10.
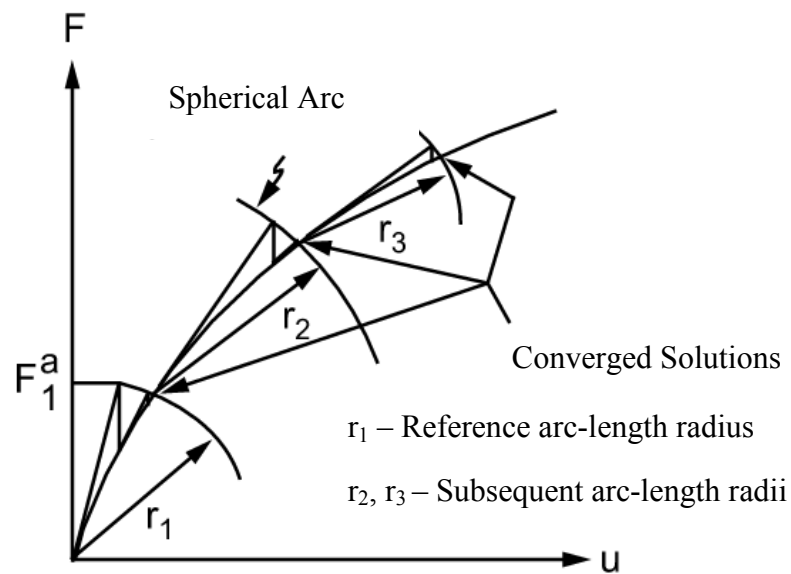
Figure 3.10: Arc Length Convergence Behavior (Crisfield 1991).

3.4.8   FINITE ELEMENT MODELING FIGURES
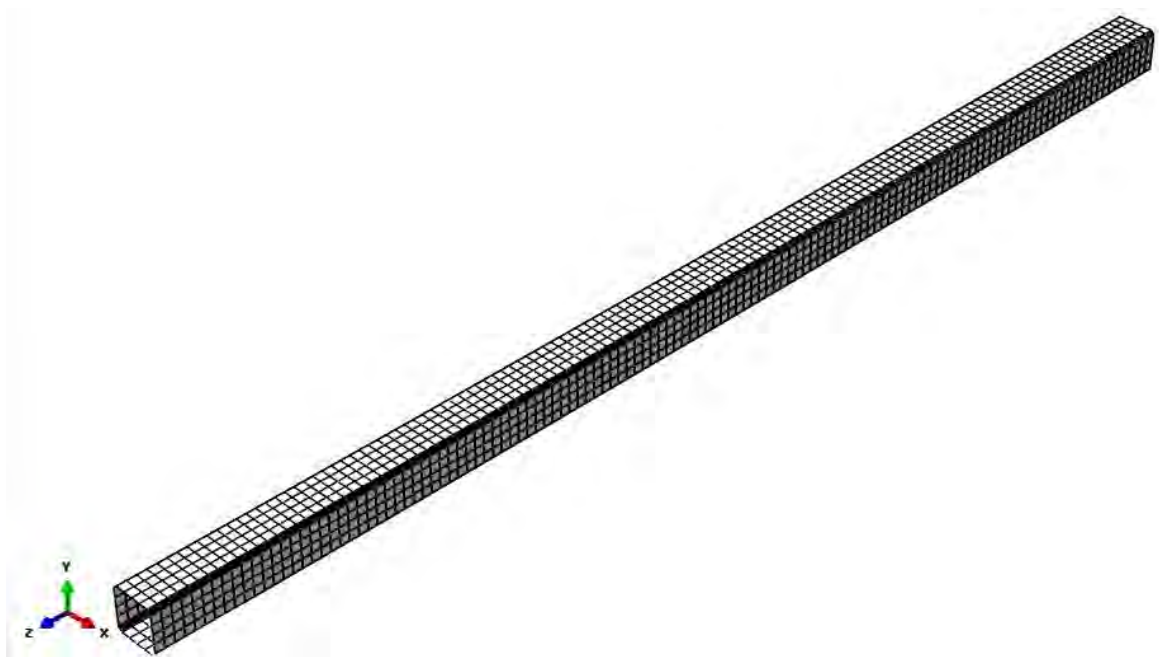
Figure 3.11: Isometric view of the Finite element mesh of HSS Column.
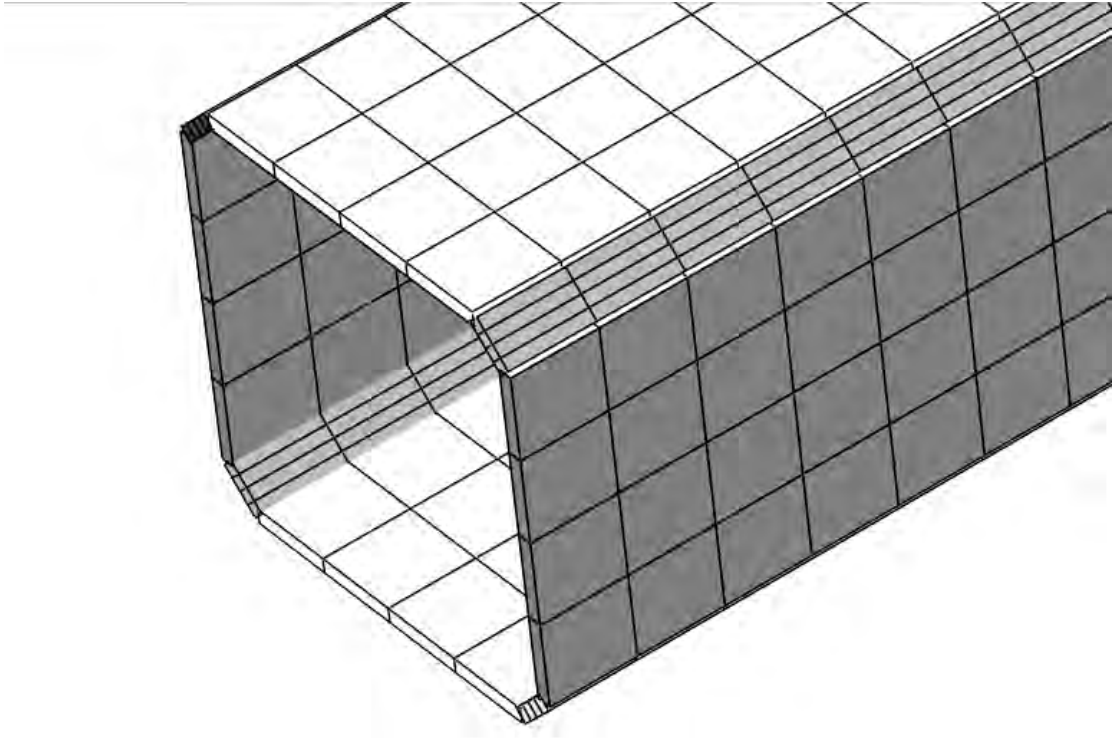
Figure 3.12: Close View of Finite element mesh of HSS Column with Actual size.

                    (a)   (b)
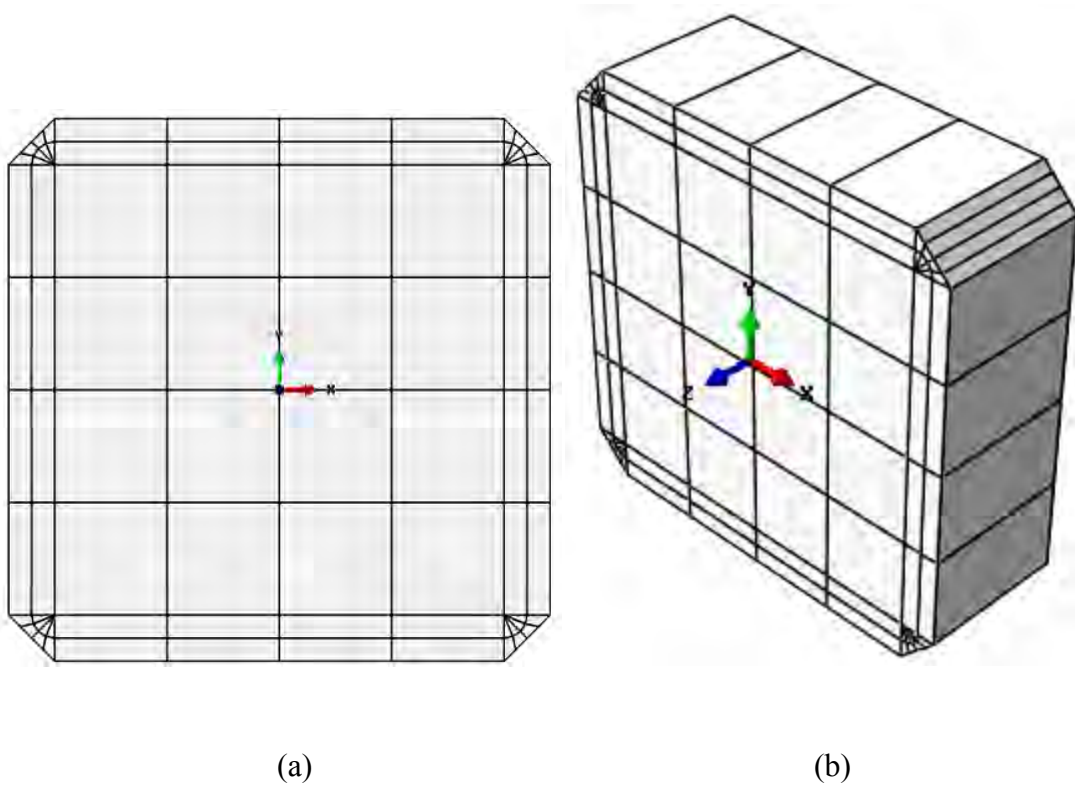
Figure 3.13: Meshing of End Plates (a) Front view (b) Isometric view with actual size.
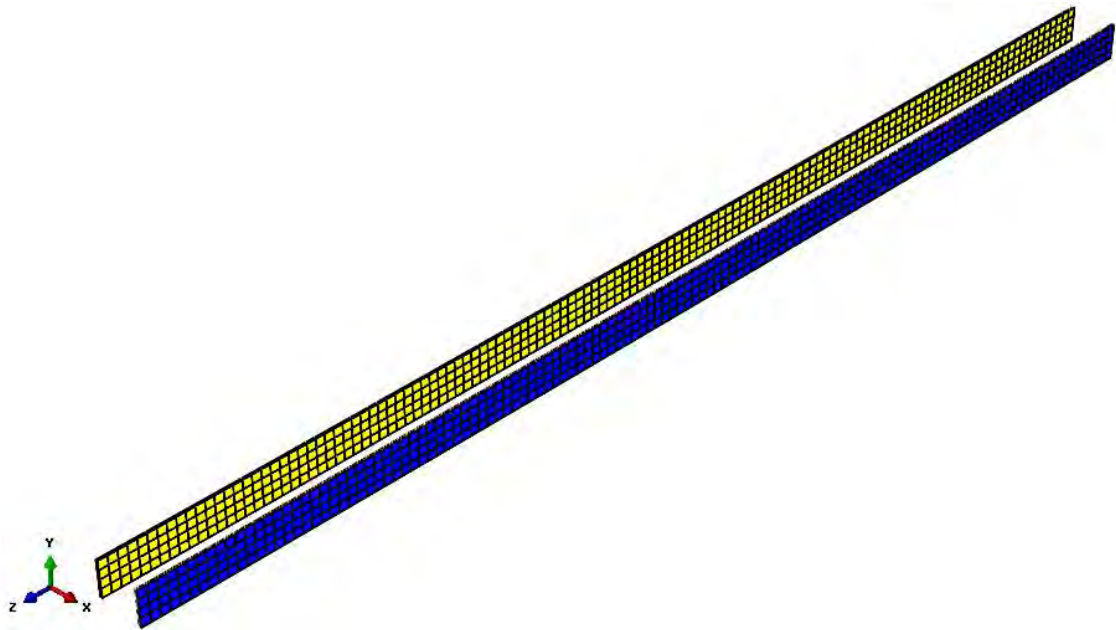
Figure 3.14: Finite Element Mesh of 2-sided CFRP materials along with Tyfo S
            Epoxy Resin and GFRP.
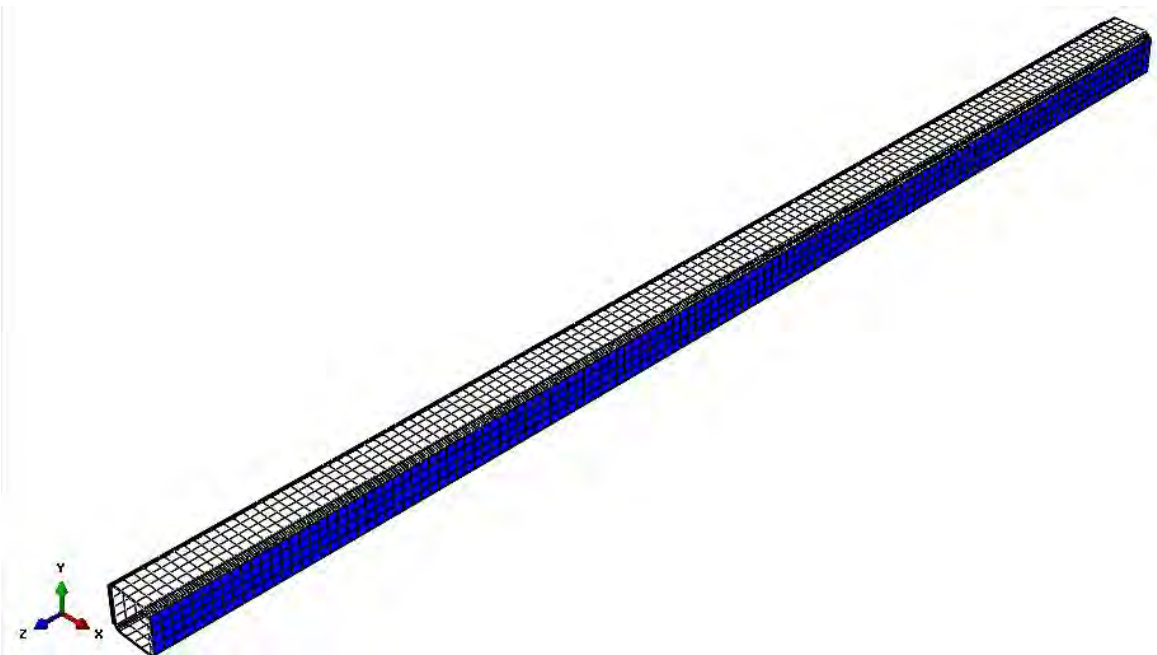
Figure 3.15: Finite Element Mesh of 2-sided CFRP materials along with Tyfo S
            Epoxy Resin and GFRP bounded around the Steel HSS column.

For better view of CFRP materials meshing different layers are shown in the
following Figure 3.16.
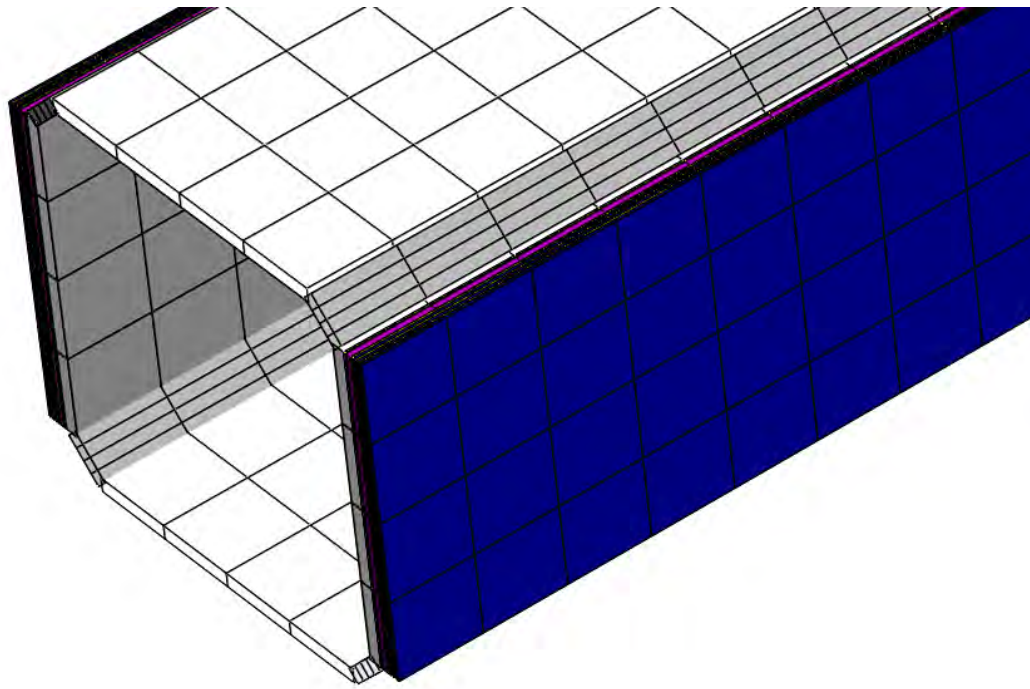
Figure 3.16: Close Isometric view of orientation of different layers with original scale.
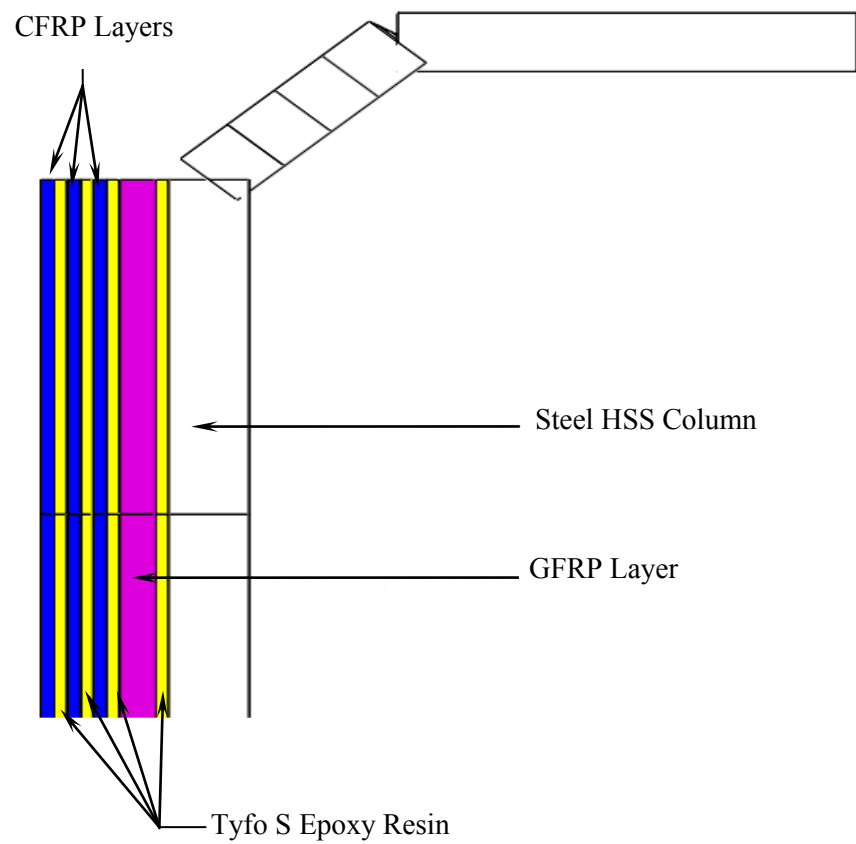
Figure 3.17: Close up view of orientation of different layers with original scale.

Similarly FRP materials can be meshed on four sides of the column specimen like following.
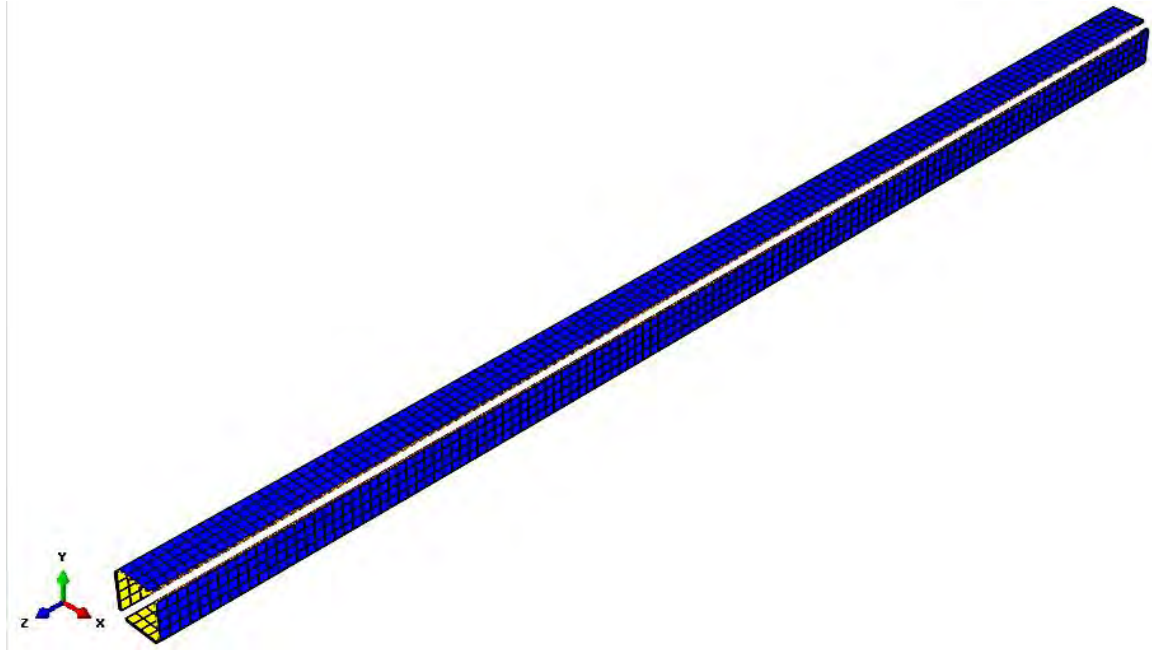
Figure 3.18: Finite Element Mesh of 4-sided CFRP materials along with Tyfo S
Epoxy Resin and GFRP.
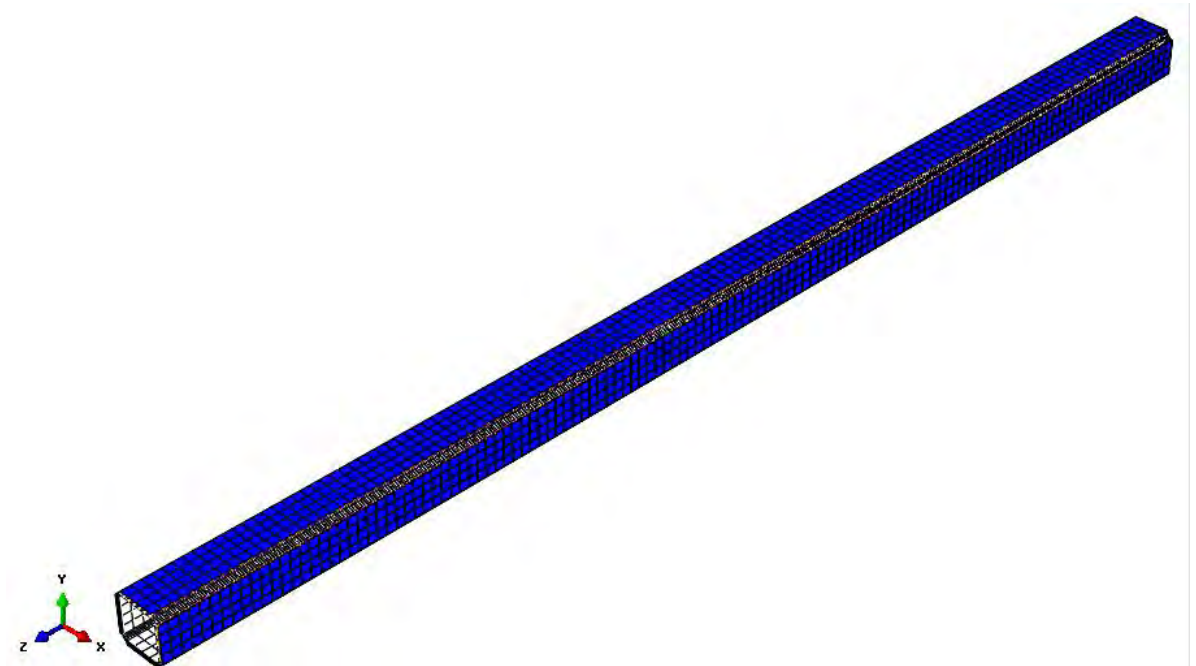
Figure 3.19: Finite Element Mesh of 4-sided CFRP materials along with Tyfo S
Epoxy Resin and GFRP bounded around the Steel HSS column.

For better view of 4-sided CFRP materials meshing different layers are shown in the following Figure 3.20.
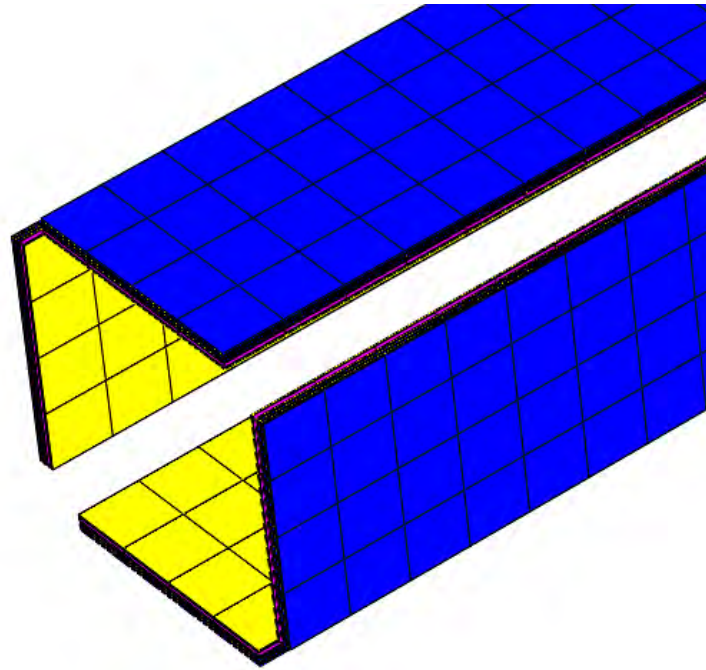
Figure 3.20: Close Isometric view of the Finite Element mesh of four sided CFRP
materials.
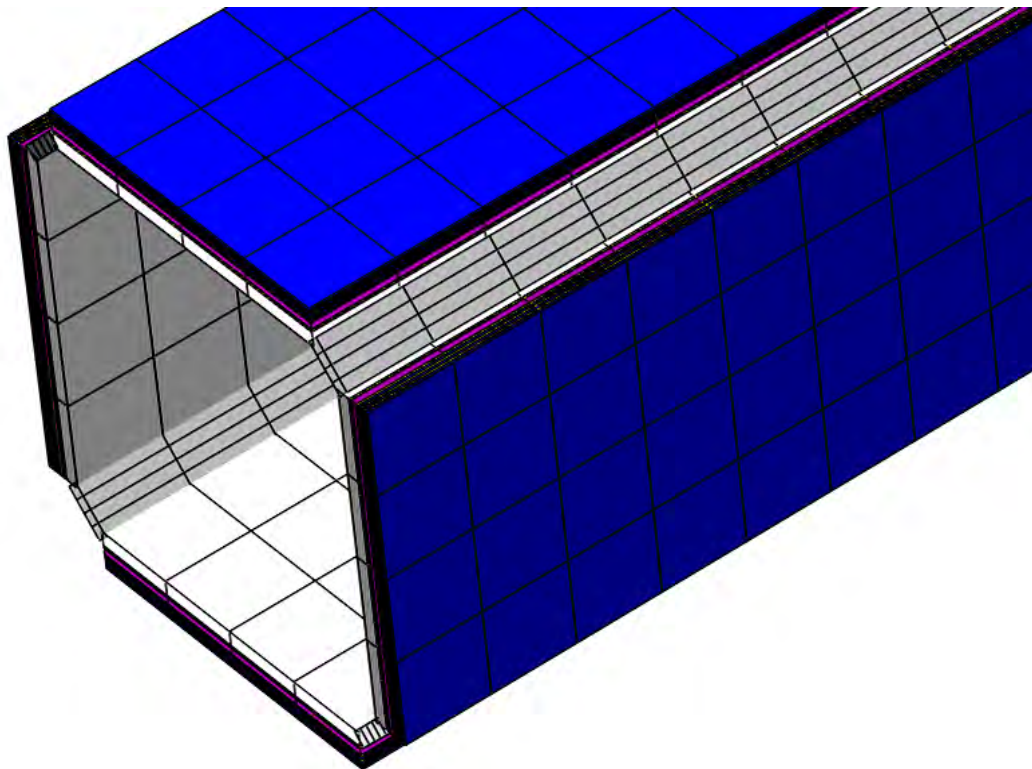
Figure 3.21: Close Isometric view of orientation of different 4-sided layers along with
steel HSS column with original scale.
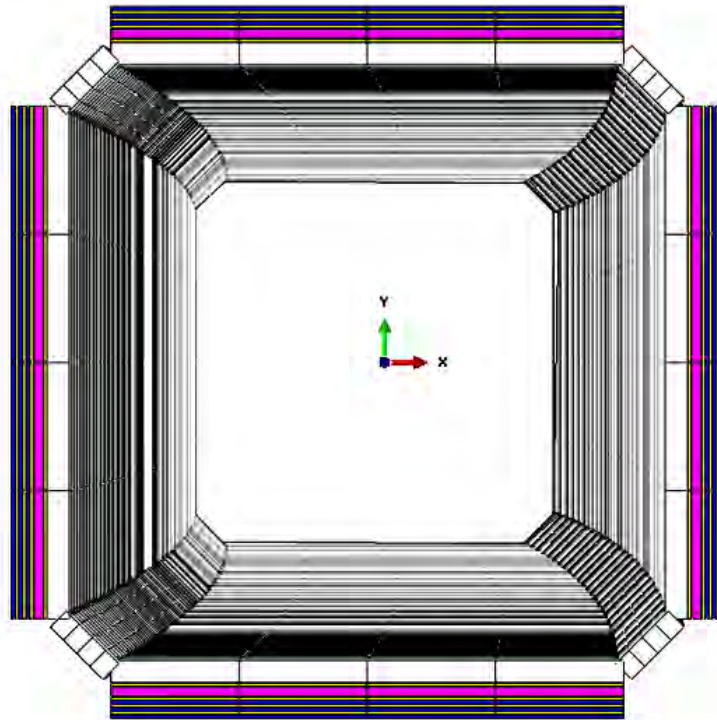
Figure 3.22: Close up view of orientation of different 4-sided layers along with steel HSS column with original scale.

Restraints against twisting at end

Boundary conditions restraining translations against x & y directions and displacement applied along the negative z direction
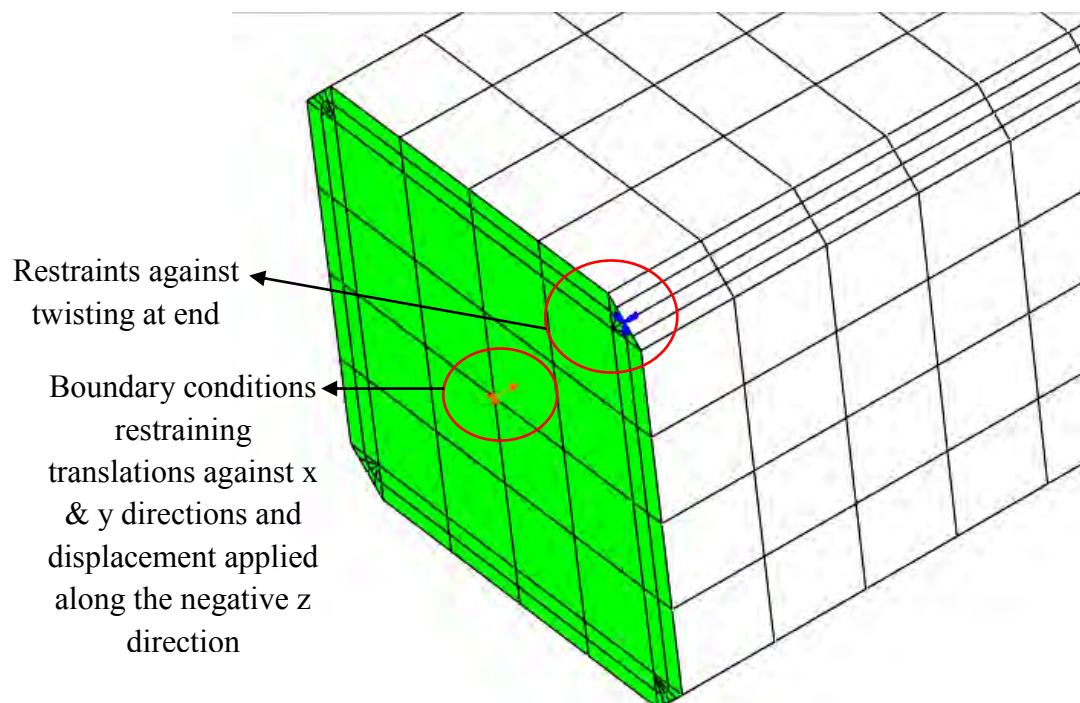
Figure 3.23: Close Isometric view of the Boundary Conditions at one end.

Boundary conditions restraining translations against x & y directions and displacement applied along the negative z direction

Boundary conditions at one corner node restraining translations against x & y directions to prevent twisting along xy plane

Boundary conditions restraining translations against y direction

Boundary conditions restraining translations against x, y, z directions

Figure 3.24: Boundary Conditions of the Proposed Model.

3.5   VERIFICATION OF HASHIN DAMAGE MODEL WITH A SIMPLE CANTILEVER PLATE

A finite element model of a simple cantilever steel plate with CFRP bonded on the upper and lower side of the steel plate has been modeled using ABAQUS 6.14-4. CFRP strips have been modeled using Hashin Damage Model (Hashin 1980; Hahin and Rotem 1973). It has been modeled to examine the damage properties of CFRP materials since it is linearly elastic in nature with brittle failure mechanism.

3.5.1   MATHEMATICAL CALCULATION FOR SIMPLE STEEL CANTILEVER PLATE WITH CFRP STRIPS
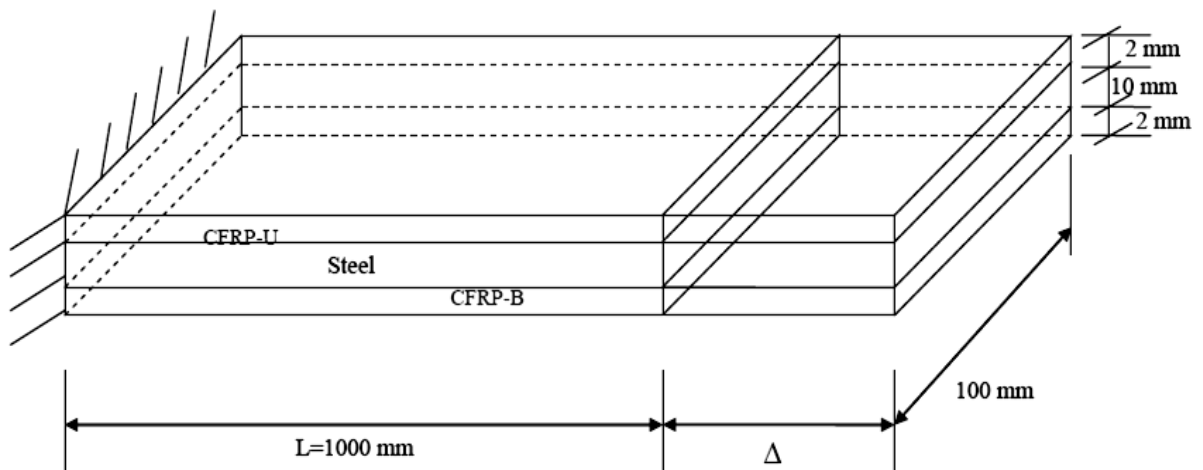
Material Properties:

1. **Steel:**

Stress (MPa)	Plastic Strain	Total Strain
400	0	0.002
410	0.0056	0.0076
420	0.0112	0.0132
430	0.0168	0.0188
440	0.0224	0.0244
450	0.028	0.03
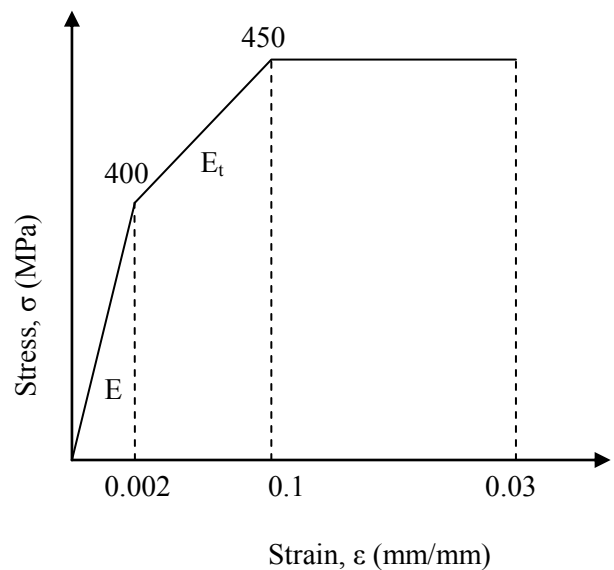
Elastic Modulus, E = 200000 MPa

Poisson's Ratio, v = 0.3

Tangent Modulus, E_t = (450-400)/(0.03-0.002) = 1785.7 MPa

Yield stress = 400 MPa

2. **CFRP:**

Elastic Modulus = 200000 MPa

Poisson's Ratio = 0.3

Tensile Strength = 2000 Mpa

Elastic, Type: Lamina

E_1 = 200000 MPa

E_2 = 100000 Mpa (Assumed)

Nu_{12} = 0.3

G_{12} = 100000 MPa (Assumed)   [Shear Modulus of Elasticity]

G_{13} = 100000 MPa (Assumed)

G_{23} = 50000 MPa (Assumed)
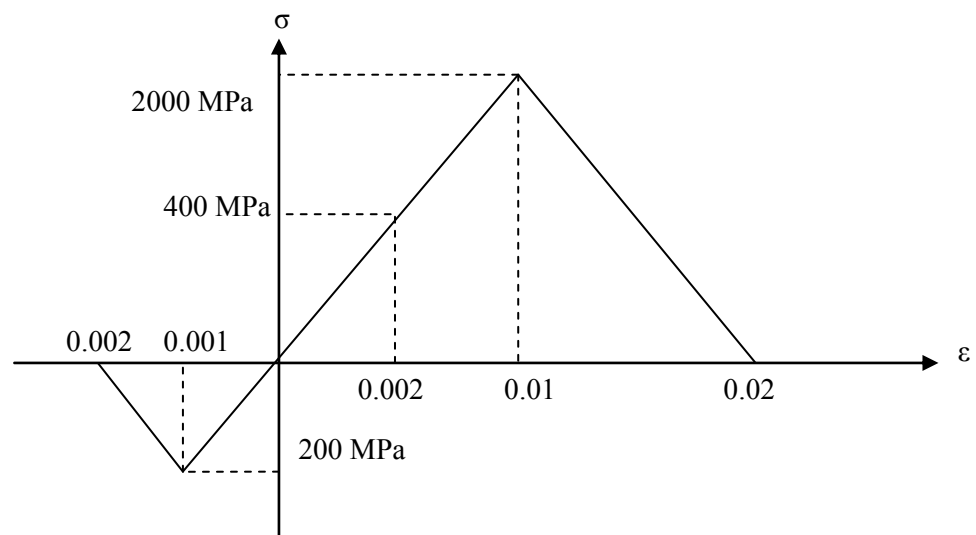
Hashin Damage: Damage Initiation

Longitudinal Tensile Strength, X^T = 2000 MPa

Longitudinal Compressive Strength, X^C = 200 MPa (Assumed 10% of tensile strength)

Transverse Tensile Strength, Y^T = 200 MPa (Assumed same)

Transverse Compressive Strength, Y^C = 200 MPa (Assumed same)

Longitudinal Shear Strength, S^L = 1200 MPa (Assumed 60% of tensile strength)

Transverse Shear Strength, S^T = 120 MPa (10% of longitudinal)

Hashin Damage: Damage Evolution

Longitudinal Tensile Fracture Energy, G_{ft} = 0.5×2000×0.02 = 20 MPa

Longitudinal Compressive Fracture Energy, G_{fc} = 0.5×200×0.002 = 0.2 MPa

Transverse Tensile Fracture Energy, G_{mt} = 2.0 (10% of longitudinal)

Transverse Compressive Fracture Energy, G_{mc} = 0.02 (10% of transverse)

Hashin Damage: Damage Stabilization

Viscosity coefficient in the longitudinal tensile direction = 0.00095 (most effective)

Viscosity coefficient in the longitudinal compressive direction = 0.00095 (most effective)

Viscosity coefficient in the transverse tensile direction = 0.00095 (most effective)

Viscosity coefficient in the transverse compressive direction = 0.00095 (most effective)

3.5.2 ANALYSIS RESULTS USING ABAQUS 6.14-4

Since the real damage properties are not known, the modeling has been done using some assumed values and then varying some parameters such as stabilization parameter of nonlinear analysis to capture the load-deflection curve as per obtained from the mathematical calculation. Convergence difficulty due to an unstable problem is usually the result of a large displacement for smaller load increments. Nonlinear stabilization can be understood as adding an artificial damper or *dashpot* element at each node of an element that supports this technique. To better conceptualize the artificial dashpot element, it has been thought as having two nodes: one is the node of the FE model that is created; the other is fixed on the ground. The program calculates

the damping force such that it is proportional to the relative pseudo velocity of the two nodes of the artificial element, which is equal to the velocity of the node belonging to the FE model. The pseudo velocity is calculated as a displacement increment divided by the time increment of the substep. Therefore, any DOF that tends to be unstable has a large displacement increment causing a large damping (stabilization) force; this force, in turn, reduces the displacements at the DOF so that stabilization is achieved. For the DOFs that are stable, the dashpot elements have little effect on the results because the displacements and the stabilization forces are small relative to the physical forces. Also the coefficient used to calculate the damping (stabilization) force is the damping factor. Although it has the same physical meaning and unit as physical damping, it is purely numerical in nonlinear stabilization. The program calculates a damping factor based on the energy dissipation ratio that is specified, or the damping factor value can be input directly (ANSYS 2016). Element and material selections have also been varied and studies have been divided into various cases listed as per following Table 3.8 to Table 3.10.

Table 3.8: Modeling features for Case 1 for verifying the Hashin Damage Model.

Finite Element Modeling Item	Steel	CFRP
Element	C3D8R	SC8R Continuum Shell
Section Assignment	Solid, Homogeneous	Shell, Composite
Elastic Material Property	Elastic, Isotropic	Elastic , Lamina
Plastic Material Property	Plastic	Hashin damage Model: Damage Initiation, Damage Evolution
Nonlinear Convergence Parameter		Damage Stabilization Parameter (varied)

Interface:

Tie Constraint: Surface to Surface, Adjust =NO, tie DOF = No

Solution Strategy: Riks Method (Crisfield 1991)
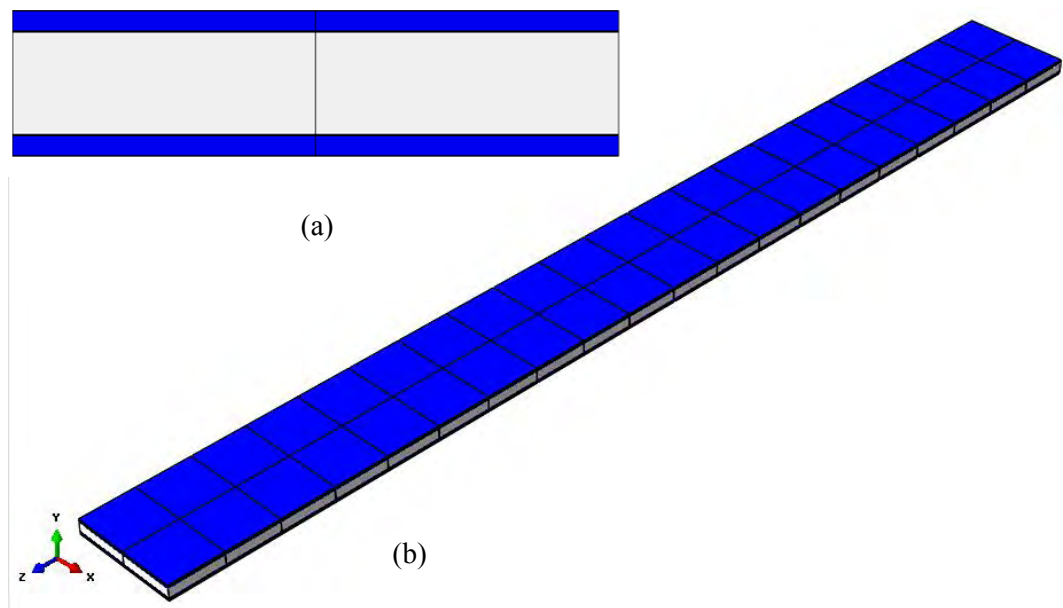
Figure 3.25: Simple Cantilever Plate Bounded by CFRP strips at the upper and lower side for Case 1 (a) Front view (b) Isometric view.
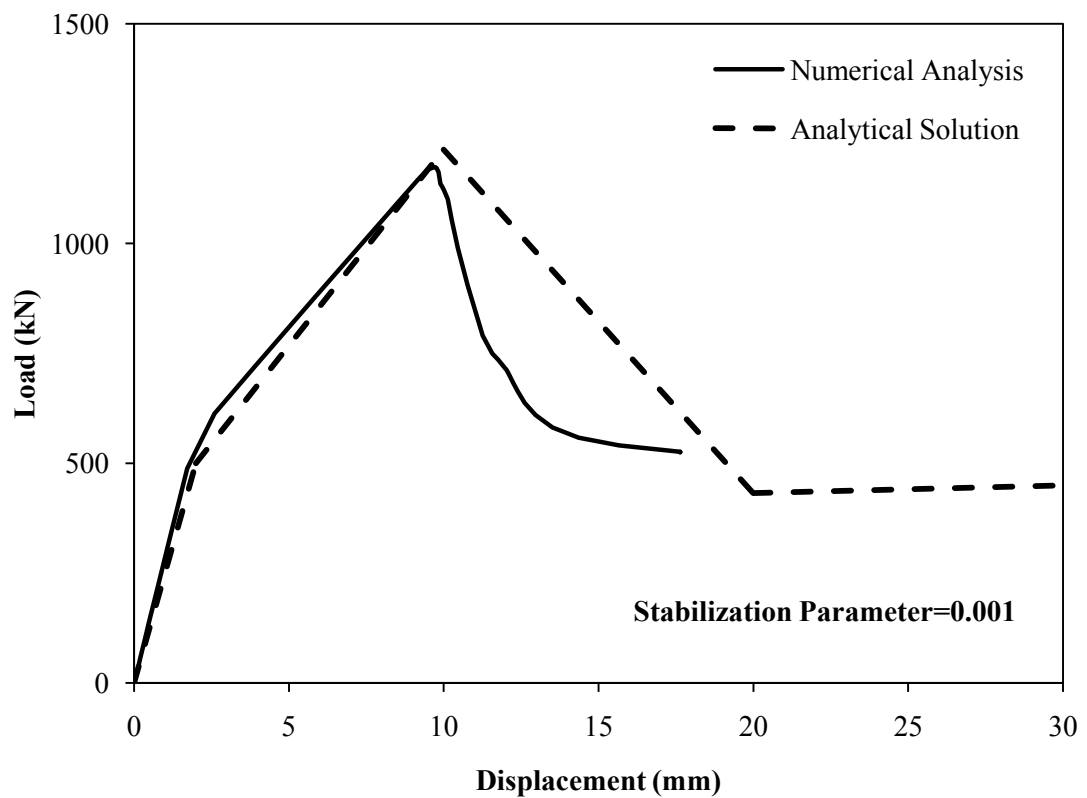
Figure 3.26: Verification of Hashin Damage Model using Abaqus for Case 1 taking the stabilization parameter as 0.001.
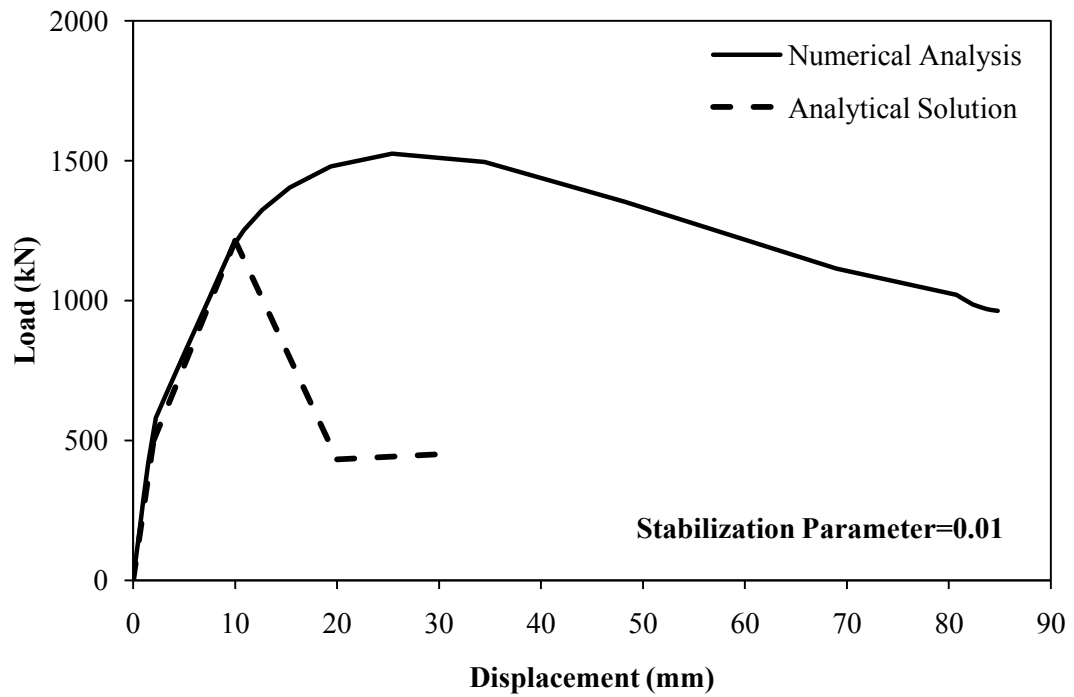
Figure 3.27: Verification of Hashin Damage Model using Abaqus for Case 1 taking the stabilization parameter as 0.01.
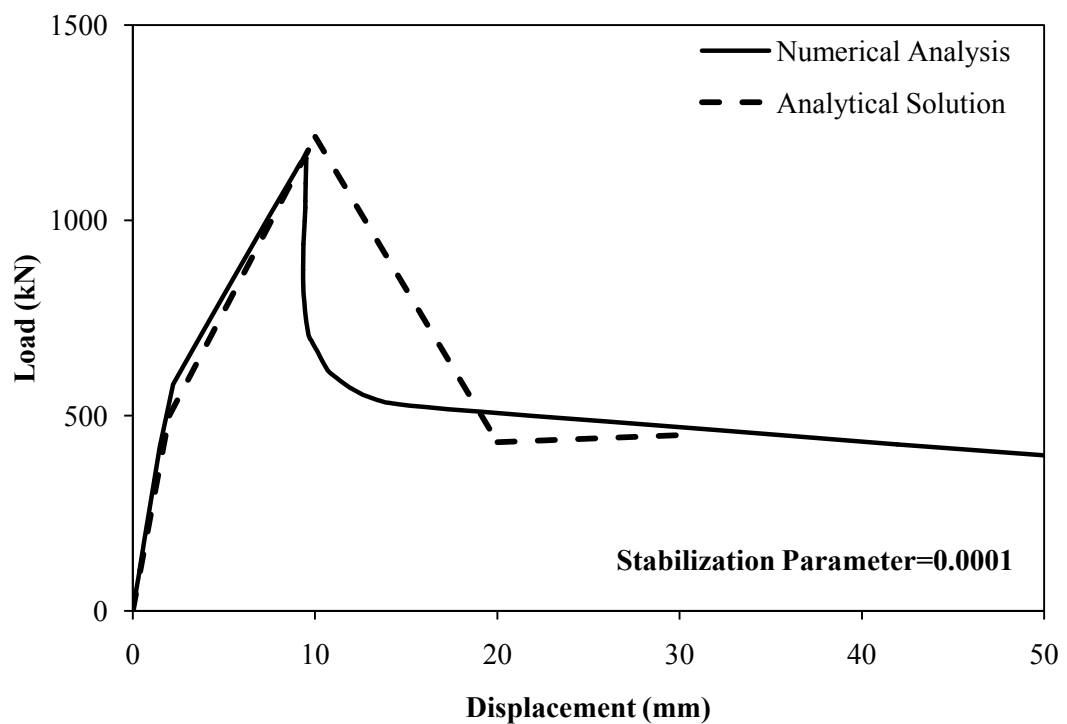
Figure 3.28: Verification of Hashin Damage Model using Abaqus for Case 1 taking the stabilization parameter as 0.0001.
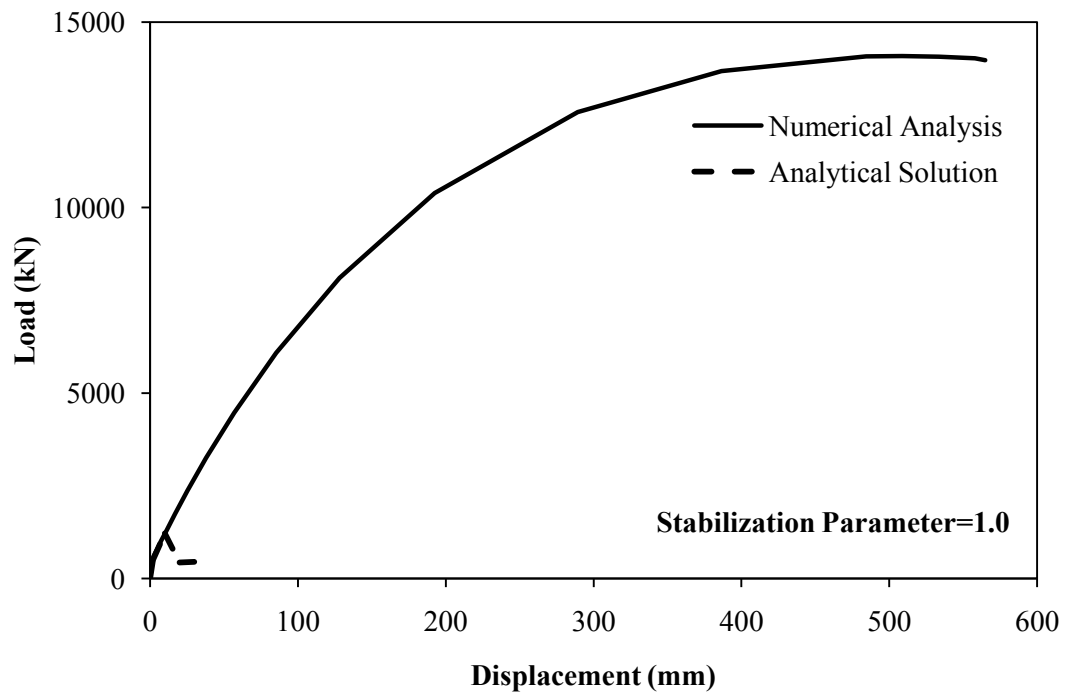
Figure 3.29: Verification of Hashin Damage Model using Abaqus Case 1 taking the stabilization parameter as 1.0.
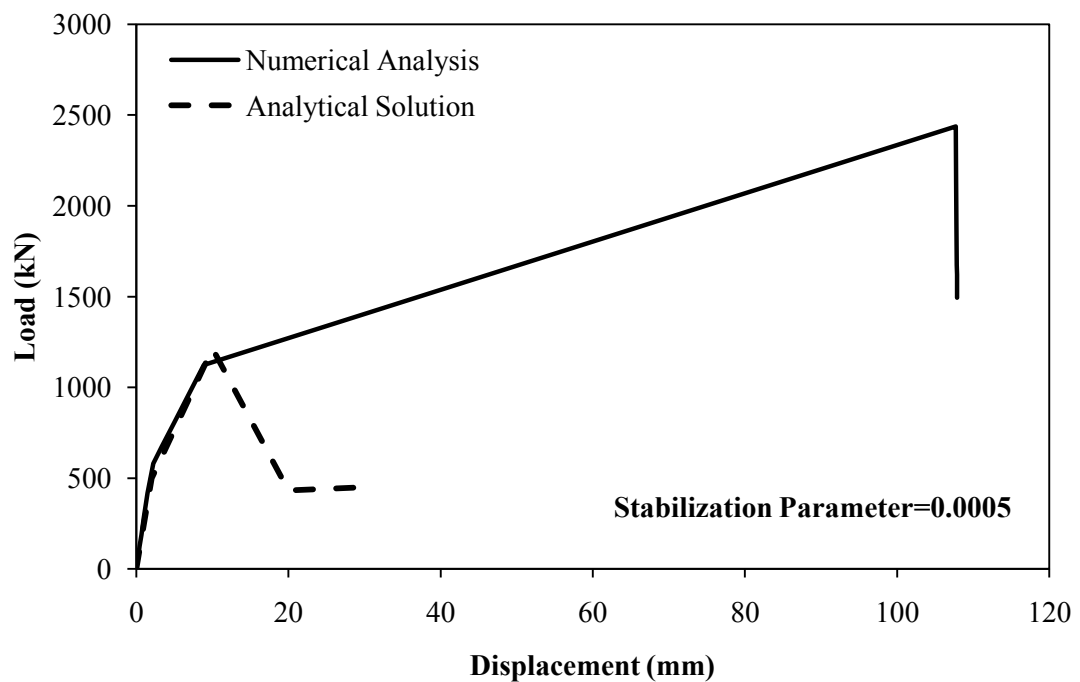
Figure 3.30: Verification of Hashin Damage Model using Abaqus for Case 1 taking the stabilization parameter as 0.0005.
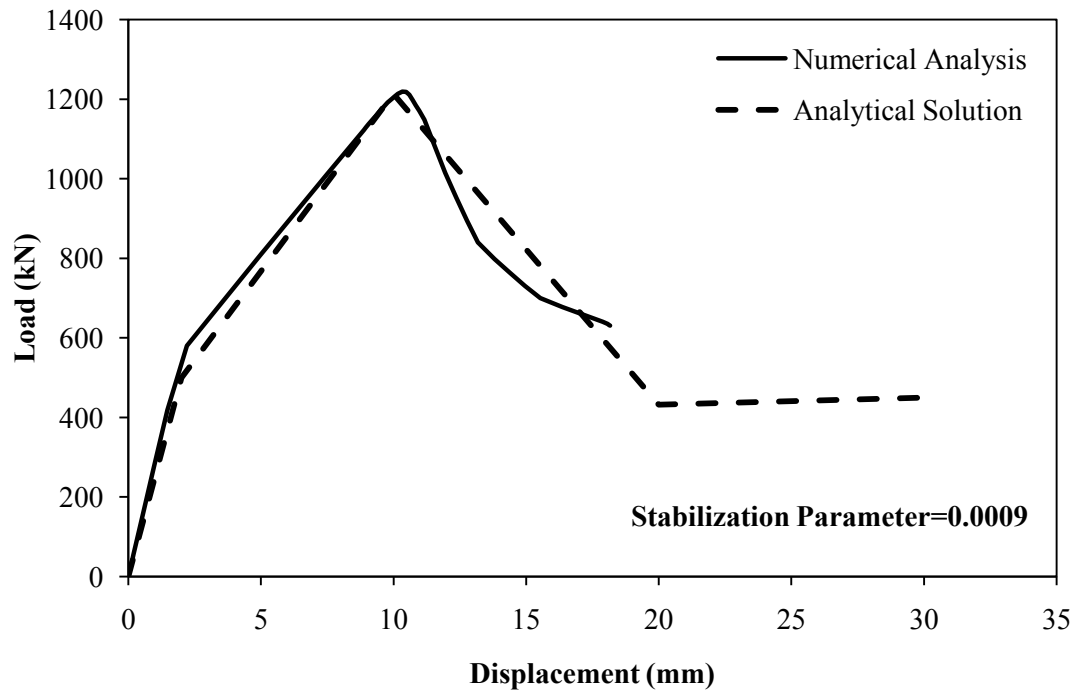
Figure 3.31: Verification of Hashin Damage Model using Abaqus for Case 1 taking the stabilization parameter as 0.0009.
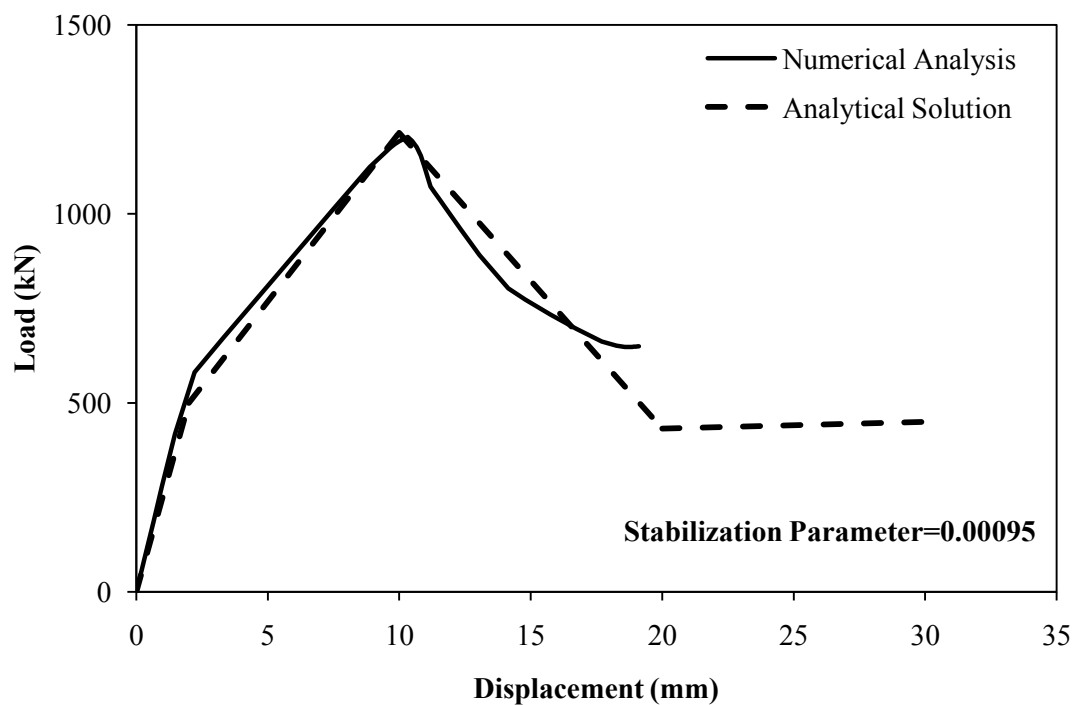
Figure 3.32: Verification of Hashin Damage Model using Abaqus for Case 1 taking the stabilization parameter as 0.00095.

Table 3.9: Modeling features for Case 2 for verifying the Hashin Damage Model.

Finite Element Modeling Item	Steel	CFRP
Element	S4R	SC8R Continuum Shell
Section Assignment	Shell, Homogeneous	Shell, Composite
Elastic Material Property	Elastic, Isotropic	Elastic , Lamina
Plastic Material Property	Plastic	Hashin damage Model: Damage Initiation, Damage Evolution
Nonlinear Convergence Parameter		Damage Stabilization Parameter : 0.00095

Interface:

Tie Constraint: Surface to Surface, Adjust =NO, tie DOF = No

Solution Strategy: Riks Method (Crisfield 1991)
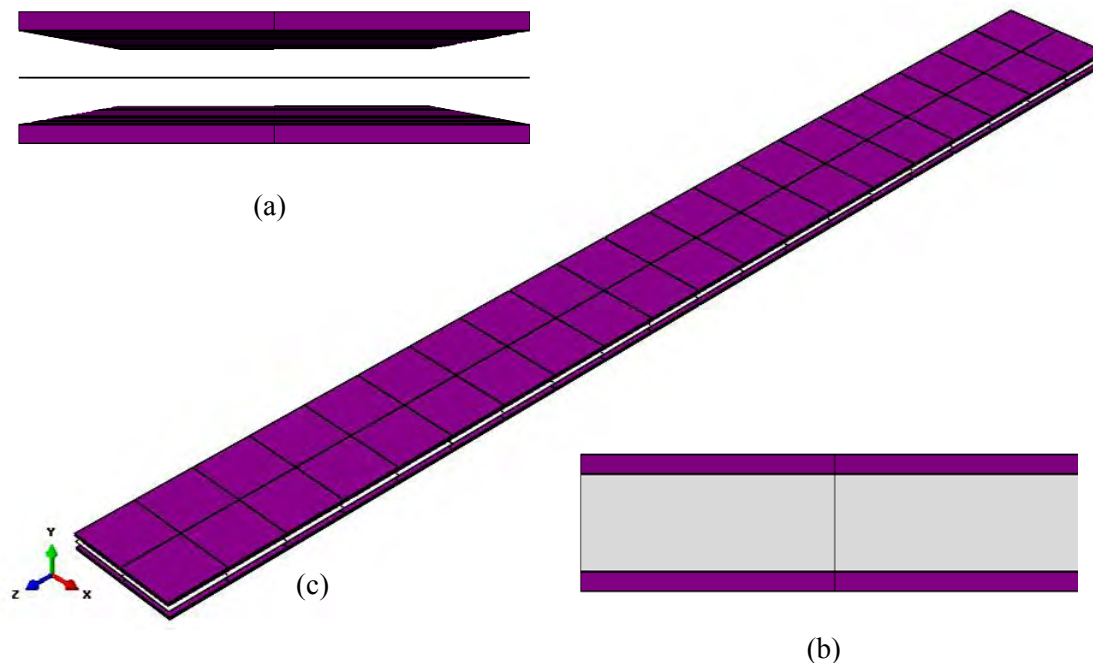
Figure 3.33: Simple Cantilever Plate Bounded by CFRP strips at the upper and
              lower side for Case 2 (a) Front view (b) Front view with original scale
              (c) Isometric view.
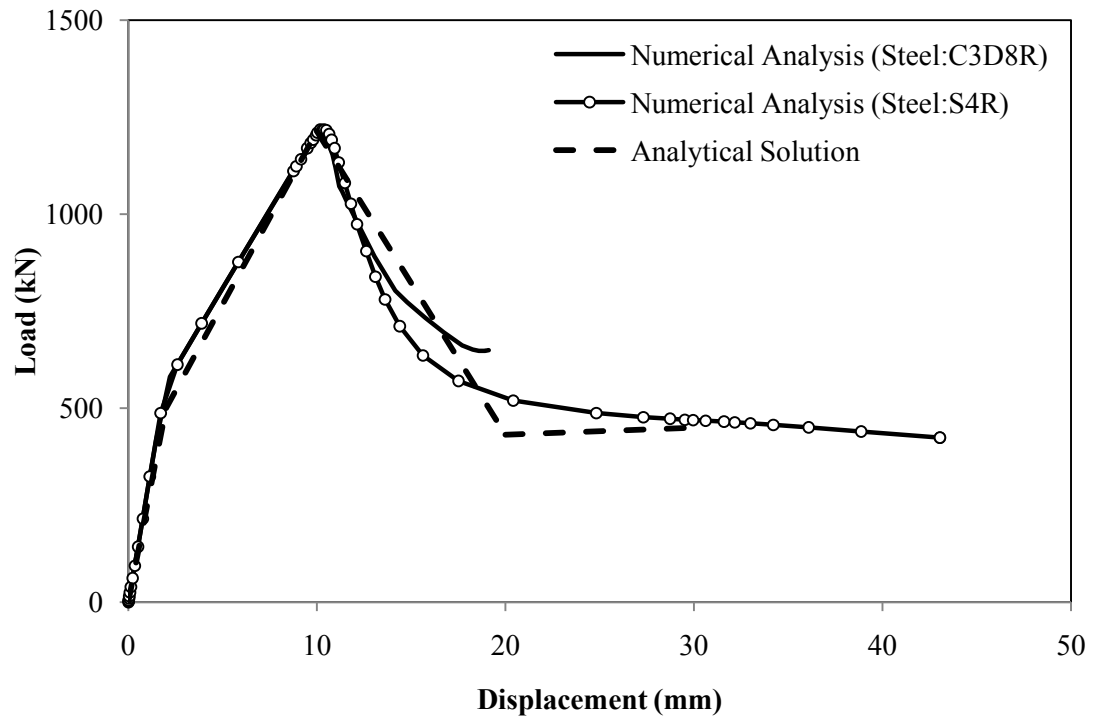
Figure 3.34: Verification of Hashin Damage Model using Abaqus for Case 2 taking the stabilization parameter as 0.00095.

Table 3.10: Modeling features for Case 3 for verifying the Hashin Damage Model.

Finite Element Modeling Item	Steel	CFRP
Element	S4R	S4R
Section Assignment	Shell, Homogeneous	Shell, Homogeneous
Elastic Material Property	Elastic, Isotropic	Elastic , Lamina
Plastic Material Property	Plastic	Hashin damage Model: Damage Initiation, Damage Evolution
Nonlinear Convergence Parameter		Damage Stabilization Parameter : 0.00095
Solution Strategy: Riks Method (Crisfield 1991)		
Interface:		
Tie Constraint: Surface to Surface, Adjust =NO, tie DOF : NO		
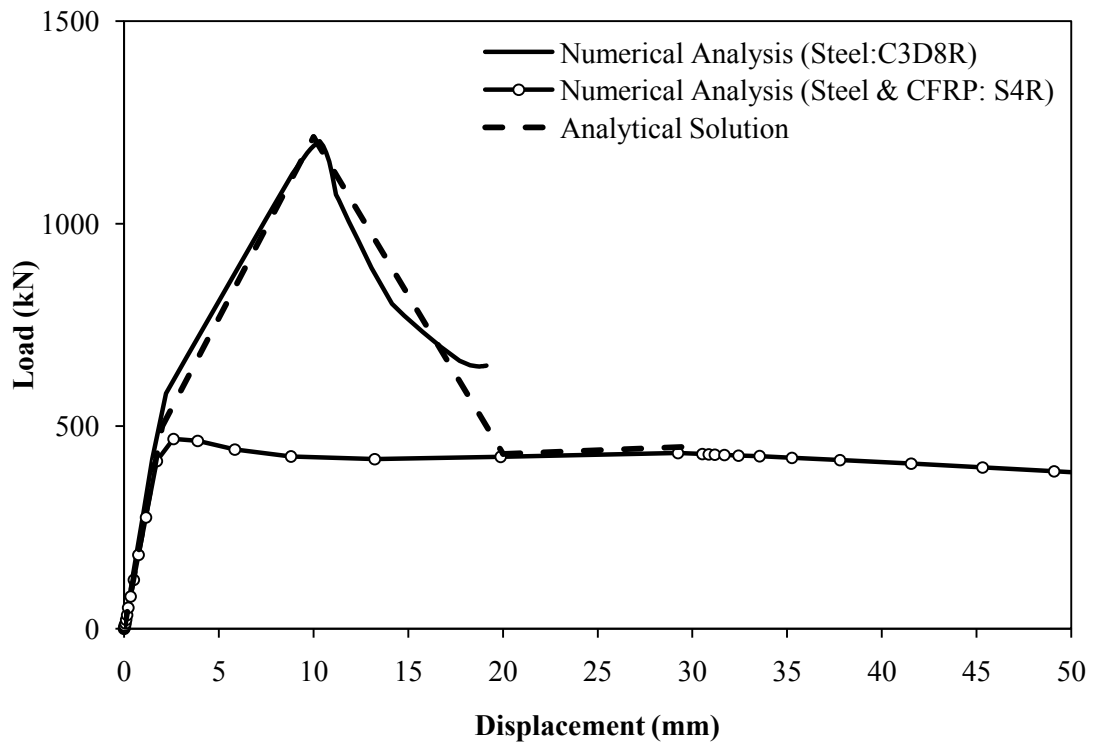
Figure 3.35: Verification of Hashin Damage Model using Abaqus for Case 3 taking the stabilization parameter as 0.00095.

Interface:

Tie Constraint: Surface to Surface, Adjust =YES, tie DOF=YES
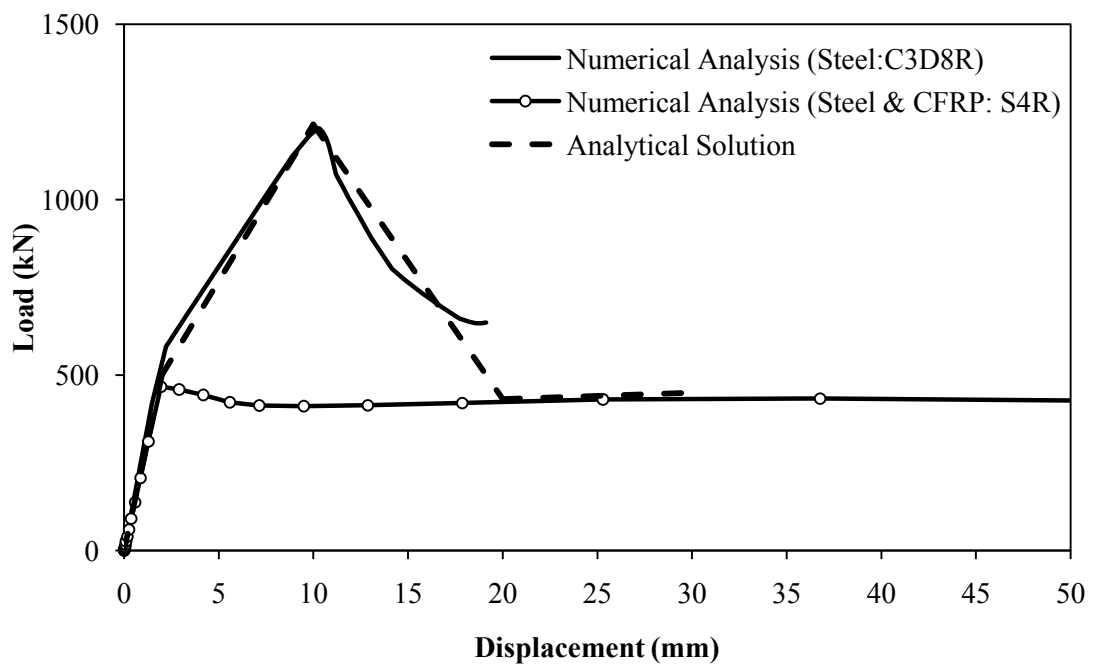
Figure 3.36: Verification of Hashin Damage Model using Abaqus for Case 3 taking the stabilization parameter as 0.00095.

Interface:

Tie Constraint: Surface to Surface, Adjust=YES, tie DOF=YES, position tolerance = 6 mm
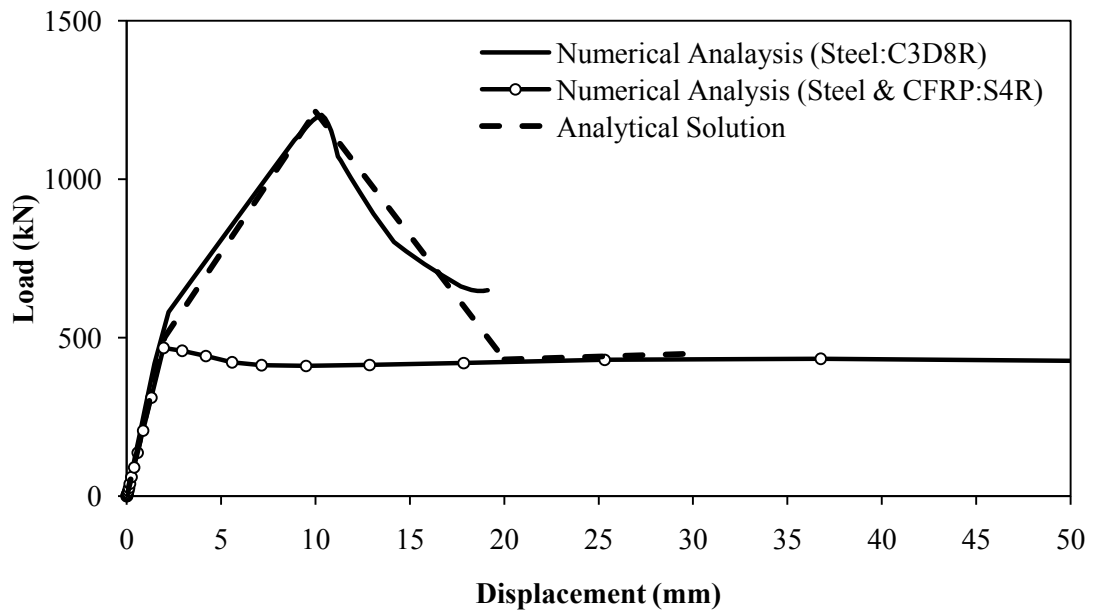
Figure 3.37: Verification of Hashin Damage Model using ABAQUS for Case 3 taking the stabilization parameter as 0.00095.

Interface:

Tie Constraint: Surface to Surface, Adjust=YES, tie DOF=YES, position tolerance = 6 mm, Damage stabilization coefficient= 0.1
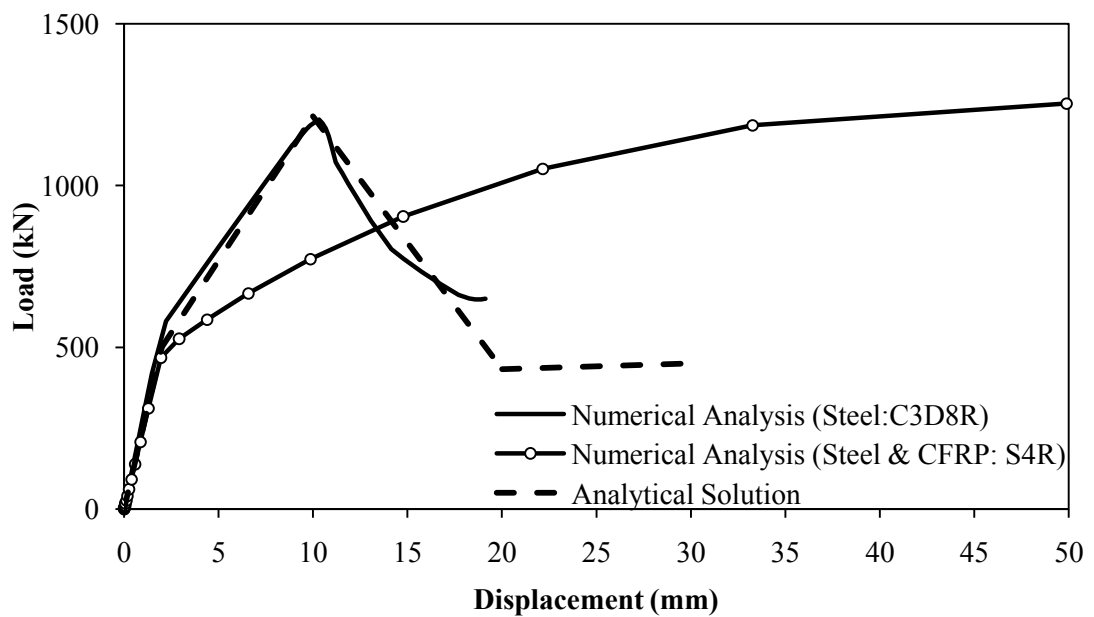
Figure 3.38: Verification of Hashin Damage Model using Abaqus for Case 3 taking the stabilization parameter as 0.00095.

In the above case studies simple cantilever plate bounded by CFRP strips at the upper and bottom side have been modeled to examine the implementation of Hashin Damage Model for modeling the CFRP materials in the proposed numerical model. Since the different input parameters of Hashin Damage Model are not known from the reference experimental study, different parameters have been assumed and varied for verification. In case study 1, steel plate and CFRP strips have been modeled using C3D8R solid element and SC8R continuum shell element respectively. Load vs. Displacement diagrams comparing the analytical solution and numerical analysis for case study 1 have been shown in Figure 3.26 to Figure 3.32 where significant variation has been identified for changing the stabilization parameter of the damage stabilization part of the Hashin Damage Model. And for stabilization parameter of about 0.00095, numerical analysis from Abaqus has shown good agreement with the analytical solution.

Again in case study 2, stabilization parameter has been taken 0.00095 but steel plate has been modeled with conventional shell element S4R. Tie constraints are used for perfect bonding approach in between steel plate and CFRP strips. Similar comparison results are obtained as shown in Figure 3.34 as per obtained in case study 1 for stabilization parameter 0.00095 as shown in Figure 3.32. By taking the 4-noded conventional shell element to model steel plate the computational time of numerical analysis has also been possible to reduce with a significant amount.

In case study 3, both the steel plate and CFRP strips have been modeled using 4-noded conventional shell element S4R. But the result does not agree with analytical solution as shown in Figure 3.35 to Figure 3.38.

By studying the three cases, it has been seen that case 2 is the best alternative option to model the simple steel cantilever plate along with the CFRP strips for the verification of the Hashin Damage Model. For this reason, in the proposed model steel HSS column has been modeled with 4-noded S4R conventional shell element and the CFRP & GFRP strips have been modeled using Hashin Damage Model taking the stabilization parameter as 0.00095 in the damage stabilization part. Also tie constraints have been used for modeling the interface in between the steel-FRP interface and also the FRP-FRP interface. This verification is conducted by trial basis since some parameters of Hashin Damage model are not available in literature

through experiment. Due to this reason, such trial basis study has been conducted to fix the parameters of Hashin Damage model to best fit with the experimental values (Kabir *et al.* 2016).

3.6 REMARKS

The finite element model developed in this Chapter using Abaqus 6.14-4 need to be verified to carry on further numerical investigation to simulate the practical conditions. If it is possible to show that numerical model can adequately simulate the experimental results than it would be really helpful in the era of numerical analysis of practical problematic situations. On account of this, experimental model used by Shaat and Fam in 2007 for their investigation is considered as reference for model verification which is described in Chapter 4 in details.

Chapter 4

EXPERIMENTAL MODEL VERIFICATION

4.1 INTRODUCTION

The finite element model developed in Chapter 3 using Abaqus 6.14-4 need to be verified to carry on further numerical investigation to simulate the practical conditions. If it is possible to show that numerical model can adequately simulate the experimental results than it would be really helpful in the era of numerical analysis of practical problematic situations. On account of this, experimental model used by Shaat and Fam in 2007 for their investigation is considered as reference in this chapter.

4.2 DETAILED DESCRIPTION OF REFERENCE EXPERIMENTAL STUDY (SHAAT AND FAM 2007)

An experimental study was carried out by Shaat and Fam (2007) to investigate the effect of adhesively bonded CFRP sheets on the behavior of axially loaded hollow structural section (HSS) slender columns. It was shown experimentally that CFRP sheets have increased the columns strengths by up to 23%. The study however revealed the sensitivity of the strengths of axially loaded slender columns to their inherent geometric out-of-straightness alignment (imperfections). Residual stresses are also a factor, which can affect the behavior of cold columns. While the major parameter intended to be studied in the experimental investigation was the effect of the number of CFRP layers, it is believed that geometric out-of-straightness values and alignment have varied inevitably among the specimens. As such, no specific correlation could be established between the amount of strength gain and amount of CFRP.

4.2.1   GEOMETRIC AND MATERIAL PROPERTIES OF TESTED SPECIMENS

The study was conducted using five slender 89×89×3.2 mm HSS column specimens, including a control (unstrengthened) specimen and three specimens strengthened with one, three and five layers of CFRP, applied to two opposite side in the plane of overall buckling. The fifth specimen was strengthened with three layers, applied to all four sides. Based on the CFRP orientation, HSS columns were designated in the following way such as 1L-2S, 3L-2S, 5L-2S, 3L-4S. Here, for example, 3L-2S indicates three CFRP layers applied on two opposite sides allowing buckling about the vertical axis y-y only. And, 3L-4S indicates three CFRP layers applied on four sides of the HSS column.

Table 4.1: Geometric properties of tested specimen (Shaat and Fam 2007).

Properties	Steel HSS Column	CFRP	GFRP	Tyfo S Epoxy Resin
Cross-sectional Dimension (mm×mm)	89×89	74×0.54	74×1.46	74×0.5
Thickness (mm)	3.2	0.54 (single layer)	1.46	0.5
Length (mm)	2380	2380	2380	2380

Table 4.2: Material properties of tested specimen (Shaat and Fam 2007).

Properties	Steel HSS Column	CFRP	GFRP	Tyfo S Epoxy Resin
Modulus of Elasticity (GPa)	200	230	14	3.18
Tensile Strength (MPa)	480	510	269	-
Yield Stress (MPa)	380	-	-	-

Details of cross-sectional geometry of experimental model of Shaat and Fam (2007) can also be understood from Figure 3.1.

4.2.2   TEST SETUP AND MEASUREMENTS

Tests were carried out in a horizontal setup as shown in Figure 4.1(b). Lubricated cylindrical bearings were used at both ends to allow free end rotation in the horizontal plane only. Specimens were braced against out-of-plane buckling using another set of free sliding rollers to allow buckling about the vertical axis y-y only. The specimens were instrumented using six linear potentiometers (LPs) to record the net axial and lateral displacements. Longitudinal strains at mid-length were measured using electric resistance and displacement-types strain gauges attached to the CFRP layers on both sides of the specimen also shown in Figure 4.1(b). The load was measured using a load cell positioned between the end of the frame and the hydraulic jack.

4.2.3   FAILURE MODE AND RESULT SUMMARY

In all specimens, failure was mainly due to excessive overall buckling Figure 4.1(e), followed by a secondary local buckling in the compression side in the form of inward buckling of the compression face and outward buckling of the side faces Figure 4.1(f). For the FRP-strengthened specimens, the secondary local buckling was associated with a combined debonding at the interface between the adhesive and steel surface and crushing of FRP sheets. For specimen 3L-4S, the FRP on the sides have also fractured due to outward local buckling Figure 4.1(g). The load versus lateral displacement, axial displacement and axial strains of all specimens are shown in the following Figure 4.2. The gain in axial strength of the FRP-strengthened specimens ranged from 13 to 23 % which did not correlate directly to the number of CFRP layers. This was attributed to the geometric imperfections among the specimens, due to out-of-straightness of different values as shown in Table 3.2, or inadvertent minor misalignment within the test setup or a combination of both (Kulak and Grodin 2002).

Figure 4.2(c) shows the load versus axial strain at the two opposite sides at midlength. The figure shows that both sides are under compression up to a certain load, where excessive buckling starts and strains at the outer surface revert to tension while strains at the inner surface show rapid increase in compression.
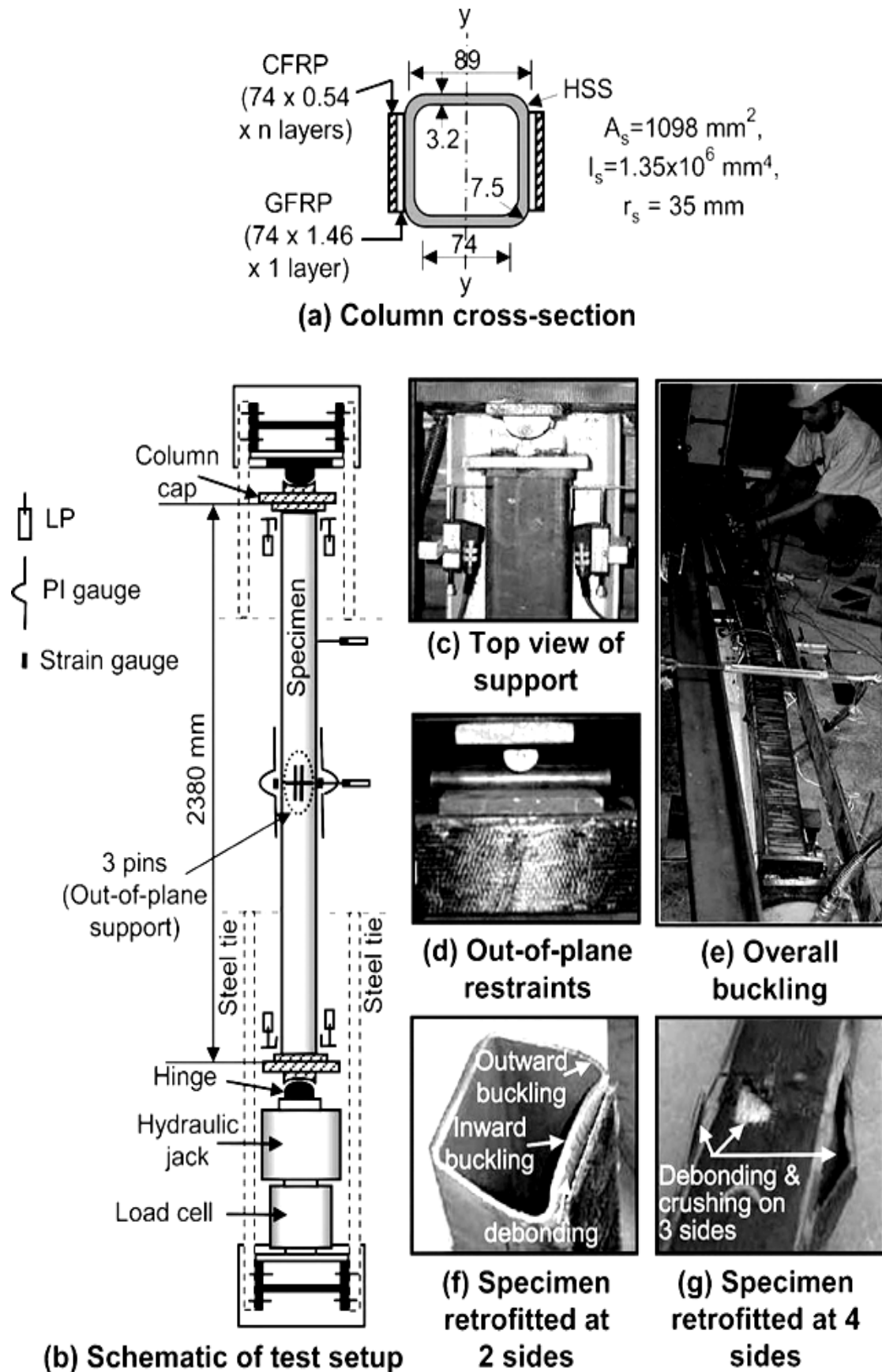
Figure 4.1: Test setup and failure mode (Shaat and Fam 2007).

(a) Load vs. lateral displacement   (b) Load vs. axial displacement   (c) Load vs. axial strain
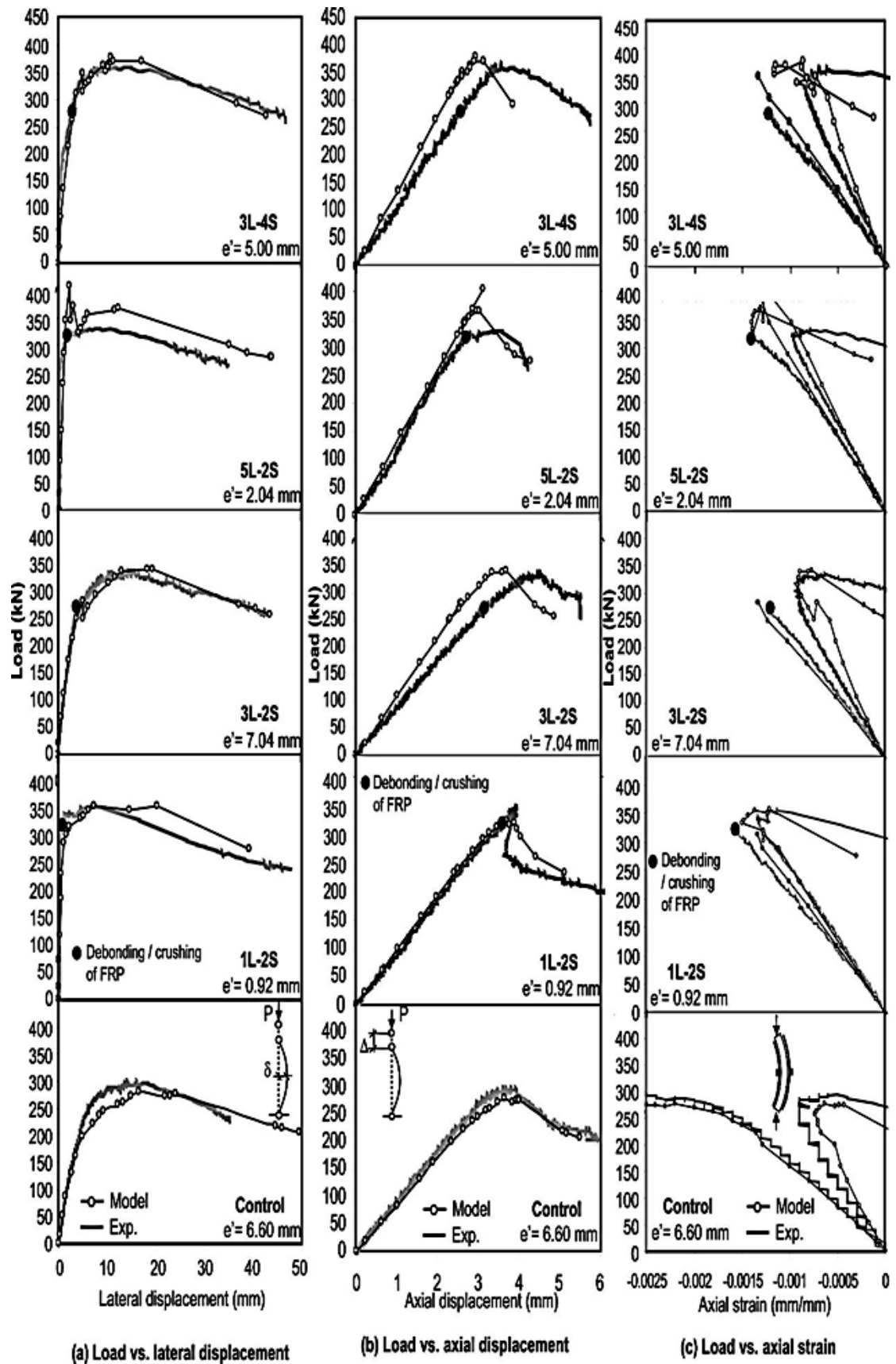
Figure 4.2: Experimental and Analytical responses of Axially loaded HSS columns
(Shaat and Fam 2007).

Strain gauges on the compression side failed due to the local buckling that followed overall buckling. By examining the strain readings, an average strain of 0.13% was defined as the strain at which CFRP failed in compression. This strain is limited to this particular case and may vary for different types of CFRP or HSS sections. No signs of FRP failure have been observed on the tension side.

Using the sectional geometric and material properties given by Shaat and Fam (2007), the model is generated similar to the way described in Chapter 3. Detailed sketches of the model from the Abaqus 6.14-4 have also been shown in Figure 3.11 to Figure 3.24 in Chapter 3.

4.3 VERIFICATION OF NUMERICAL MODEL

The numerical simulation has been carried out based on the developed finite element model and the results obtained from numerical analysis were standardized against the corresponding experimental data (Shaat and Fam 2007). The ultimate load, load-deflection curves and failure mode of the unstrengthened and composite HSS columns having various FRP strips executed by FE models are compared with the experimental results. The finite element model have been developed following different combinations in respect of element, material and bonding since there is no definite approach for modeling steel HSS column retrofitted with multilayer FRP strips along with the FRP damage properties. Present analysis results have also been compared with the past analysis results from Devi and Amanat's study (2015)[1].

4.3.1   VERIFICATION OF EXPERIMENTAL MODEL (SHAAT AND FAM 2007)

4.3.1.1 Description of Different Case Studies

For the purpose of verifying the reference experimental model study has been organized in various cases. For each case study verification of Abaqus analysis has been done with the Shaat and Fam (2007) test results. And finally a case study has been proposed for future parametric study which has shown the good agreement with the test results. Brief details of different case studies are following and further represented in a Table 4.3.

Case Study-I:

- Steel HSS column, steel end loading plate, Glass Fiber Reinforced Polymer (GFRP) and Carbon Fiber Reinforced Polymer (CFRP) materials have been modeled using 4-noded conventional shell element S4R.

- Tyfo S Epoxy Resin, the material used for bonding, has also been modeled using element S4R.

- Materials for steel HSS column and steel end loading plate have been modeled as per described in Chapter 3.

- GFRP, CFRP strengthening materials and Epoxy resin bonding materials have been modeled assuming elasto-plastic material.

- Perfect bonding approach has been adopted at the interface in between the steel-FRP and FRP-FRP. Tie constraints have been implemented in between surface to surface for modeling this feature.

Case Study-II (Alternate 1 & 2):

- Steel HSS column, steel end loading plate, Glass Fiber Reinforced Polymer (GFRP) and Carbon Fiber Reinforced Polymer (CFRP) materials have been modeled using 4-noded conventional shell element S4R.

- Tyfo S Epoxy Resin, the material used for bonding, has also been modeled using element S4R.

- Materials for steel HSS column and steel end loading plate have been modeled as per described in Chapter 3.

- GFRP and CFRP strips have been modeled using the Hashin Damage Model specially used for fiber reinforced material modeling verified in chapter 3. The elastic lamina properties have been taken as shown in Table 3.5. The material properties of Hashin Damage Model are taken as shown in Table 3.6 along with the second option of the Table 3.7.

- Epoxy resin has been modeled assuming elasto-plastic material.

- Perfect bonding approach has been adopted at the interface in between the steel-FRP and FRP-FRP. Tie constraints have been implemented in between surface to surface for modeling this feature.

Case Study-III (Alternate 1 & 2):

- Steel HSS column and steel end loading plate have been modeled using 4-noded conventional shell element S4R.

- CFRP and GFRP strips have been modeled using 8-noded continuum shell element SC8R.

- Tyfo S Epoxy Resin has not been incorporated in the finite element model.

- Materials for steel HSS column and steel end loading plate have been modeled as per described in Chapter 3.

- GFRP and CFRP strips have been modeled using the Hashin Damage Model specially used for fiber reinforced material modeling verified in chapter 3. The elastic lamina properties have been taken as shown in Table 3.5. The material properties of Hashin Damage Model are taken as shown in Table 3.6 along with the second option of the Table 3.7.

- Perfect bonding approach has been adopted at the interface in between the steel-FRP and FRP-FRP. Tie constraints have been implemented in between surface to surface for modeling this feature.

Case Study-IV:

- Steel HSS column and steel end loading plate have been modeled using 4-noded conventional shell element S4R.

- Tyfo S Epoxy Resin has also been modeled using element S4R.

- CFRP and GFRP strips have been modeled using 8-noded continuum shell element SC8R.

- GFRP and CFRP strips have been modeled using the Hashin Damage Model specially used for fiber reinforced material modeling verified in chapter 3. The elastic lamina properties have been taken as shown in Table 3.5. The material properties of Hashin Damage Model are taken as shown in Table 3.6 along with the first option of the Table 3.7.

- Hashin Damage Model has also been applied to the Tyfo S Epoxy Resin as per the assumption taken for GFRP and CFRP.

- Perfect bonding approach has been adopted at the interface in between the steel-FRP and FRP-FRP. Tie constraints have been implemented in between surface to surface for modeling this feature.

Table 4.3: Details of Different Case Studies in a Summarized way.

Case	Steel HSS Column		End Loading Plate		GFRP and CFRP Strips		Tyfo S Epoxy Resin		Interface
	Element	Material	Element	Material	Element	Material	Element	Material	
Case I	S4R	Steel Nonlinear	S4R	Steel Linear	S4R	Elasto-plastic	S4R	Elasto-plastic	Tie Constraint
Case II (Alternate 1 & 2)	S4R	Steel Nonlinear	S4R	Steel Linear	S4R	Elastic, Lamina and Hashin Damage Model	S4R	Elasto-plastic	Tie Constraint
Case III (Alternate 1 & 2)	S4R	Steel Nonlinear	S4R	Steel Linear	SC8R	Elastic, Lamina and Hashin Damage Model	N/A		Tie Constraint
Case IV	S4R	Steel Nonlinear	S4R	Steel Linear	SC8R	Elastic, Lamina and Hashin Damage Model	S4R	Elastic, Lamina and Hashin Damage Model	Tie Constraint

4.3.1.2 Verification of the Load Vs. Axial Displacement Behavior

Graphical representations of different case studies verifying the numerical analysis with the experimental test results of Shaat and Fam (2007) are shown in Figure 4.3 to 4.23.
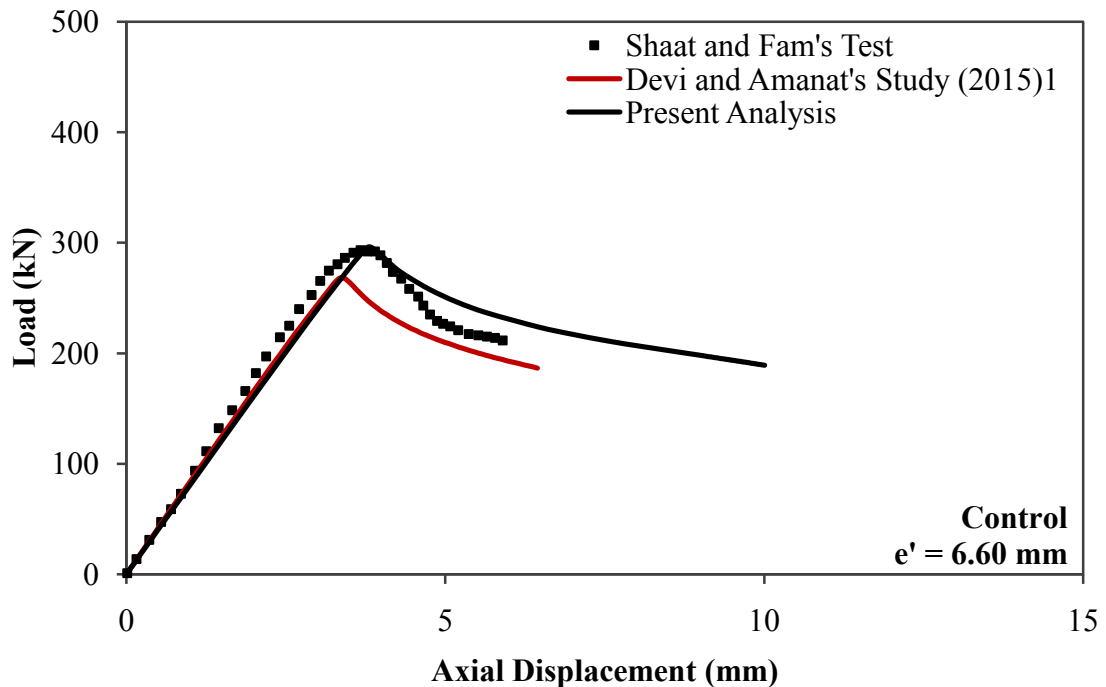
Figure 4.3: Load vs. Axial Displacement Behavior for Axially Loaded

Control/Unstrengthened HSS Column Specimen.
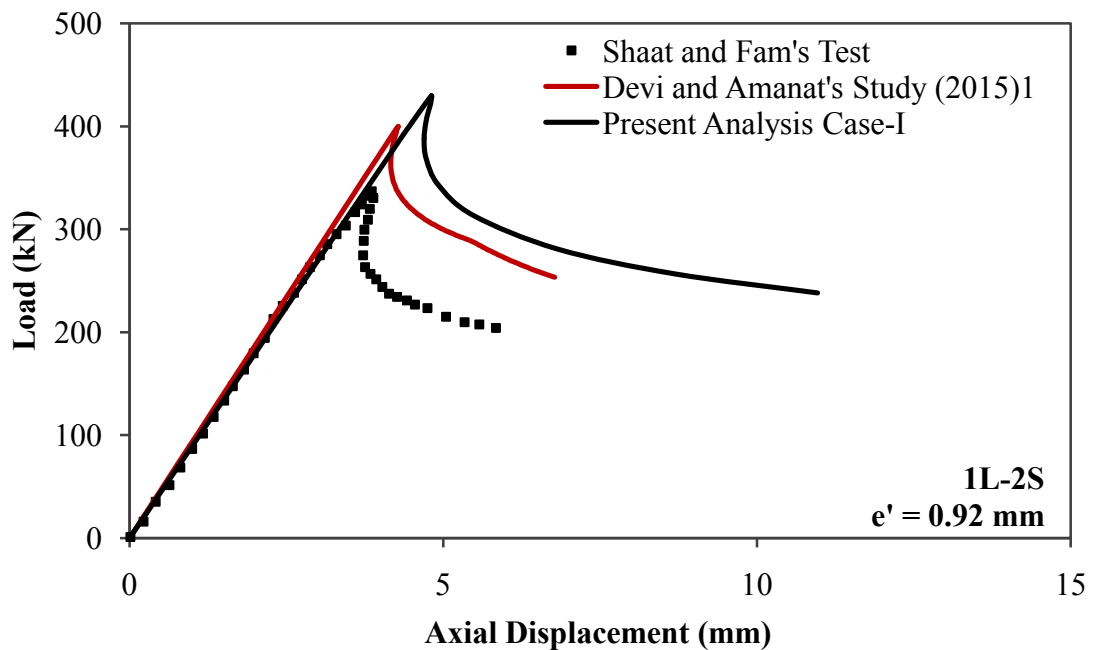
Figure 4.4: Load vs. Axial Displacement Behavior for Axially Loaded Strengthened

HSS Column Specimen (One layer and two sided CFRP) for Case Study-I.
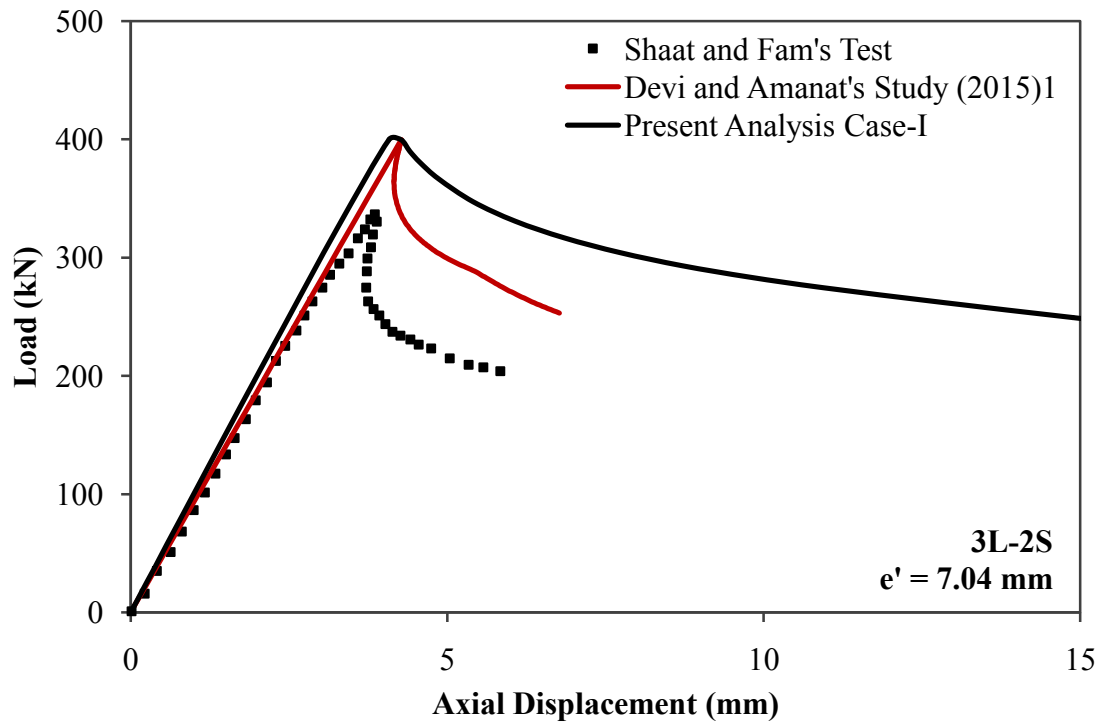
Figure 4.5: Load vs. Axial Displacement Behavior for Axially Loaded Strengthened
HSS Column Specimen (Three layers and two sided CFRP) for Case
Study-I.
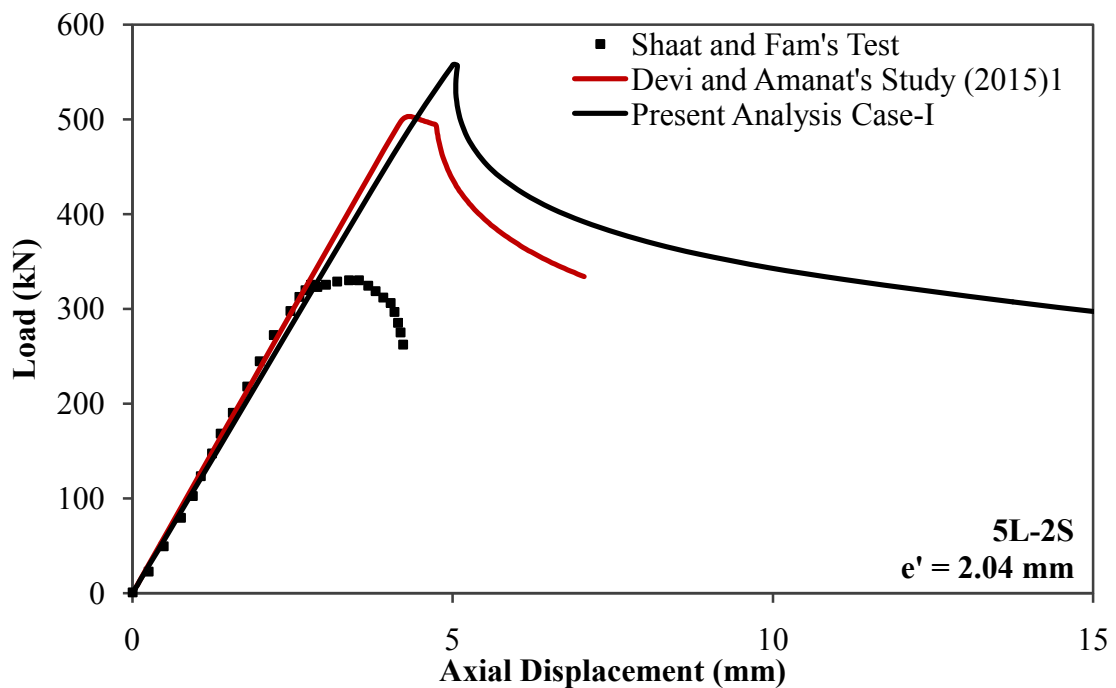
Figure 4.6: Load vs. Axial Displacement Behavior for Axially Loaded Strengthened
HSS Column Specimen (Five layers and two sided CFRP) for Case Study-
I.
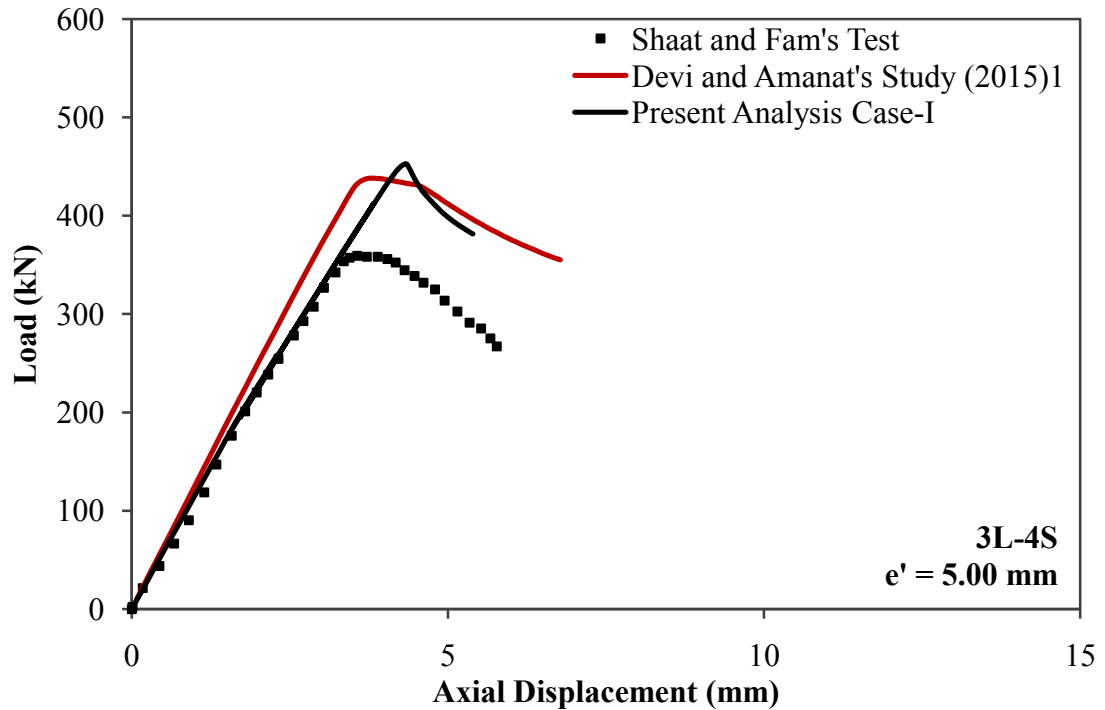
Figure 4.7: Load vs. Axial Displacement Behavior for Axially Loaded Strengthened HSS Column Specimen (Three layers and four sided CFRP) for Case Study-I.
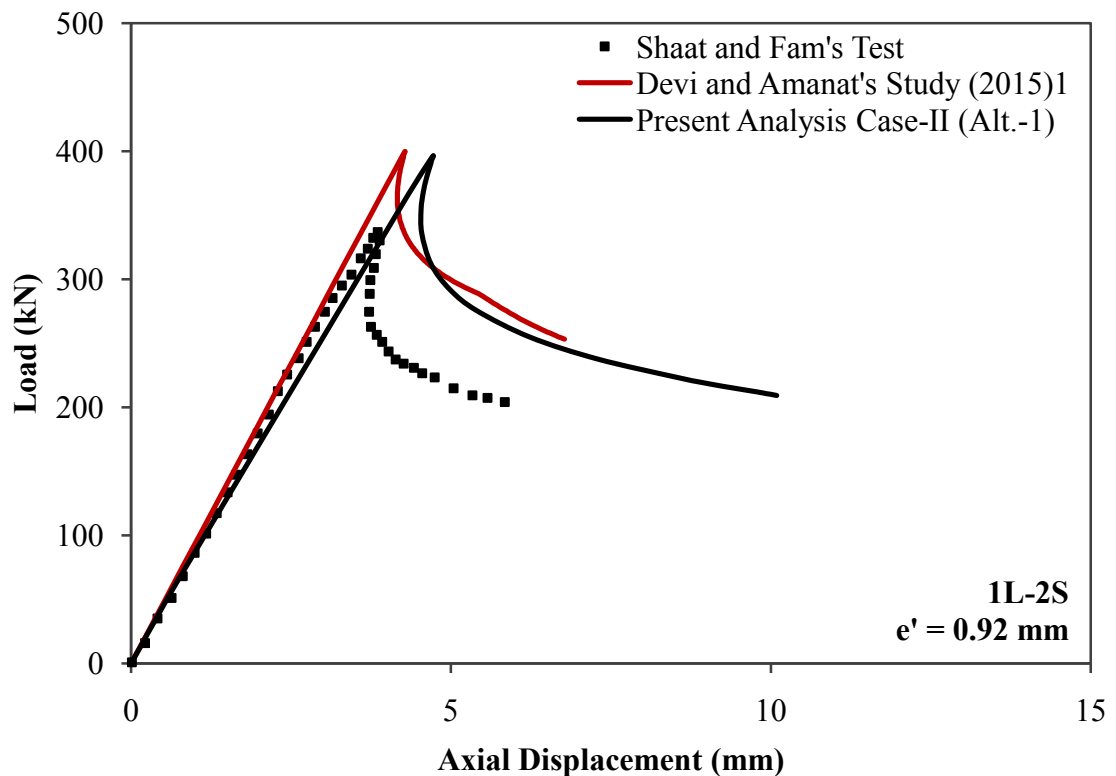
Figure 4.8: Load vs. Axial Displacement Behavior for Axially Loaded Strengthened HSS Column Specimen (One layer and two sided CFRP) for Case Study-II (Alt.-1).
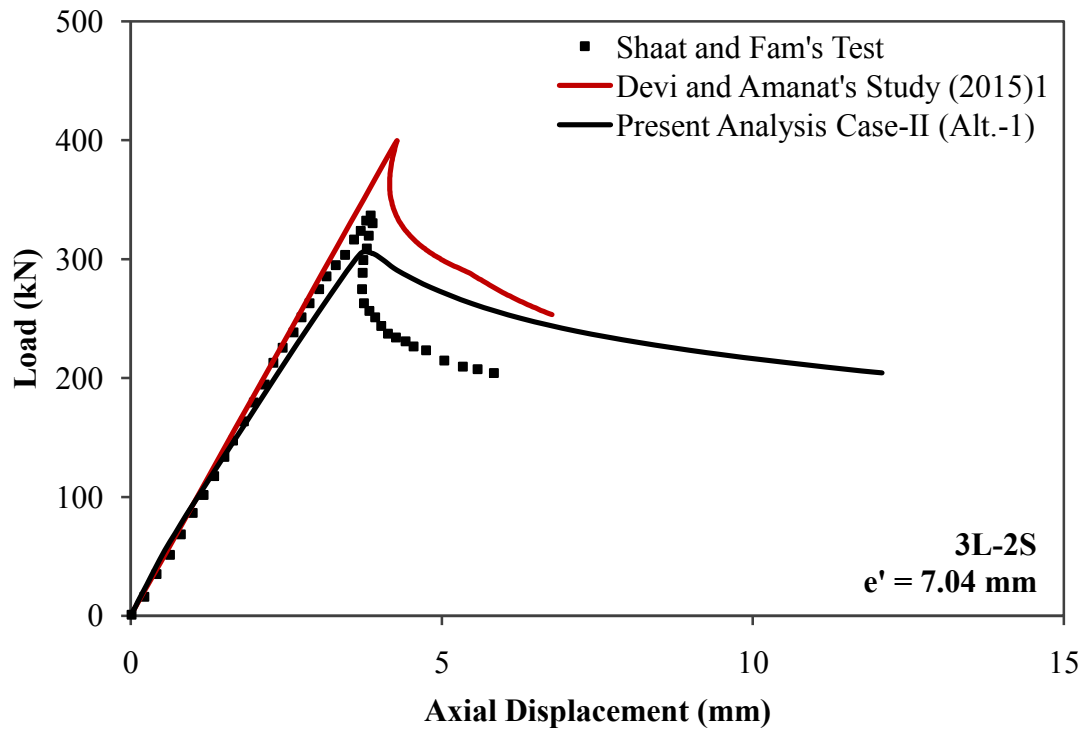
Figure 4.9: Load vs. Axial Displacement Behavior for Axially Loaded Strengthened HSS Column Specimen (Three layers and two sided CFRP) for Case Study-II (Alt.-1).
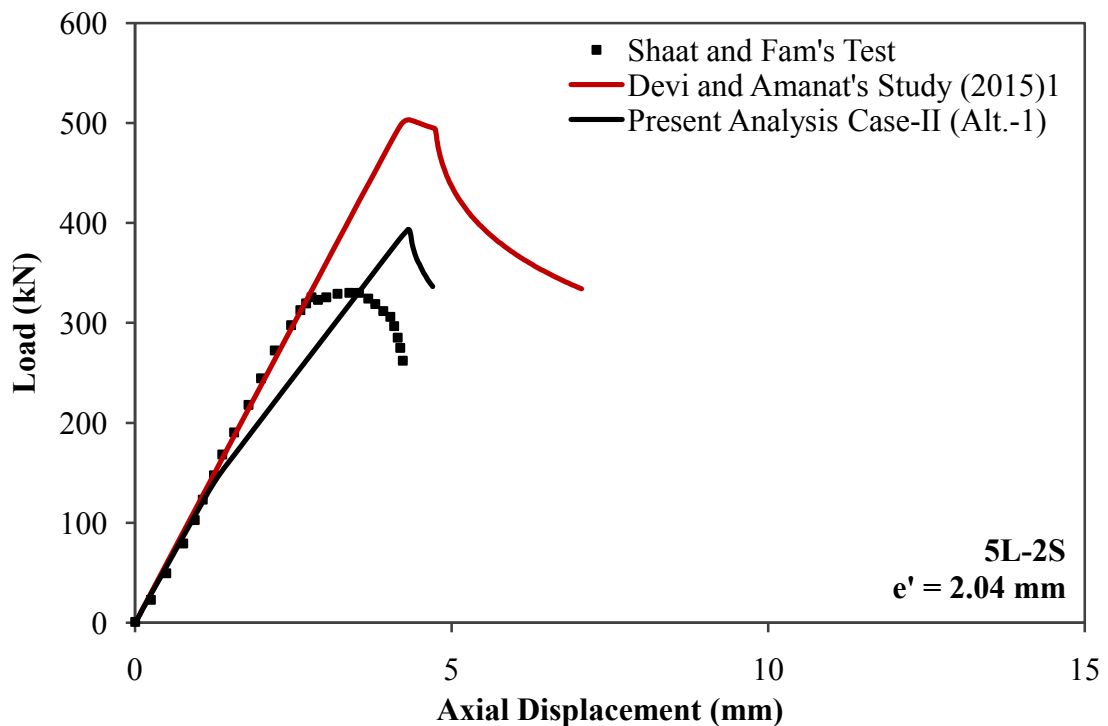
Figure 4.10: Load vs. Axial Displacement Behavior for Axially Loaded Strengthened HSS Column Specimen (Five layers and two sided CFRP) for Case Study-II (Alt.-1).
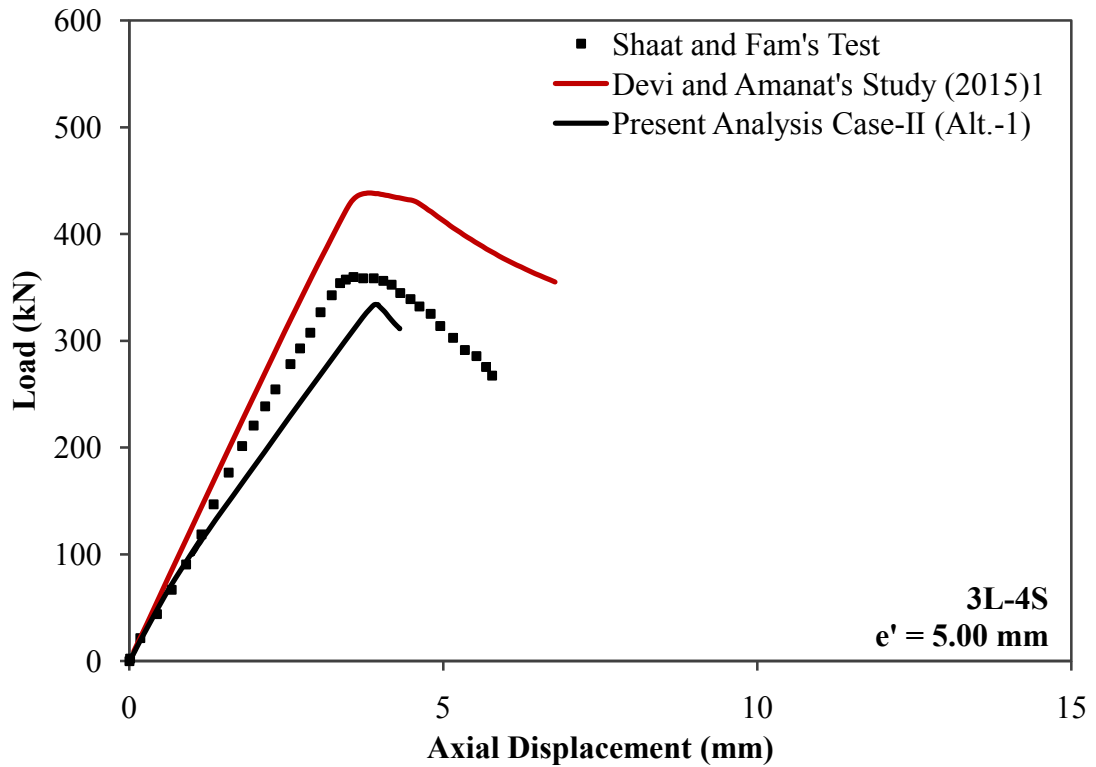
Figure 4.11: Load vs. Axial Displacement Behavior for Axially Loaded Strengthened HSS Column Specimen (Three layers and four sided CFRP) for Case Study-II (Alt.-1).
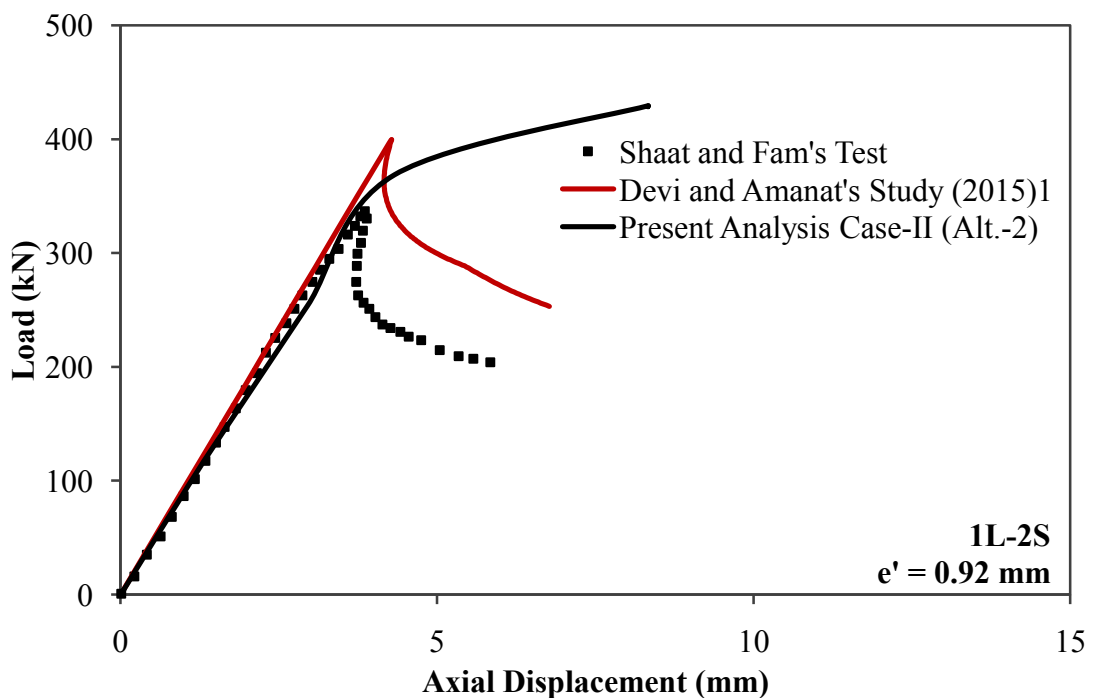
Figure 4.12: Load vs. Axial Displacement Behavior for Axially Loaded Strengthened HSS Column Specimen (One layer and two sided CFRP) for Case Study-II (Alt.-2).
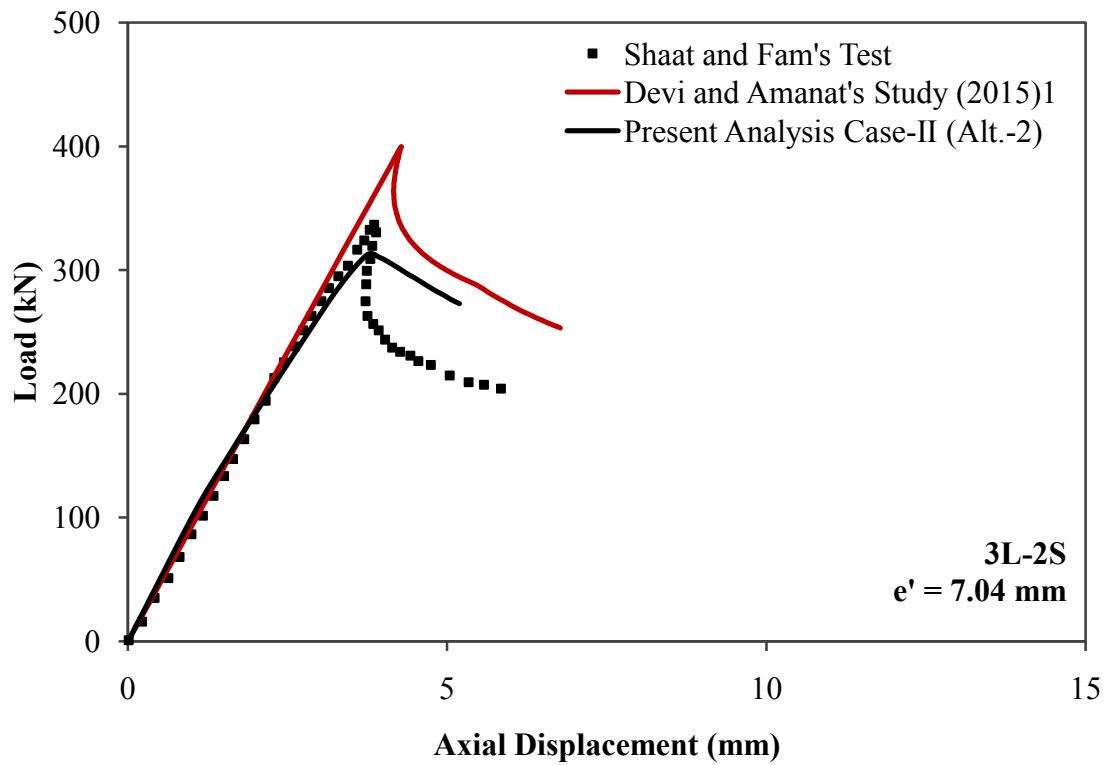
Figure 4.13: Load vs. Axial Displacement Behavior for Axially Loaded Strengthened HSS Column Specimen (Three layers and two sided CFRP) for Case Study-II (Alt.-2) Modified.
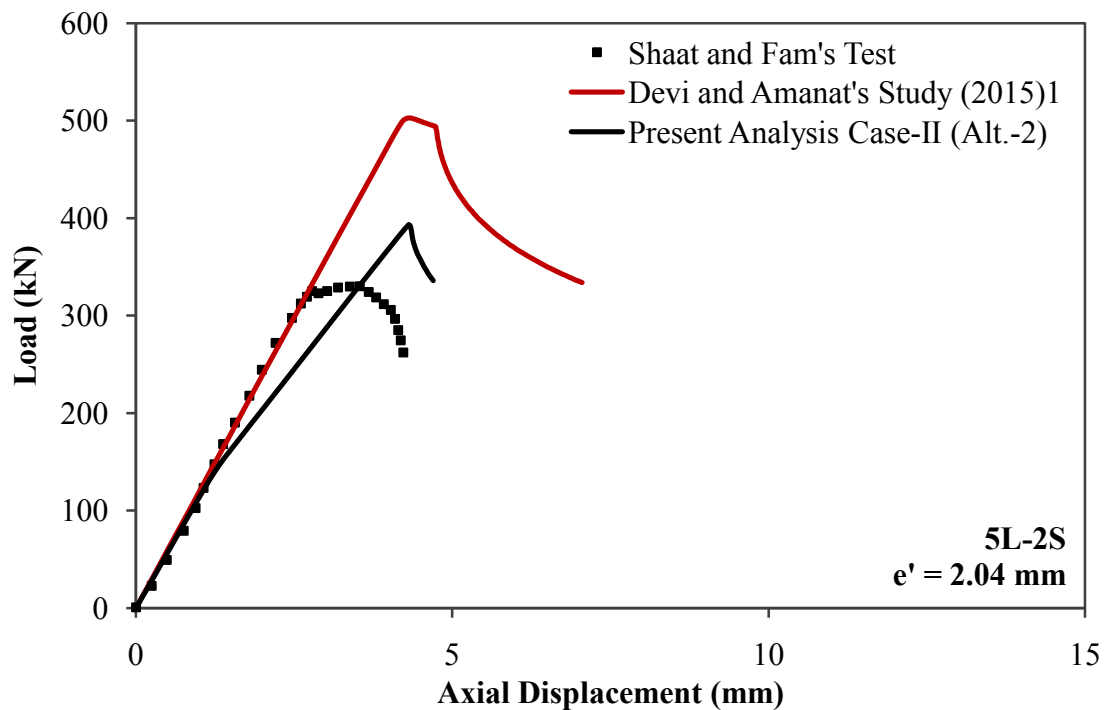
Figure 4.14: Load vs. Axial Displacement Behavior for Axially Loaded Strengthened HSS Column Specimen (Five layers and two sided CFRP) for Case Study-II (Alt.-2).
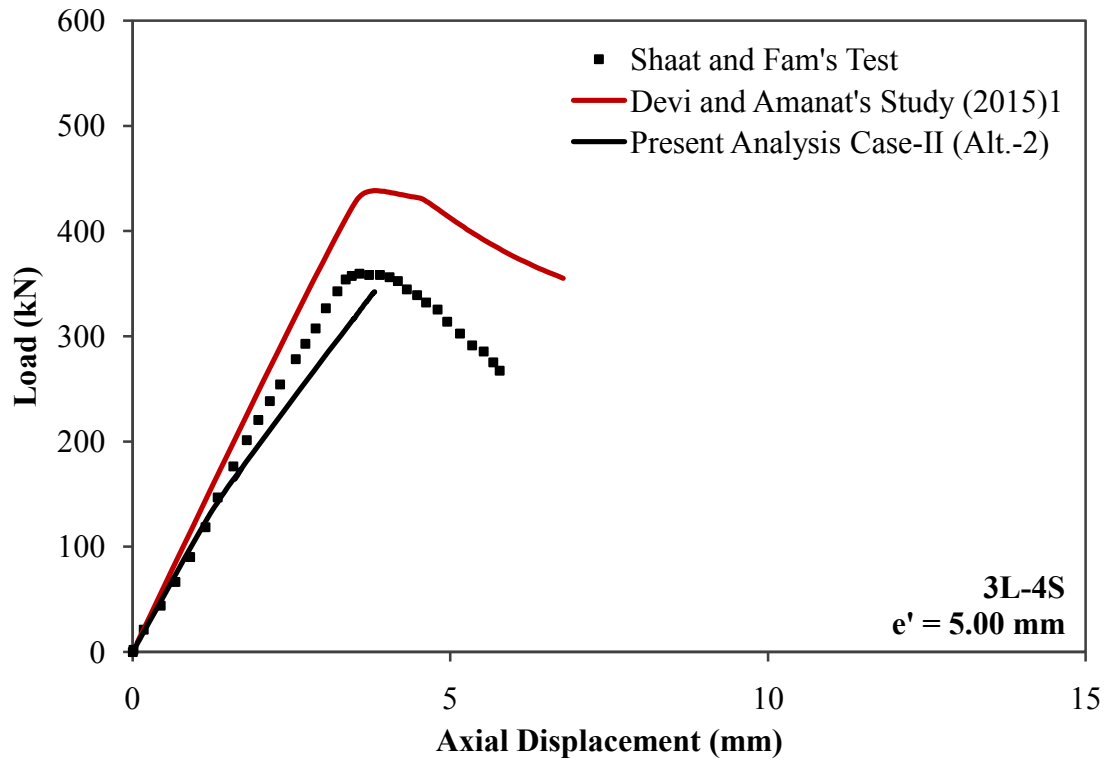
Figure 4.15: Load vs. Axial Displacement Behavior for Axially Loaded Strengthened
HSS Column Specimen (Three layers and four sided CFRP) for Case
Study-II (Alt.-2).
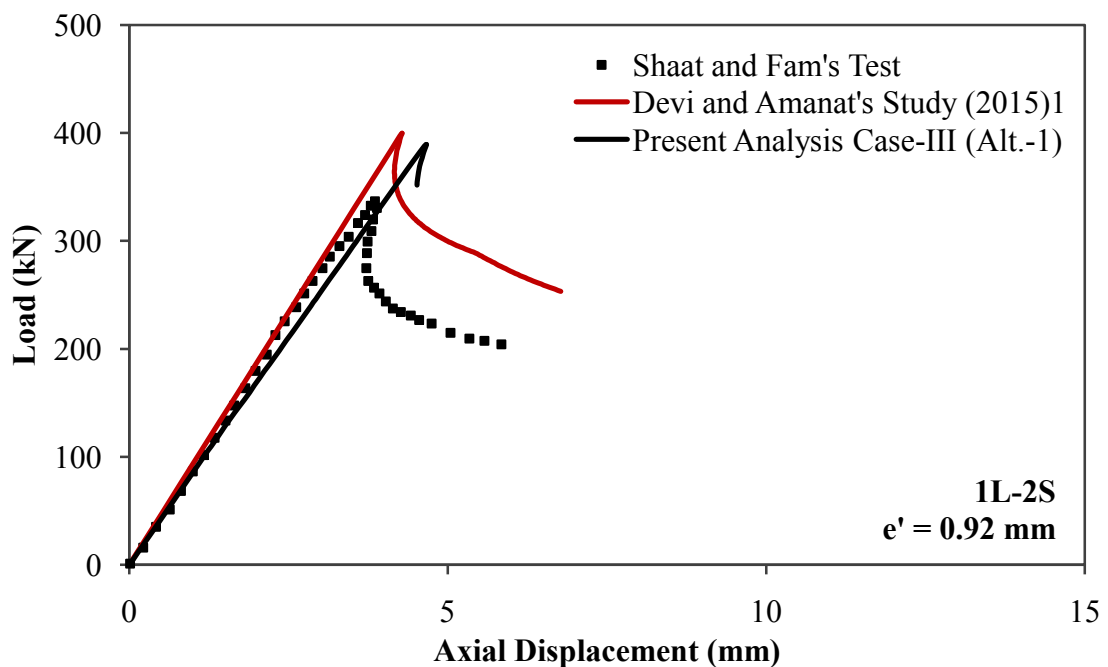
Figure 4.16: Load vs. Axial Displacement Behavior for Axially Loaded Strengthened
HSS Column Specimen (One layer and two sided CFRP) for Case Study-
III (Alt.-1).
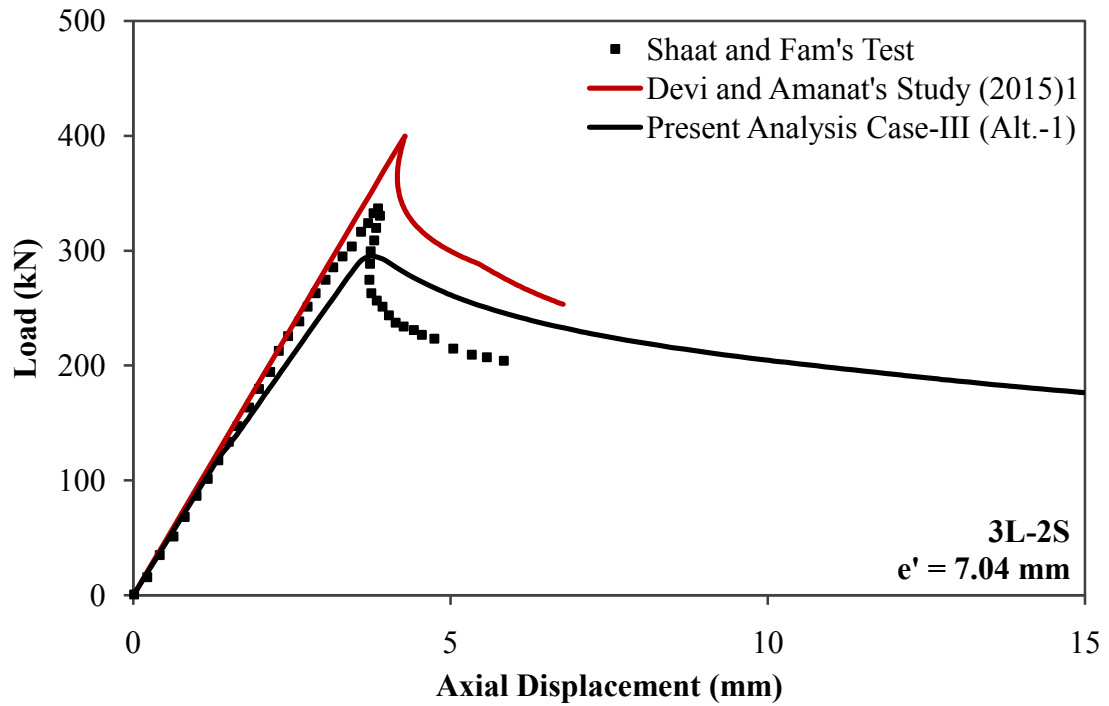
Figure 4.17: Load vs. Axial Displacement Behavior for Axially Loaded Strengthened HSS Column Specimen (Three layers and two sided CFRP) for Case Study-III(Alt.-1).
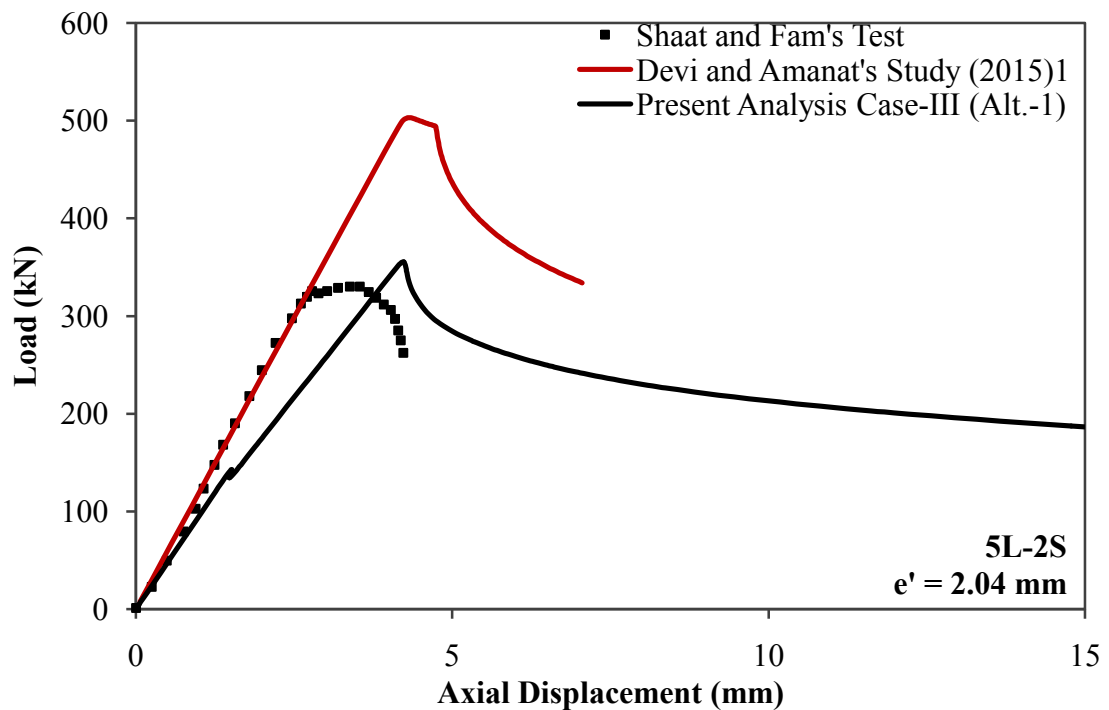
Figure 4.18: Load vs. Axial Displacement Behavior for Axially Loaded Strengthened HSS Column Specimen (Five layers and two sided CFRP) for Case Study-III (Alt.-1).
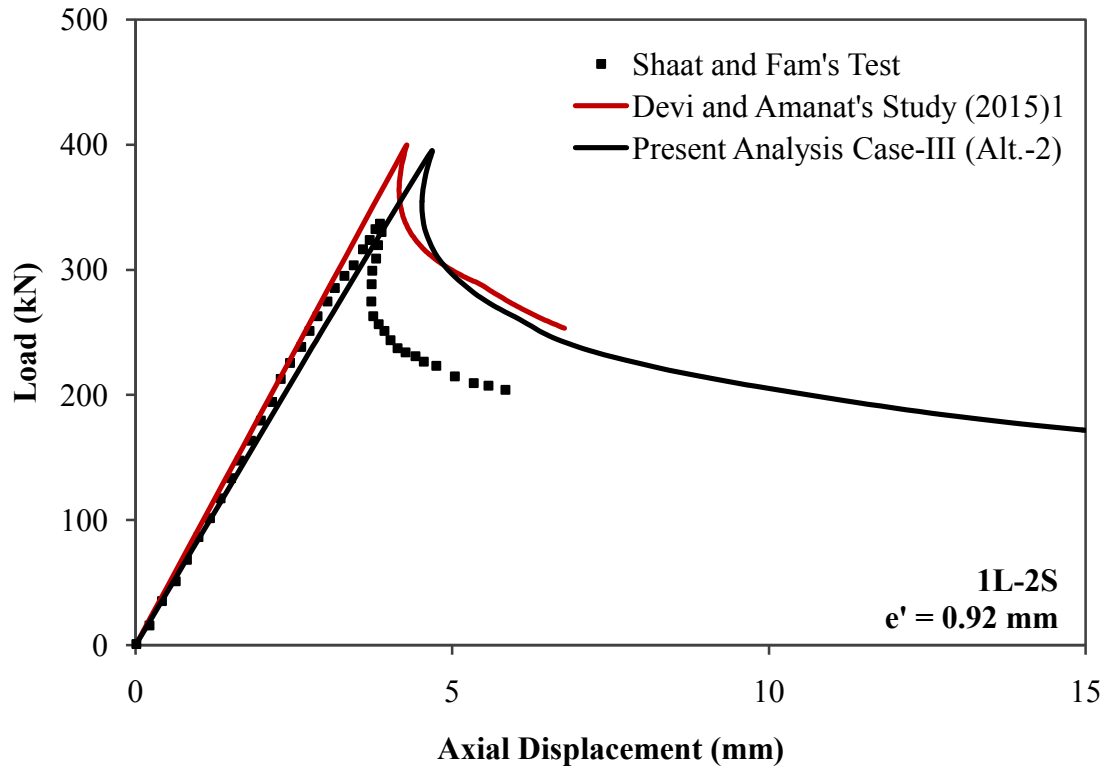
Figure 4.19: Load vs. Axial Displacement Behavior for Axially Loaded Strengthened HSS Column Specimen (One layer and two sided CFRP) for Case Study-III (Alt.-2).
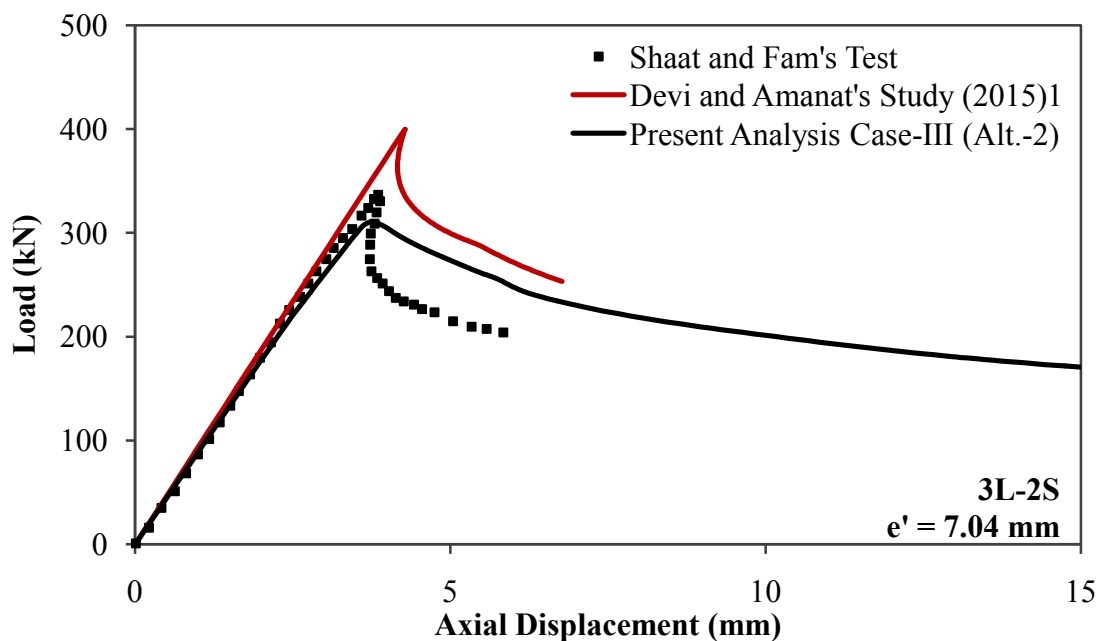
Figure 4.20: Load vs. Axial Displacement Behavior for Axially Loaded Strengthened HSS Column Specimen (Three layers and two sided CFRP) for Case Study-III(Alt.-2).
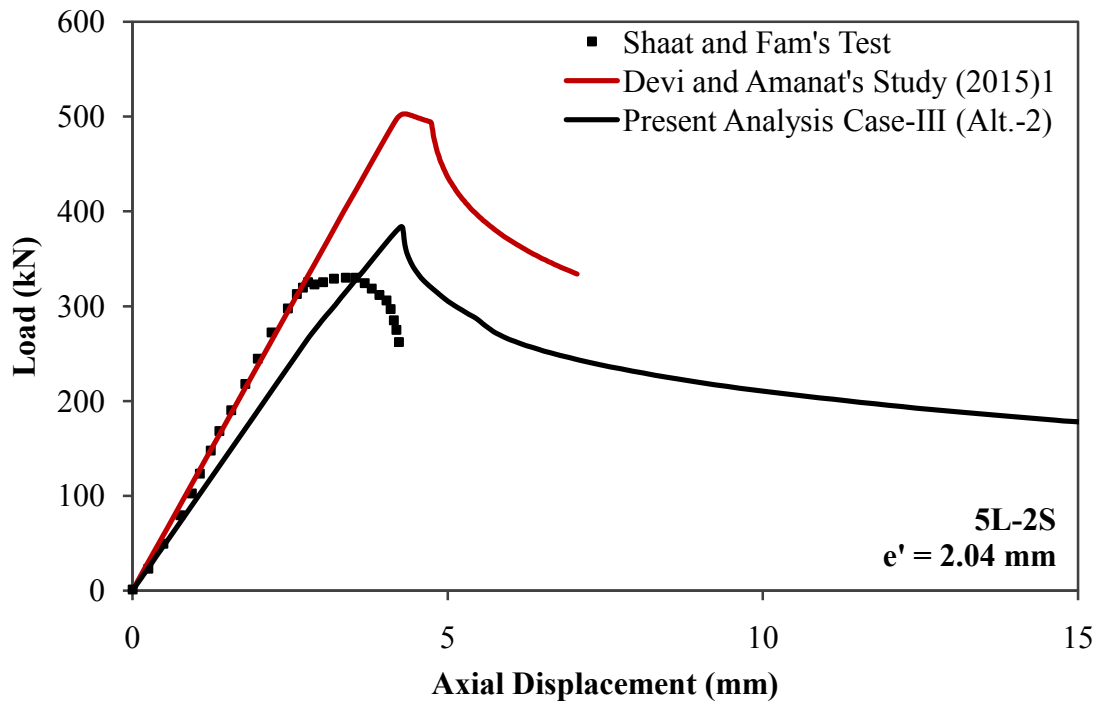
Figure 4.21: Load vs. Axial Displacement Behavior for Axially Loaded Strengthened HSS Column Specimen (Five layers and two sided CFRP) for Case Study-III (Alt.-2).
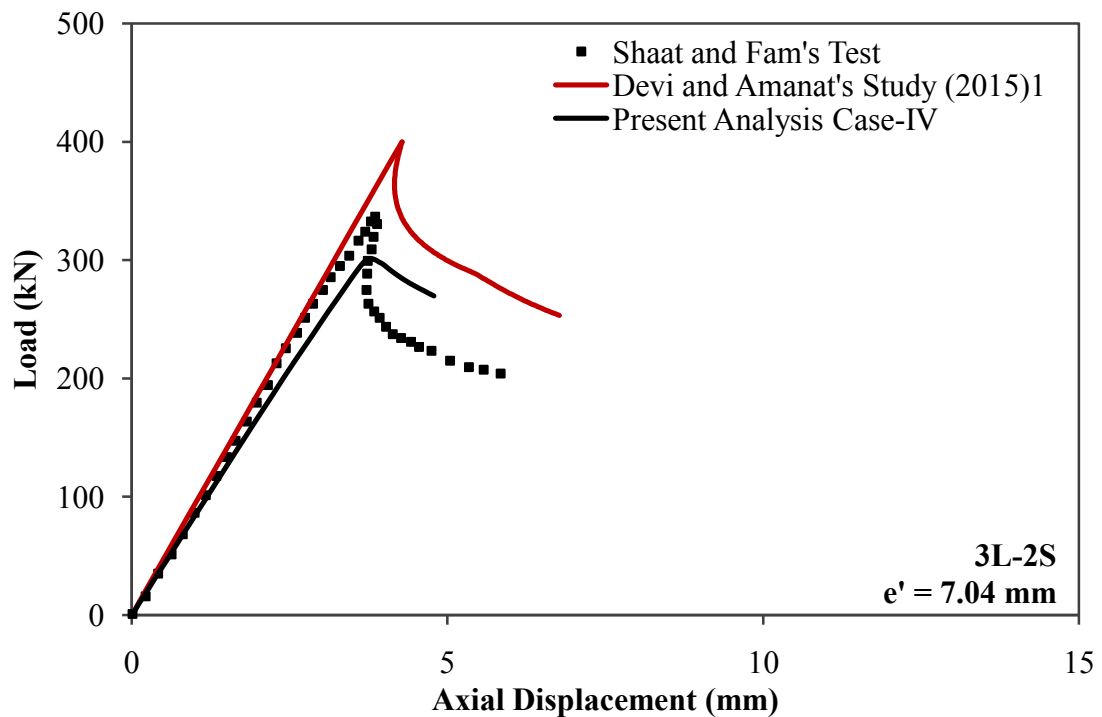
Figure 4.22: Load vs. Axial Displacement Behavior for Axially Loaded Strengthened HSS Column Specimen (Three layers and two sided CFRP) for Case Study-IV.
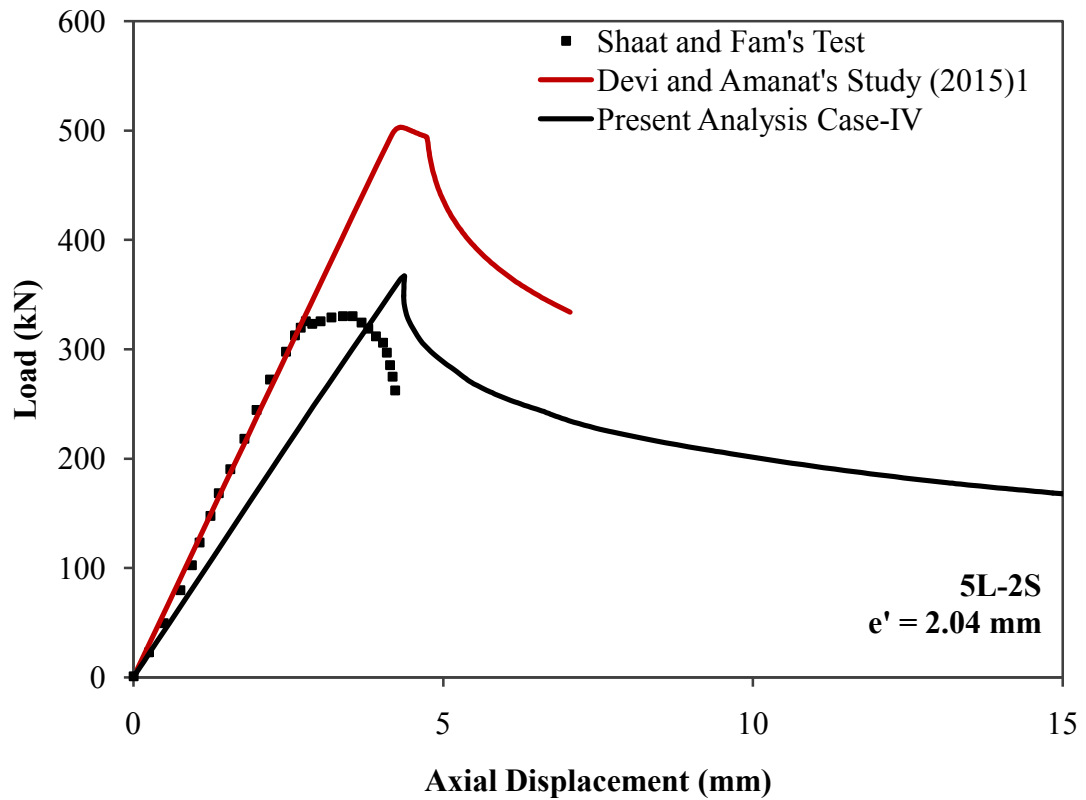
Figure 4.23: Load vs. Axial Displacement Behavior for Axially Loaded Strengthened HSS Column Specimen (Five layers and two sided CFRP) for Case Study-IV.

4.3.2   VERIFICATION OF AXIAL STRENGTH GAIN FROM NUMERICAL MODEL COMPARED TO EXPERIMENTAL MODEL RESULTS

This can be carried out by comparing the maximum load of the column obtained from both models, numerical and experimental. A summary of the numerical and experimental ultimate loads is presented in Table 4.4.

Table 4.4: Comparison between Experimental and Numerical Model Results.

Specimen Identification	$\frac{KL}{r}$	e' (mm)	Maximum Load (kN)				(Devi and Amanat's Study (2015)[1]/ Exp.) Ratio	(Present Analysis/ Exp.) Ratio
			Exp. of Shaat and Fam (2007)	Devi and Amanat's Study (2015)[1]	Present Analysis Cases	Present Analysis		
89 × 89 × 3.2 (Control)	68	6.60	295	268.33	-	295.296	0.91	1.001
89 × 89 × 3.2 (1L-2S)	68	0.92	355	399.69	Case-I	429.527	1.13	1.209
					Case-II (Alt.-1)	396.389		1.117
					Case-II (Alt.-2)	429.452		1.209
					Case-III (Alt.-1)	389.231		1.096
					Case-III (Alt.-2)	395.144		1.113
					Case-IV	393.373		1.108
89 × 89 × 3.2 (3L-2S)	68	7.04	335	363.68	Case-I	399.929	1.09	1.194
					Case-II (Alt.-1)	304.795		0.910
					Case-II (Alt.-2)	312.342		0.932
					Case-III (Alt.-1)	295.492		0.882
					Case-III (Alt.-2)	310.86		0.930
					Case-IV	300.857		0.90
89 × 89 × 3.2 (5L-2S)	68	2.04	332	503.02	Case-I	557.322	1.52	1.679
					Case-II (Alt.-1)	390.123		1.175
					Case-II (Alt.-2)	393.405		1.185
					Case-III (Alt.-1)	355.371		1.070
					Case-III (Alt.-2)	383.807		1.156
					Case-IV	367.143		1.106
89 × 89 × 3.2 (3L-4S)	68	5.00	362	438.31	Case-I	452.849	1.21	1.251
					Case-II (Alt.-1)	333.603		0.922
					Case-II (Alt.-2)	342.387		0.946
					Case-III (Alt.-1)	343.9		0.95
					Case-III (Alt.-2)	356.57		0.985
					Case-IV	404.354		1.117

4.3.3   COMPARISON OF DEFORMED SHAPES IN BETWEEN EXPERIMENTAL AND NUMERICAL MODEL

For all the experimental models, failure was mainly due to excessive overall buckling [Figure 4.24(a)], followed by a secondary local buckling in the compression side in the form of inward buckling of the compression face and outward buckling of the side faces [Figure 4.24(b)].

(b) Specimen
retrofitted at
2 sides

(a)Overall
Buckling

(c) Specimen
retrofitted at
4 sides
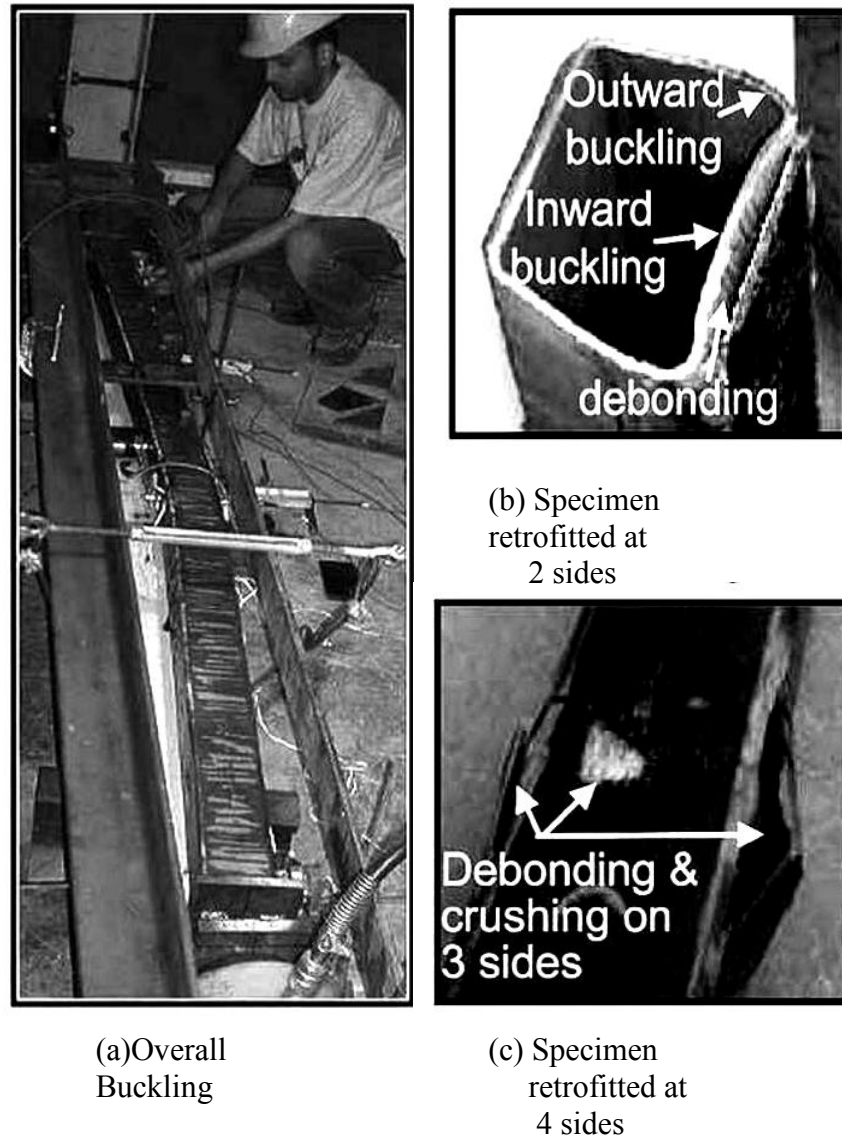
Figure 4.24: Failure Modes of the Experimental Models (Shaat and Fam 2007).

For the FRP-strengthened specimens, the secondary local buckling was associated with a combined debonding at the interface between the adhesive and steel surface and crushing of FRP sheets. For specimen 3L-4S, the FRP on the sides have also fractured due to outward local buckling [Figure 4.24(c)].

In the numerical model, for control and all other strengthened specimens are subjected to overall buckling similar to that of experimental model [Figure 4.24 (a)]. The deformed shapes related to such phenomenon are shown in Figure 4.25. Moreover, the strengthened specimens are subjected to secondary local buckling in the compression side as shown in Figure 4.26, which is also have resemblance with the failure mode of experimental model [Figure 4.24 (b)] and also with the practical local buckling phenomenon [Figure 2.4].
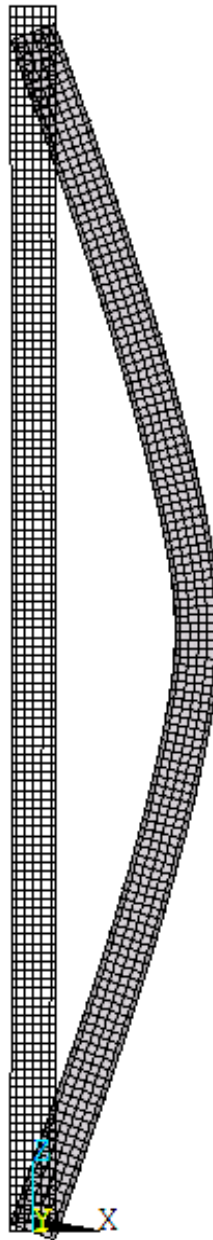
Figure 4.25: Deformed shape along with Undeformed shape of 1L-2S Strengthened Column Specimen obtained from Finite Element Model.
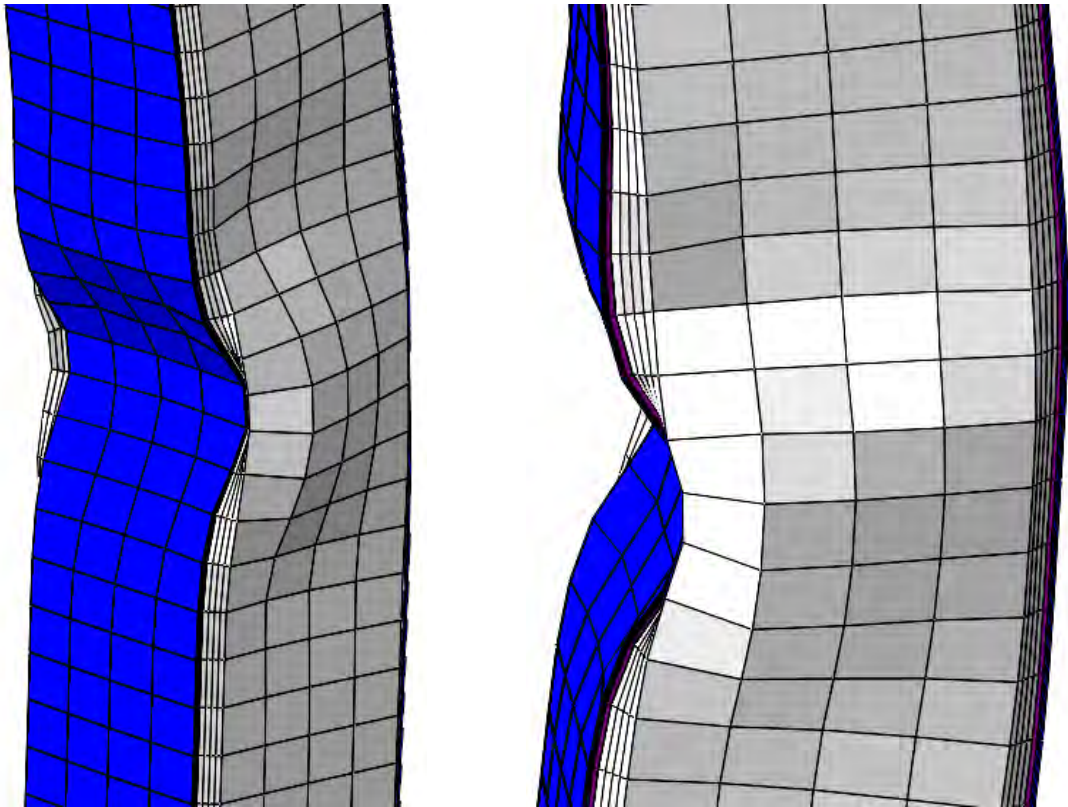
Figure 4.26: Close view of Deflected shape.

4.3.4 DISCUSSION AGAINST VERIFICATION OF EXPERIMENTAL MODEL (SHAAT AND FAM 2007) AND PROPOSED NUMERICAL MODEL FOR PARAMETRIC STUDY

From the graphical representation of verification, Case-II (Alt.-2), Case-III (Alt.-2) and Case-IV shows good agreement with the Shaat and Fam's (2007) test results in respect of peak load and stiffness as shown in Figure 4.3 to Figure 4.23. Again comparative graphical representation has also been conducted among the three best case studies considered as shown in Figure 4.27 to Figure 4.31. It is seen that Case-III (Alt.-2) governs over Case-IV (Figure 4.27 & Figure 4.28) since in Case-III (Alt.-2), peak load is near experimental maximum load and also stiffness of the composite material is closer to the experimental model stiffness. Case-III (Alt.-2) has also been compared with the Case-II (Alt.-2) where similar results has been obtained in respect of peak load and stiffness as shown in Figure 4.29 to Figure 4.31. But computational time is much less in Case-III (Alt.-2) than Case-II (Alt.-2). Thus it has been decided to conduct the further parametric studies with the key modeling features of Case-III (Alt.-2). From Table 4.4, it is seen that the results obtained from the present analysis

is close enough to the results obtained from experimental study. So the proposed model can be satisfactorily used for further parametric study.
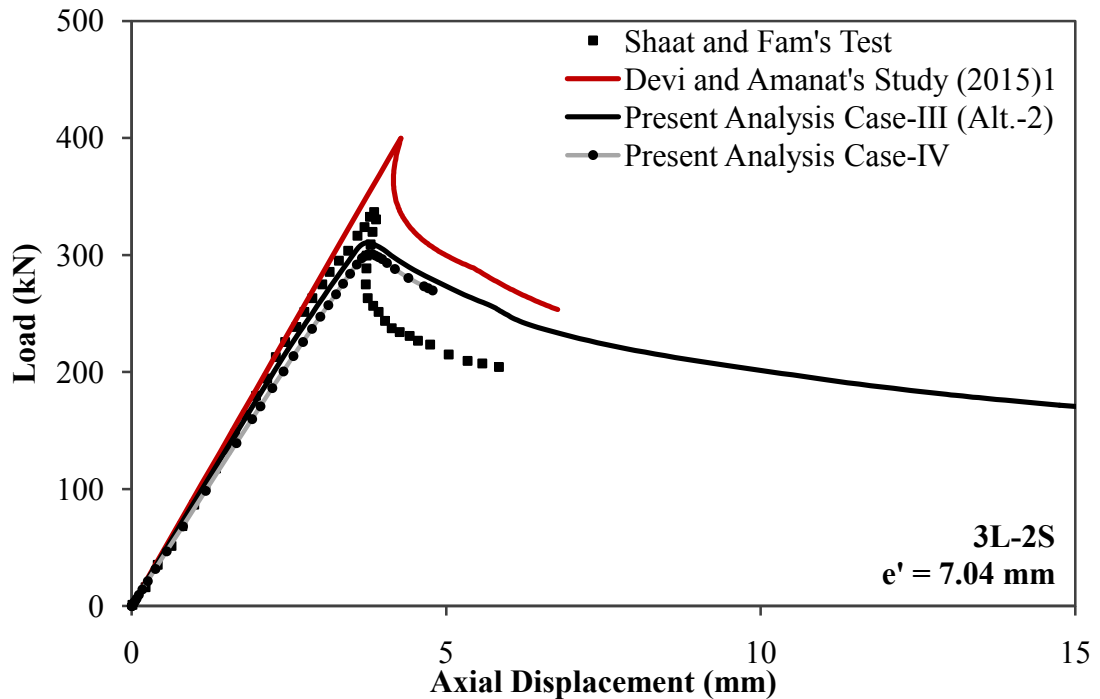
Figure 4.27: Load vs. Axial Displacement Behavior for Axially Loaded Strengthened HSS Column Specimen Comparing Case-III (Alt.-2) and Case-IV (Three layers and two sided CFRP).
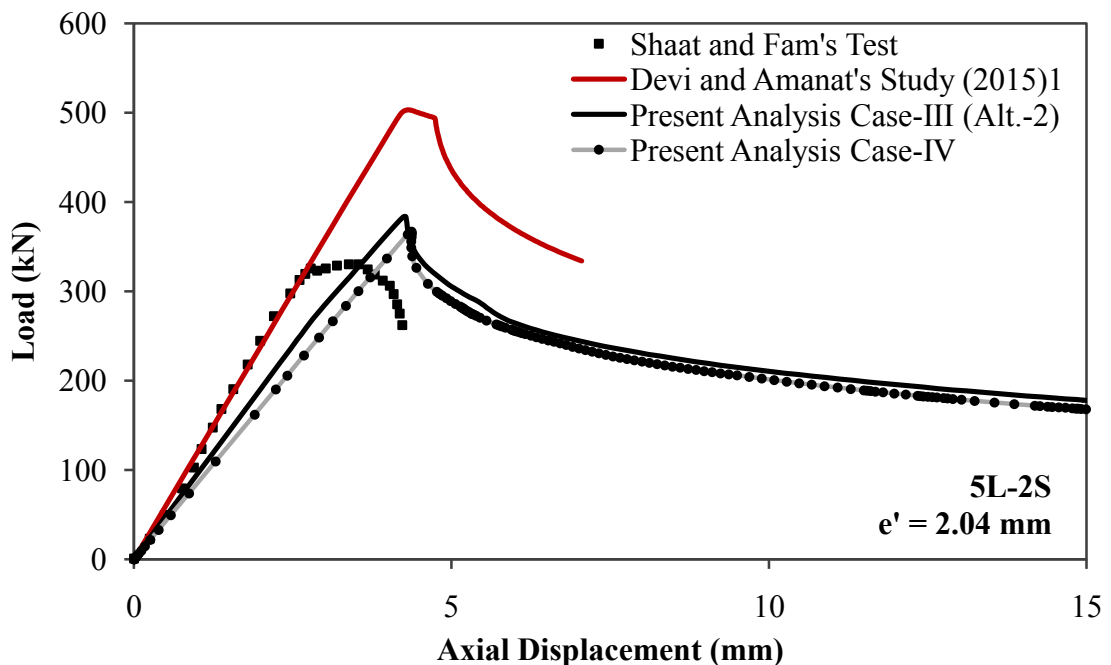
Figure 4.28: Load vs. Axial Displacement Behavior for Axially Loaded Strengthened HSS Column Specimen Comparing Case-III (Alt.-2) and Case-IV (Five layers and two sided CFRP).
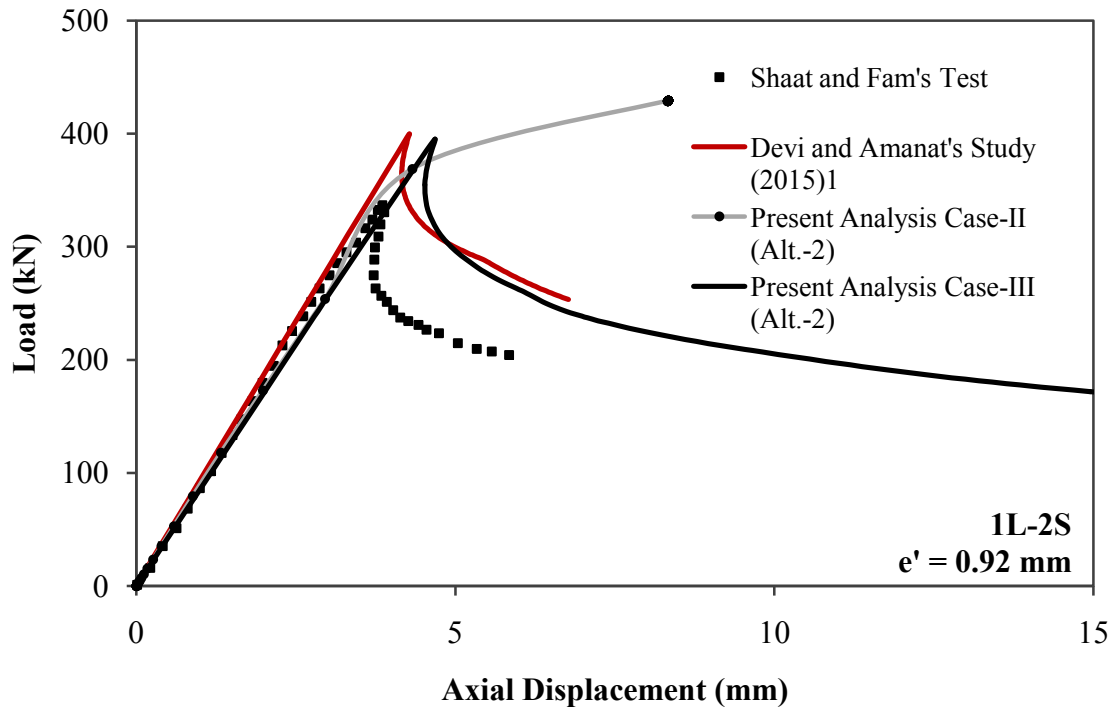
Figure 4.29: Load vs. Axial Displacement Behavior for Axially Loaded Strengthened
HSS Column Specimen Comparing Case-II (Alt.-2) and Case-III (Alt.-2)
(One layer and two sided CFRP).
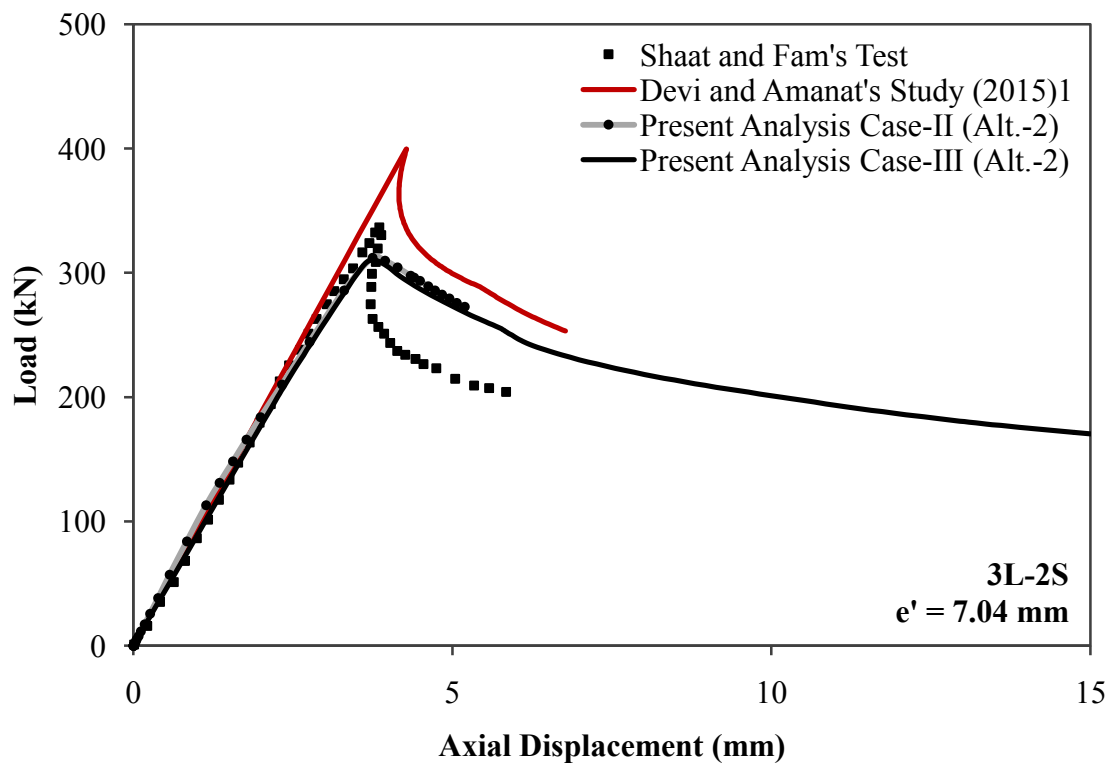
Figure 4.30: Load vs. Axial Displacement Behavior for Axially Loaded Strengthened
HSS Column Specimen Comparing Case-II (Alt.-2) and Case-III (Alt.-2)
(Three layers and two sided CFRP).
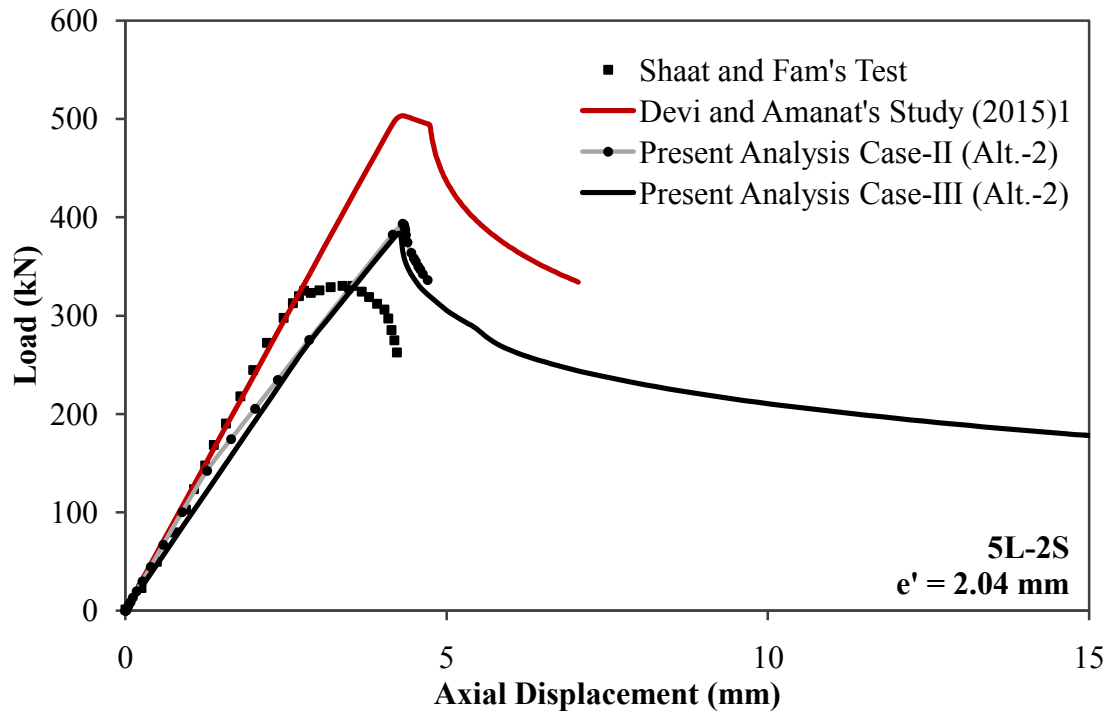
Figure 4.31: Load vs. Axial Displacement Behavior for Axially Loaded Strengthened
            HSS Column Specimen Comparing Case-II (Alt.-2) and Case-III (Alt.-2)
            (Five layers and two sided CFRP).

4.4 REMARKS

As a summary of this Chapter, it can be said that the finite element model developed in Chapter 3 is adequate enough to simulate the experimental test results. Therefore the same model can be used for further numerical study instead of performing experimental research works. The parametric study using this model has been carried out in the following Chapter 5.

Chapter 5

PARAMETRIC STUDY WITH DISCUSSIONS

5.1   INTRODUCTION

The finite element model developed in Chapter 3 using Abaqus 6.14-4 has been verified with reference to the experimental study performed by Shaat and Fam in 2007 in Chapter 4 to conclude whether the model is adequate enough for the numerical simulation of practical test results and satisfactory results has been obtained. Now using this proposed finite element model a parametric study on AISC square HSS (Hollow Structural Section) column sections will be carried out in this chapter. Preference has been given on the study of non-compact sections, since such sections are more susceptible to buckling related problem. Better achievement in strengthening such non-compact sections could be followed by the easy application of strengthening in the compact sections.

5.2   DETAILS OF SQUARE HSS SECTIONS FROM AISC MANUAL OF STEEL CONSTRUCTION (13th EDITION, 2005)

The square HSS sections available in the AISC manual are provided in Table A-1 in the Appendix A portion. Now for the sections tabulated, compactness criteria need to be checked to decide on whether a particular section would have adequate width to thickness ratio against local buckling phenomenon.

5.3   CHECK OF COMPACTNESS CRITERIA OF SQUARE HOLLOW STRUCTURAL SECTIONS (HSS) FROM AISC MANUAL

For such typical square HSS sections, shown in Figure 5.1, to be compact sections, criteria need to be fulfilled is

$$\frac{b}{t} \leq \frac{253}{\sqrt{F_y}} \qquad (5.1)$$

which is given in the Table 2.1. If the compactness criterion is not fulfilled, the section will then be considered as non-compact section.
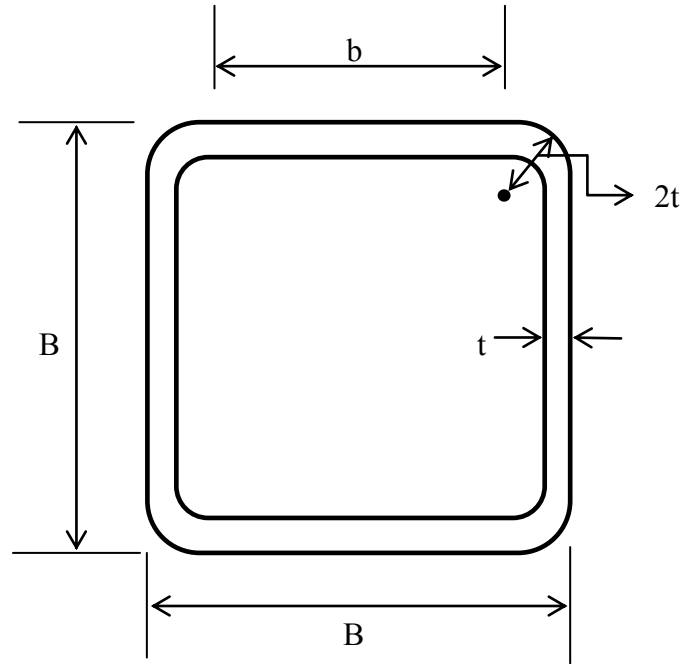
Figure 5.1: Typical Square HSS Section.

Let us consider an AISC section HSS16×16×⅜ for which

$B = 16 \text{ in}$

Design wall thickness, $t = 0.349 \text{ in}$

Therefore, $b = 16 - 3t = 16 - 3 \times 0.349 = 14.953 \text{ in}$

$$\frac{b}{t} = \frac{14.953}{0.349} = 42.84$$

Now,

$$\frac{253}{\sqrt{F_y}} = \frac{253}{\sqrt{(380 \times 145)/1000}} = 34.1$$

Since $\dfrac{b}{t} > \dfrac{253}{\sqrt{F_y}}$ the section HSS16×16×⅜ is a non-compact section. The compactness criteria for each of the AISC square HSS sections are given in the Appendix A portion.

5.4 PARAMETRIC STUDY ON SQUARE HOLLOW STRUCTURAL SECTIONS (HSS)

As we see from Table A-1 in Appendix A, most of the sections are non-compact with their least thicknesses. Some of the non-compact sections and one compact section are chosen for parametric study since non-compact sections are more susceptible to buckling phenomenon. So if the capacity of such non-compact sections can be increased adequately by strengthening with CFRP retrofitting materials, other compact sections may be strengthened without facing any problem.

5.4.1 AISC SQUARE HSS SECTIONS SELECTED FOR PARAMETRIC STUDY

The AISC square HSS sections chosen for parametric study are listed in Table 5.1.

5.4.2 TABULAR REPRESENTATION OF PARAMETRIC STUDY

In this section the finite element model has been used in a parametric study to evaluate the effect of slenderness ratios (varying from $0.25C_c$ to $1.5C_c$ with an increment of $0.25C_c$) and effect of number of CFRP layers (control, 1, 3, and 5 layers). Therefore a total of 168 square HSS column sections, 24 of each, are taken to conduct the parametric study. Material properties are kept same as those used in the experimental analysis. Complete results obtained from the numerical simulation using ABAQUS 6.14-4 for the chosen AISC sections are given in Table B-1a to Table B-2g of Appendix B portion. For discussion purpose, works have been carried out with results of few sections in this Chapter. The results obtained from the tabular representation are then discussed considering the effects of number of CFRP layers the effect of slenderness ratios and also the effects of cross sectional geometry in the last portion of this chapter.

Table 5.1: Dimensions and Section Properties of chosen AISC Square HSS Sections
for Parametric Study.

Shape (Compact/ Non-compact)	Design Wall Thickness, t (in)	Nominal Wt. (lb/ft)	Area, A (in.^{2})	I (in.^{4})	r (in.)	$\dfrac{b}{t}$	$\dfrac{253}{\sqrt{F_y}}$
HSS16×16× 5/16 (Non-compact)	0.291	65.82	18.1	739	6.39	52.0	34.1
HSS14×14× 5/16 (Non-compact)	0.291	57.31	15.7	490	5.58	45.1	34.1
HSS12×12× 3/16 (Non-compact)	0.174	29.82	8.15	189	4.82	66.0	34.1
HSS9×9× ⅛ (Non-compact)	0.116	14.95	4.09	53.5	3.62	74.6	34.1
HSS7×7× ⅛ (Non-compact)	0.116	11.55	3.16	24.8	2.80	57.3	34.1
HSS5×5× ⅛ (Non-compact)	0.116	8.15	2.23	8.80	1.99	40.1	34.1
HSS3×3× ⅛ (Compact)	0.116	4.75	1.30	1.78	1.17	22.9	34.1

5.4.3   GRAPHICAL REPRESENTATION OF PARAMETRIC STUDY

Results obtained from the numerical simulation are shown in Figure 5.2 to Figure

5.14.
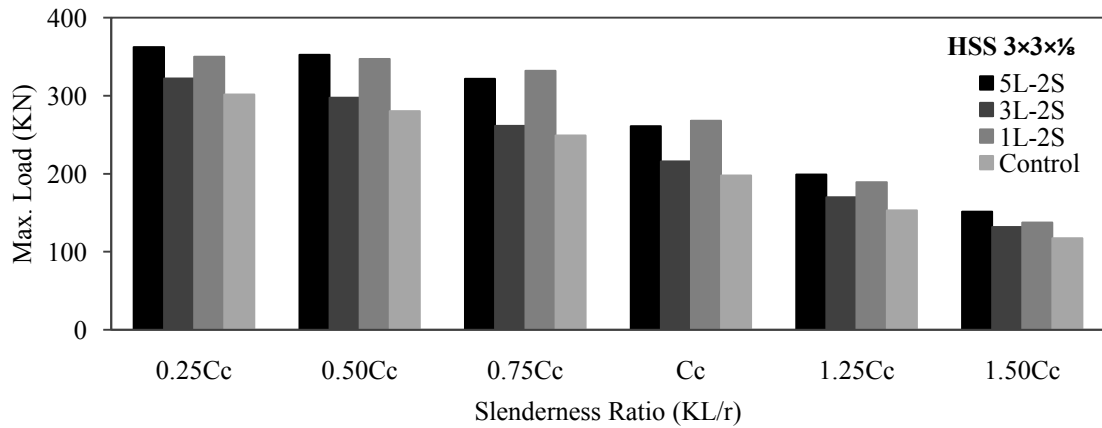
Figure 5.2: Maximum load obtained with varying slenderness ratio and varying no. of CFRP layers for AISC steel column HSS 3×3×⅛.
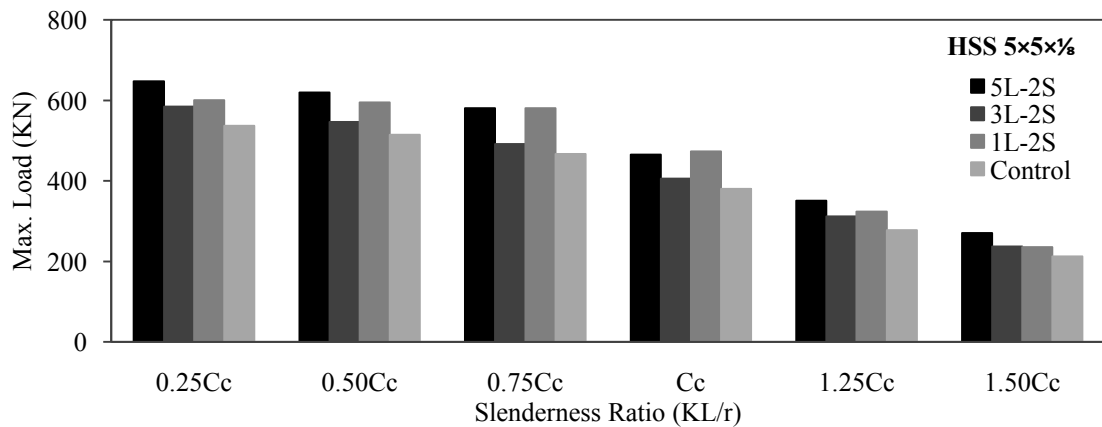
Figure 5.3: Maximum load obtained with varying slenderness ratio and varying no. of CFRP layers for AISC steel column HSS 5×5×⅛.
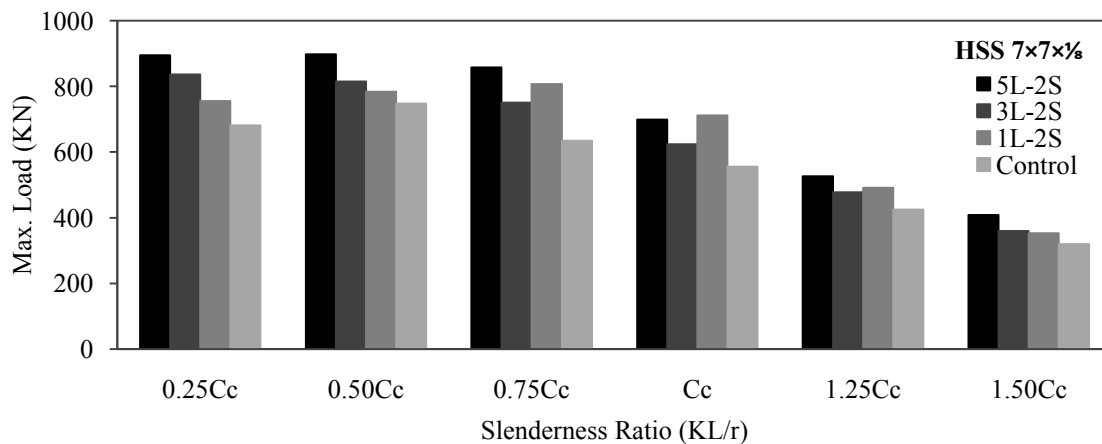
Figure 5.4: Maximum load obtained with varying slenderness ratio and varying no. of CFRP layers for AISC steel column HSS 7×7×⅛.
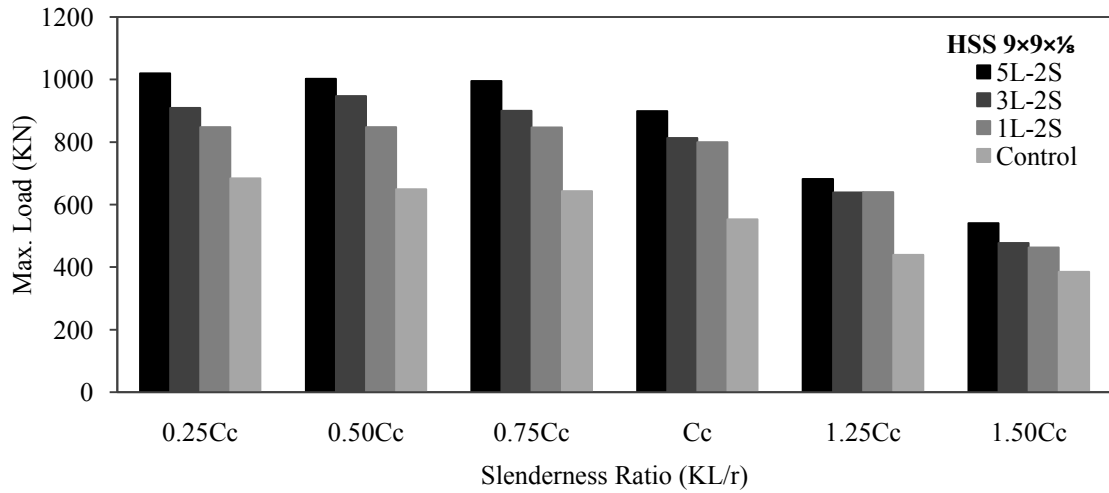
Figure 5.5: Maximum load obtained with varying slenderness ratio and varying no. of CFRP layers for AISC steel column HSS 9×9×⅛.
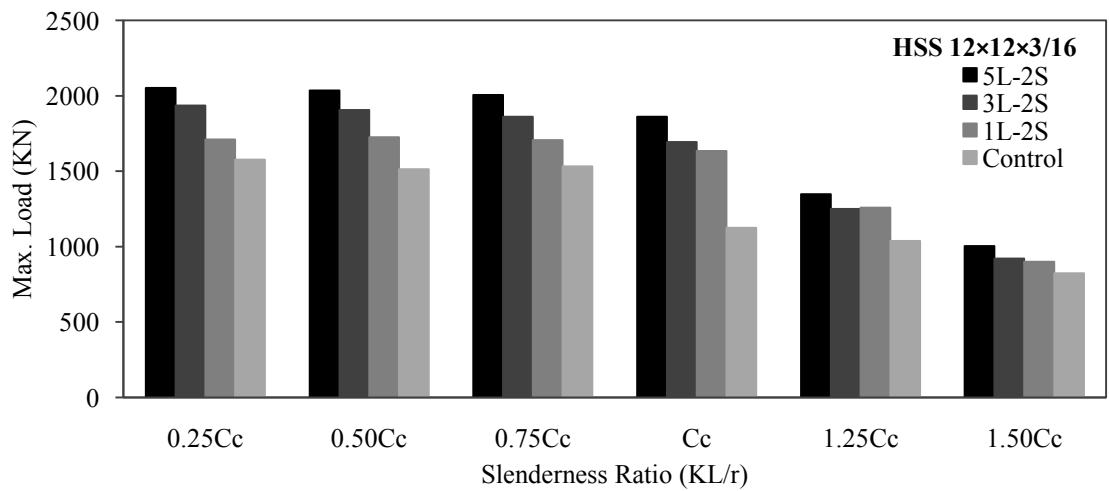
Figure 5.6: Maximum load obtained with varying slenderness ratio and varying no. of CFRP layers for AISC steel column HSS 12×12×3/16.
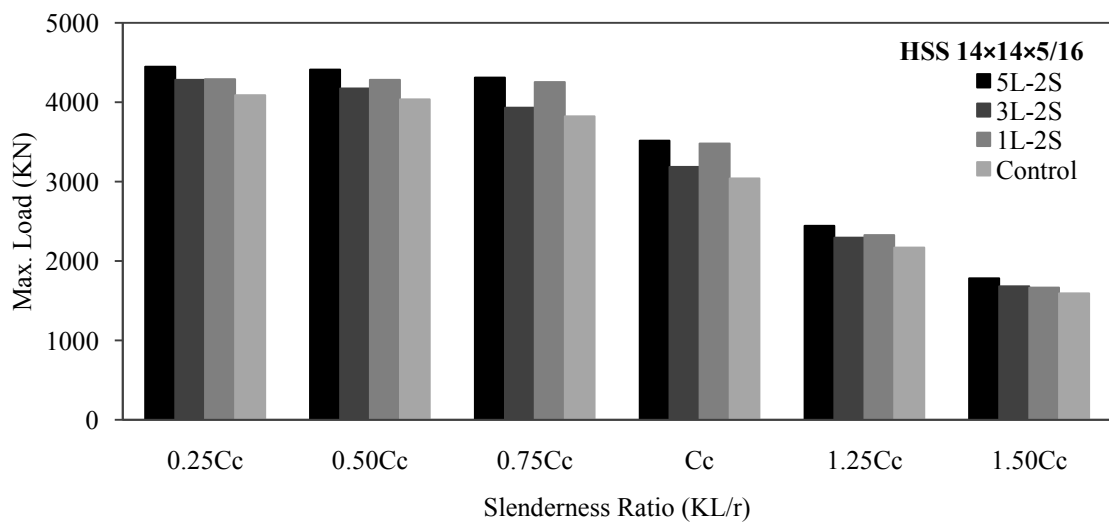
Figure 5.7: Maximum load obtained with varying slenderness ratio and varying no. of CFRP layers for AISC steel column HSS 14×14×5/16.
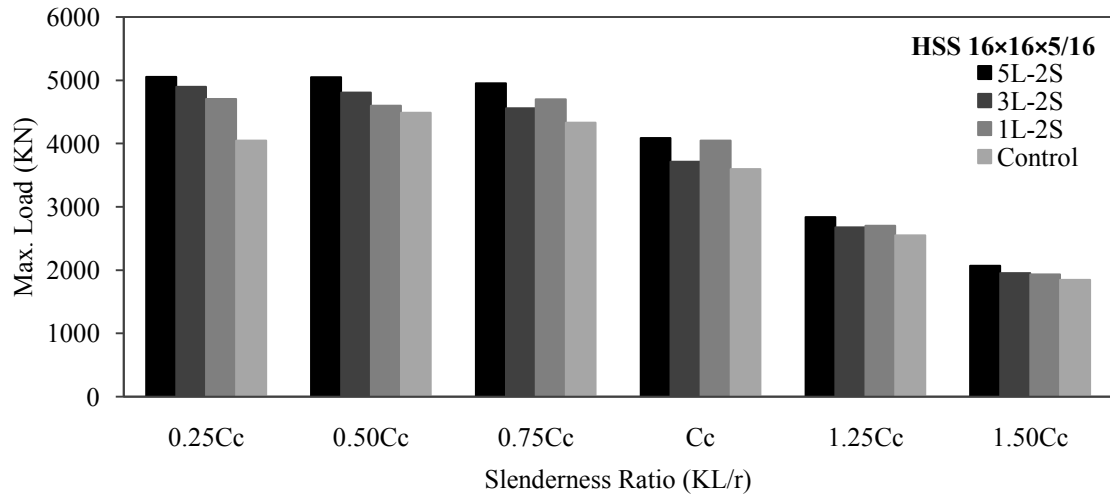
Figure 5.8: Maximum load obtained with varying slenderness ratio and varying no. of CFRP layers for AISC steel column HSS 16×16×5/16.
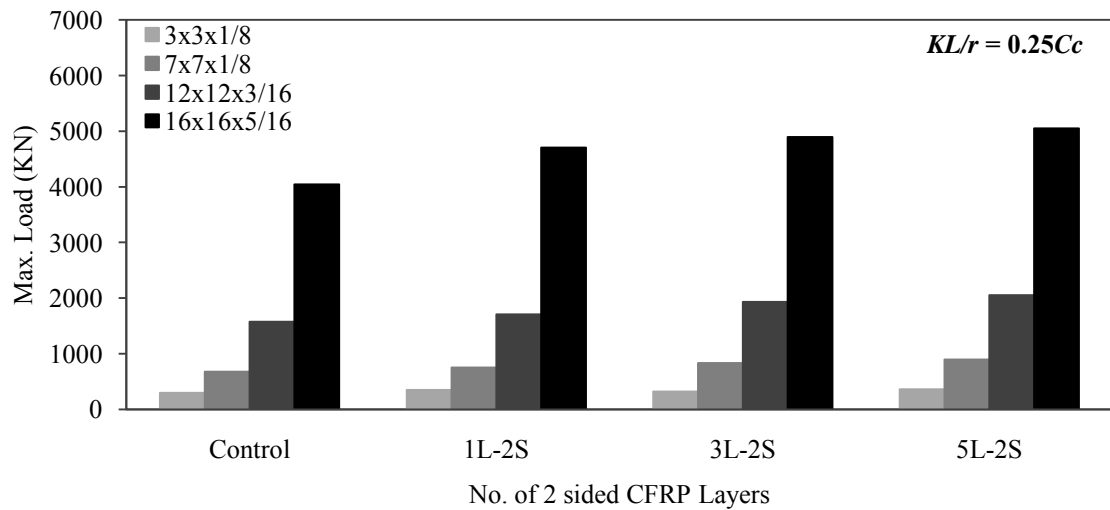
Figure 5.9: Effect of number of CFRP layers on the strength of AISC HSS column sections for slenderness ratio of $0.25C_c$.
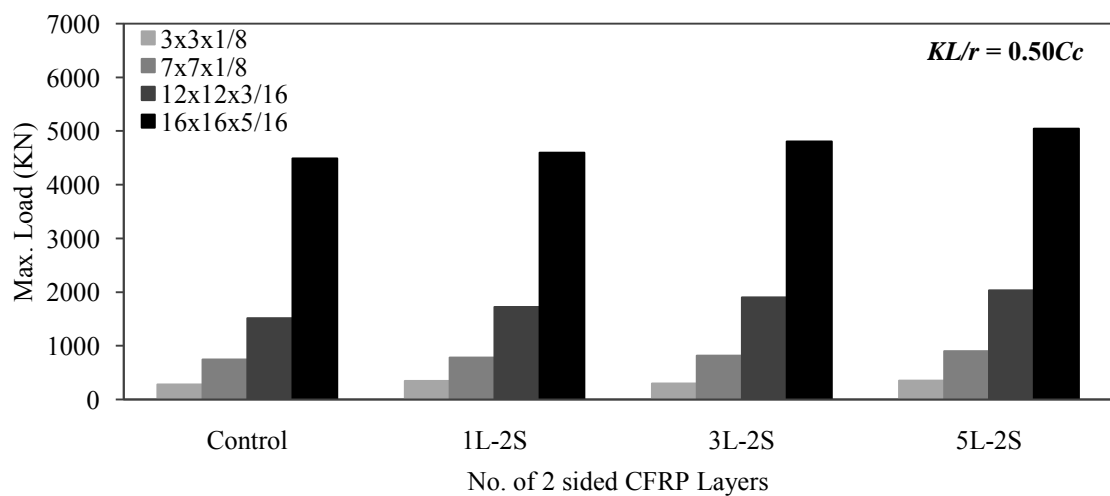
Figure 5.10: Effect of number of CFRP layers on the strength of AISC HSS column sections for slenderness ratio of $0.50C_c$.
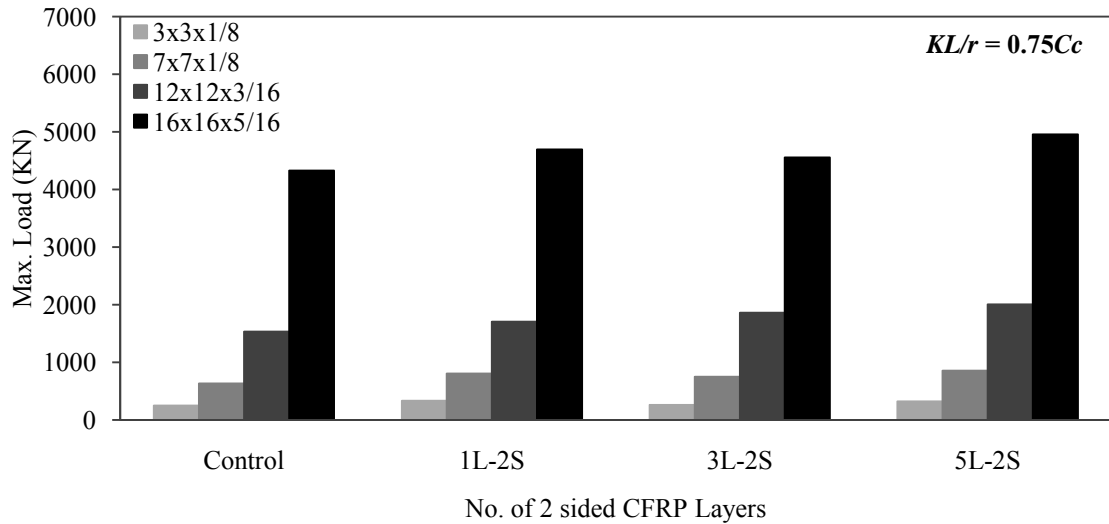
Figure 5.11: Effect of number of CFRP layers on the strength of AISC HSS column sections for slenderness ratio of $0.75C_c$.
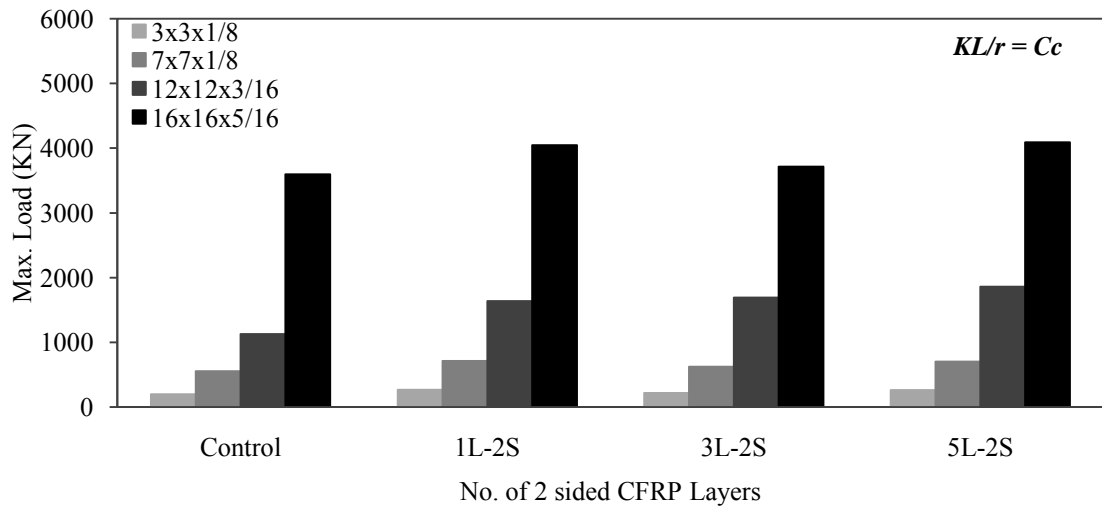
Figure 5.12: Effect of number of CFRP layers on the strength of AISC HSS column sections for slenderness ratio of C_c.
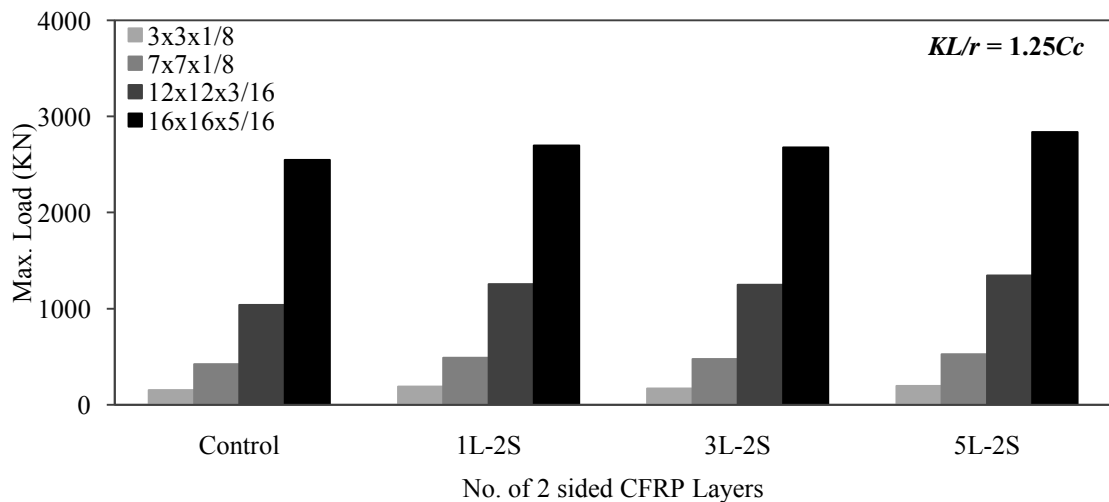
Figure 5.13: Effect of number of CFRP layers on the strength of AISC HSS column sections for slenderness ratio of $1.25C_c$.
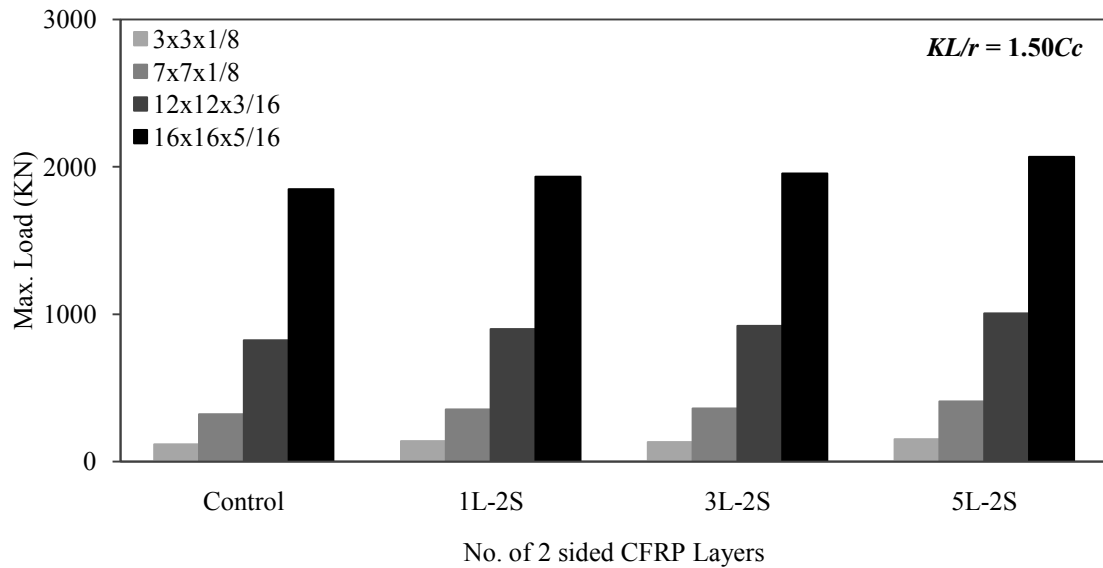
Figure 5.14: Effect of number of CFRP layers on the strength of AISC HSS column sections for slenderness ratio of $1.50C_c$.

5.5   DISCUSSION ON RESULTS

Based on the above parametric study on non-compact AISC square HSS sections, observations made from the tabular and graphical representations have been discussed in the following section.

5.5.1   EFFECT OF NUMBER OF CFRP LAYERS ON STRENGTH

The effect of number of CFRP layers on the behavior of AISC HSS column sections under compressive load have been observed by using bar charts presented in Figure 5.2 to Figure 5.14 and by using Table B-1a to B-1g which clearly shows that the application of CFRP materials to the unstrengthened square HSS column sections is capable of increasing their strength. Whenever the steel HSS column is subjected to deformation due to axial loading, the external bonding of CFRP strips provides sufficient restraining effect against elastic deformation and also delayed the local buckling and as a result the ultimate strength capacity is increased. Application of CFRP causes an increase in effective thickness which reduces the width-to-thickness ratio of cross sectional elements. This decrease in the slenderness of cross-sectional elements actually results in a delayed local buckling which ultimately enhances overall buckling strength of columns.
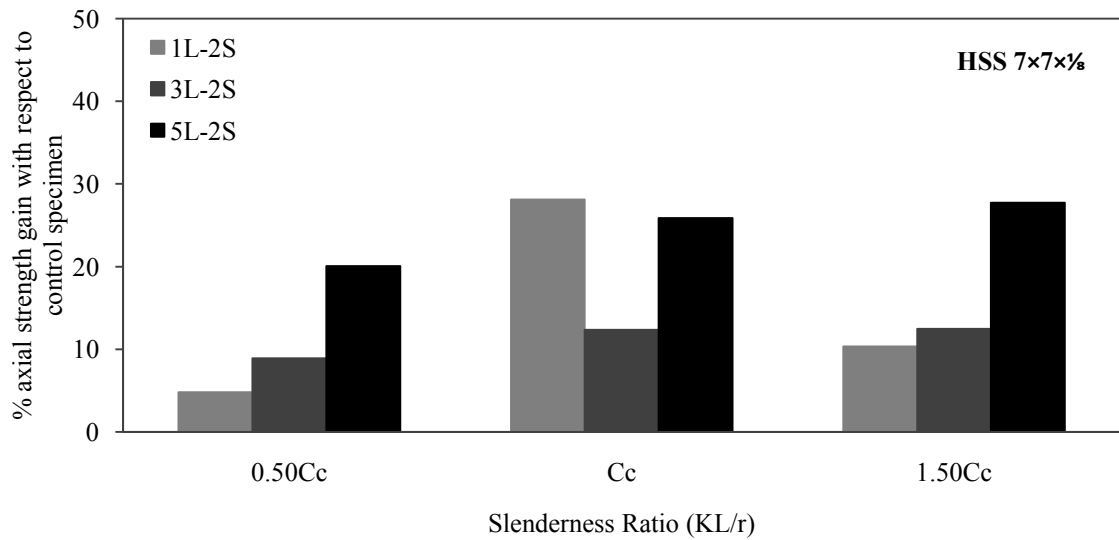
Figure 5.15: Percentage gain in axial strength for a relatively smaller section HSS 7×7×⅛.
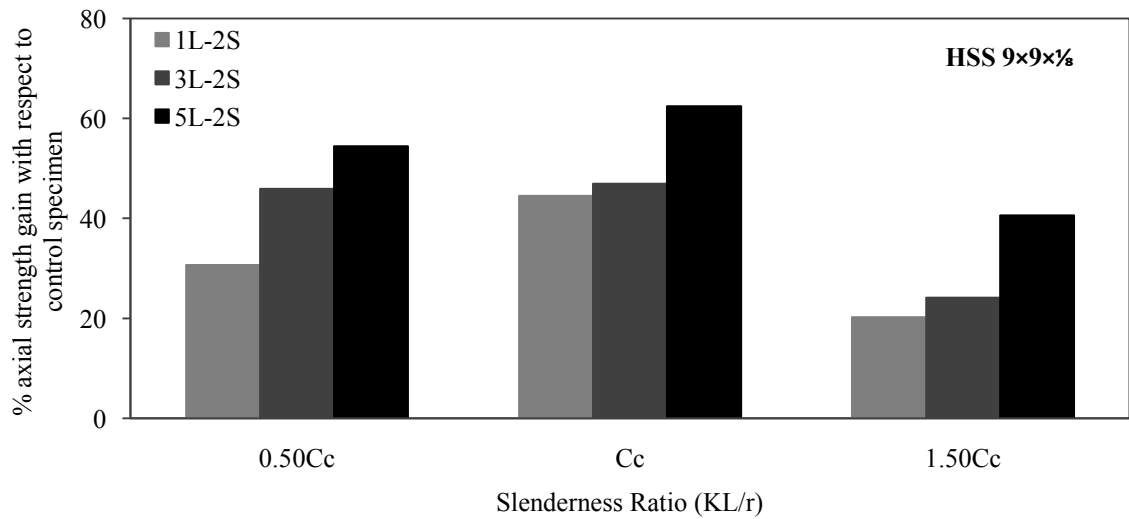
Figure 5.16: Percentage gain in axial strength for a relatively smaller section HSS 9×9×⅛.
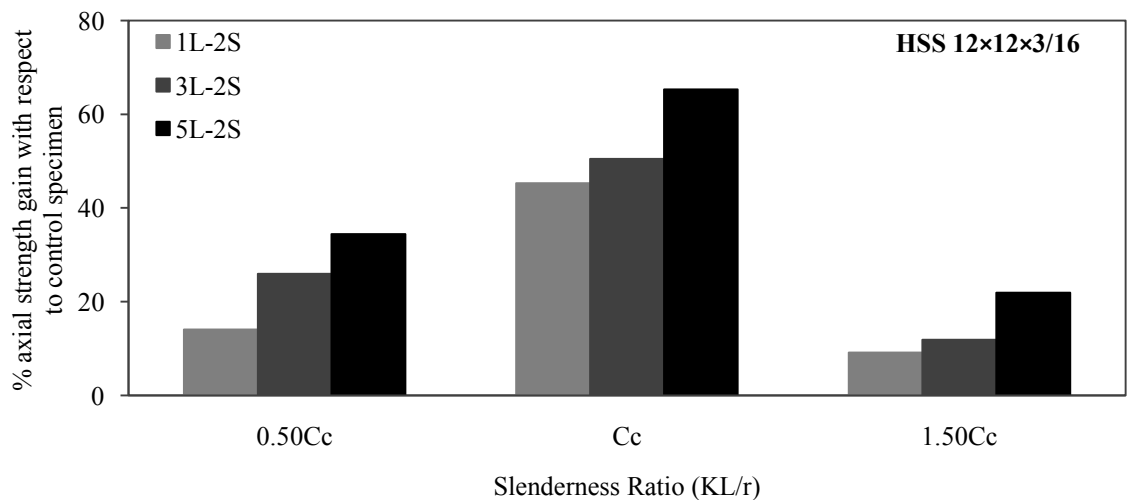
Figure 5.17: Percentage gain in axial strength for a relatively smaller section HSS 12×12×3/16.
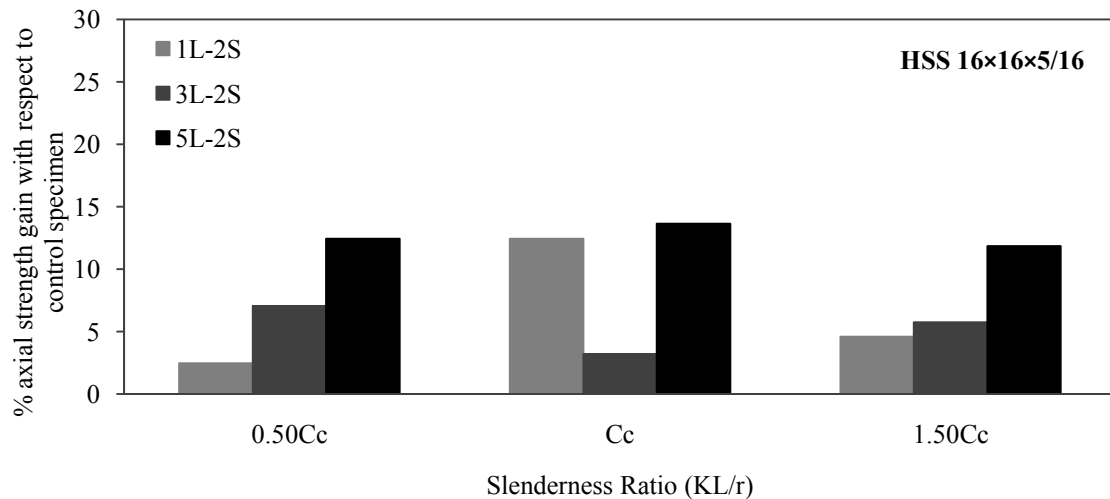
Figure 5.18: Percentage gain in axial strength for a relatively smaller section HSS
16×16×5/16.

The axial strength gain increases with the increase in the number of CFRP layers (Figure 5.15 to Figure 5.18). But in most cases, the strength gains, however, do not correlate directly to the number of CFRP layers. This attributes to the less percentage of axial strength gain with the application of three layers of CFRP strips rather than the application of single layer and five layers of CFRP strips. This phenomenon is acceptable since it matches with the experimental study as shown in Table 4.4. The effectiveness of CFRP retrofitting increases as the values of the out-of-straightness of the column increases (Shaat and Fam 2007). Again compared to the previous numerical study of Devi and Amanat (2015)[1], it can be said that the present study is more acceptable since in this study damage properties of CFRP and GFRP materials have been incorporated whereas in Devi and Amanat (2015)[1]'s study linear material properties of CFRP and GFRP have been considered. This is attributed to the dependence of axial strength gain on the number of CFRP layers in Devi and Amanat (2015)[1]'s study. So the present study also governs over previous numerical study of Devi and Amanat (2015)[1].

5.5.2   EFFECT OF CROSS SECTIONAL GEOMETRY ON STRENGTH

For relatively large AISC square HSS columns, such as for HSS16×16×5/16 and HSS14×14×5/16, with width-to-thickness (*b/t*) ratio of 52.0 and 45.1 respectively, the percentage gain in axial strength is only approximately by about 1 to 20% due to CFRP strengthening with increasing number of layers (1, 3 and 5) (Figure 5.18).

Addition of CFRP layers does not significantly contribute in increasing the effective thickness or reducing the width-to-thickness ratio of the elements of the section to improve the compactness criteria (b/t = 34.1) (Table 5.1). The axial load carrying capacity is generally governed by the local buckling which depends on the width-thickness ratio of cross-sectional elements. Since width-to-thickness ratio does not decrease significantly, therefore strength gain is also not very significant. Percentage axial strength gain of may be increased through the use of thicker CFRP strips.

On the other hand, for comparatively medium AISC square HSS sections such as for HSS12×12×3/16 and HSS9×9×⅛, with *b/t* ratio of 66.0 and 74.6 respectively, the percentage gain in axial strength is approximately by up to 65% due to CFRP strengthening with increasing number of layers (1, 3 and 5) (Figure 5.16 and Figure 5.17) compared to comparatively larger and smaller sections. In buckling related problems, compression capacity is generally proportional to the inverse of the square of the width-to-thickness (*b/t*) ratio. Therefore a moderate amount of reduction in *b/t* ratio causes large increase in capacity which eventually prevents or delays the onset of local buckling.

Again for comparatively small AISC square HSS sections such as for HSS7×7×⅛, HSS5×5×⅛ and HSS3×3×⅛, with *b/t* ratio of 57.3, 40.1 and 22.9 respectively, the axial strength gain is approximately by up to 35% (Figure 5.15). For smaller AISC HSS sections, width-to-thickness ratio is comparatively less than medium and large HSS sections and therefore these sections are closer to compactness. For compact or close to compact sections, axial strength is generally governed by material strength (for *KL/r* < C_c) or section geometry (*KL/r* > C_c). Since compressive strength of CFRP is very small compared to steel, it contributes insignificantly. For this reason, strength increase for smaller sections (for *KL/r* < C_c) is less significant.

For this reason, the percentage gain in axial strength for medium AISC HSS sections increase significantly rather than the small and larger AISC square HSS sections.

5.6   REMARKS

Considering the effects of CFRP layers, slenderness ratios and cross-sectional geometry for all AISC square HSS column sections it can be conclude that the

application of CFRP materials can increase the capacity of AISC square HSS columns but not more than 2 times the capacity of unstrengthened columns. Again AISC HSS sections with higher width-to-thickness ratios will be more benefitted than AISC HSS sections with lower width-to-thickness ratios due to CFRP strengthening.

Chapter 6

CONCLUSION

6.1 GENERAL

Nonlinear 3D finite element models have been developed using Abaqus 6.14-4 finite element software to investigate the behavior of slender steel HSS columns strengthened using multilayer CFRP strips. A static, Riks solution strategy (Crisfield 1991) was implemented in the numerical model to trace a stable post peak response in the load-deflection curve. To investigate the performance of this FEM model, simulations were conducted reported in the literature (Shaat and Fam 2007) and it has shown good agreement. The proposed model is then used for performing the parametric study on some of the non-compact HSS column sections from AISC Manual (13th edition, 2005) with varying aspect ratio, CFRP thickness, number of layers, CFRP tensile strength, initial out of straightness, eccentricity in load application, CFRP orientation and slenderness ratios. Based on the parametric study some important relationships have been observed which are pointed out in the following section.

6.2 OUTCOMES OF THE STUDY

The investigation on non-compact AISC square HSS column sections by finite element method concludes with following outcomes.

1. From the present study it can be conclude that the FE modeling technique presented is reasonably accurate in predicting the ultimate compression capacity of CFRP retrofitted HSS sections. So that instead of experimental study, the proposed finite element modeling technique can be satisfactorily used to predict the behavior of the steel HSS columns as well as other steel sections strengthened by multilayer CFRP retrofitting materials strips.

2. Carbon Fiber Reinforced Polymer (CFRP) materials are capable of increasing the axial load capacity of the steel HSS columns. The axial strength of column specimens can be possible to increase by two-thirds to that of control/unstrengthened specimens.

3. For columns of short and intermediate lengths ($KL/r < C_c$) variation in strength is less significant. When column length increases ($KL/r > C_c$), strength decreases significantly as expected.

4. Medium sized HSS sections benefit most from CFRP strengthening compared to larger or smaller sized sections. This is because addition of CFRP layers decreases the b/t ratio more for medium sized sections and hence brings the section closer to compactness and delays local buckling which contributes to significant increase in capacity.

5. The capacity generally increases with the increase in the number of CFRP layers. The application of CFRP strips increases the effective thickness of the steel HSS column reducing the slenderness value of the cross-sectional elements which ultimately results in a delayed local buckling as well as increasing the overall buckling strength of columns. In some cases, the strength gains, however, do not correlate directly to the number of CFRP layers. Similar phenomena were also experimentally observed by Shaat and Fam (2006, 2007).

6.3 SCOPES FOR FUTURE INVESTIGATION

The following recommendations for future research work may be suggested.

1. In the present study only the non-compact square Hollow Structural Sections (HSS) have been investigated. Other compact and non-compact HSS sections with varying cross sectional properties can be used for further investigation to check the effectiveness of CFRP strengthening.

2. Present study considers CFRP materials with tensile strength of 510 MPa to get resemblance with the experimental work. But now-a-days CFRP materials can be found with strength of 2000 to 4000 MPa or may be more than that. Further investigation can be carried out considering the varying material properties of CFRP materials.

3. In the present study effect of change of initial out-of-straightness on the capacity of column section has not been considered. But it could be an effective parameter of interest.

4. In the present study concentric loading is assumed to investigate. Considering eccentricity in load application further investigation can be carried out.

5. Further study should be carried on more detailed description of failure of CFRP materials.

REFERENCES

ANSYS Academic Research (2016), Release 16.2, Help System, Coupled Field Analysis Guide, ANSYS, Inc.

Al-Zubaidy, H., Al-Mahaidi, R. and Zhao, X. L. (2013). "Finite element modelling of CFRP/steel double strap joints subjected to dynamic tensile loadings.", *Composite Structures*, 99, pp. 48-61.

Abaqus (2013). "Abaqus Analysis User's Manual.", Dassult Systèmes Simulia Corporation, Providence, RI, USA.

Al-Hammoud, R., Soudki, K. and Topper, T. (2011). "Fatigue flexural behavior of corroded reinforced concrete beams with CFRP sheets.", *Journal of Composites for Construction*, 15(1), pp. 42-51.

AISC Committee on Manuals and Textbooks, (2005). *Steel Construction Manual*, (13th Edition), American Institute of Steel Construction, Inc., USA.

Bambach, M. R. (2014). "6 - Strengthening of thin-walled (hollow) steel sections using fibre-reinforced polymer (FRP) composites.", *Rehabilitation of Metallic Civil Infrastructure using Fiber Reinforced Polymer (FRP) Composites*, pp. 140-168.

Badawi, M. and Soudki, K. (2010). "CFRP repair of RC beams with shear-span and full-span corrosions.", *Journal of Composites for Construction*, 14(3), pp. 323-335.

Bambach, M. R., Jama, H. H. and Elchalakani, M. (2009)[1]. "Axial capacity and design of thin-walled steel SHS strengthened with CFRP.", *Thin-Walled Structures*, 47 (10), pp. 1112-1121.

Bambach, M. R., Elchalakani, M. and Zhao, X. L. (2009)[2]. "Composite steel-CFRP SHS tubes under axial impact.", *Composite Structures*, 87(3), pp. 282-292.

Balaguru, P., Nanni, A. and Giancaspro, J. (2009). *FRP composites for reinforced and prestressed concrete structures*, Tailor & Francis, New York, USA.

Bambach, M. R. and Elchalakani, M. (2007). "Plastic mechanism analysis of steel SHS strengthened with CFRP under large axial deformation.", *Thin-Walled Structures*, 45(2), pp. 159-170.

Buyukozturk, O., Oguz G. and Erdem K. (2004). "Progress on understanding debonding problems in reinforced concrete and steel members strengthened using FRP composites." *Construction and Building* Materials, 18(1) pp. 9-19.

Bathe, K. J. (1976). *Numerical Methods in Finite Element Analysis*, Prentice-Hall.

Carolin, A., Paulsson, B. and Elfgren, L. (2015). "Assessment of the strengthening of an RC railway bridge with CFRP utilizing a full-scale failure test and finite-element analysis.", *Journal of Structural Engineering*, 141, SPECIAL ISSUE: Field Testing of Bridges and Buildings, D4014008.

Crisfield, M. A. (1991). *Non-linear Finite Element Analysis of Solids and Structures*, Volume 1: Essentials, John Wiley & Sons Ltd., England.

Devi, U. and Amanat, K. M. (2015)[1]. "Non-linear finite element investigation on the behavior of CFRP strengthened steel square HSS columns under compression", *International Journal of Steel Structures*, Springer, ISSN: 1598-2351, 15(3), pp 671-680.

Devi, U. and Amanat, K. M. (2015)[2]. "Numerical simulation of steel HSS columns strengthened using CFRP", *Journal of Civil Engineering*, The Institution of Engineers, Bangladesh., CE 42(2), pp. 209-216.

Dawood, M., Sumner, E. and Rizkalla, S. (2006). "Strengthening steel bridges with new high modulus CFRP materials.", *Third international conference on bridge maintenance, safety and management (IABMAS'06),* Portugal.

Di Sarno, L. and Elnashai, A. S. (2005). "Innovative strategies for seismic retrofitting of steel and composite frames.", *Journal of Progress in Structural Engineering and Materials*, 7(3), pp. 115-135.

Darwish, M. N. (2000). "Upgrading reinforced concrete columns by jacketing with carbon fiber-reinforced plastic (CFRP) sheets.", *ACI Special Publication,* 193, pp. 488-502.

El-Saikaly, G., Godat, A. and Chaallal, O. (2014). "New anchorage technique for FRP shear-strengthened RC T-beams using CFRP rope.", *Journal of Composites for Construction*, 10.1061/(ASCE)CC.1943-5614.0000530, 04014064.

Ehsani, M. R. and Saadatmanesh, H. (1990). "Fiber composite plates for strengthening bridge beams.", *Composite Structures*, 15(4), pp. 343-355.

Faggiani, A. and Falzon, B. G. (2010). "Predicting low-velocity impact damage on a stiffened composite panel.", *Composites Part A*, 41, pp. 737–49.

Fawzia, S. (2007). "Bond characteristics between steel and carbon fibre reinforced polymer (CFRP) composites (PhD Thesis).", Melbourne: Monash University.

Falzon, B. G. and Hitchings, D. (1999). "Besant T. Fracture mechanics using a 3D composite element.", *Composite Structures*, 45, pp. 29–39.

Garcia, R., Jemaa, Y., Helal, Y., Guadagnini, M. and Pilakoutas, K. (2014). "Seismic strengthening of severely damaged beam-column RC joints using CFRP.", *Journal of Composites for Construction*, 18(2), 04013048.

Gajdosova, K. and Bilcik, J. (2013). "Full-scale testing of CFRP-strengthened slender reinforced concrete columns.", *Journal of Composites for Construction*, 17(2), pp. 239-248.

Gardner, L. and Nethercot, D. A. (2004)[1]. "Experiments on stainless steel hollow sections – Part 1: Material and cross-sectional behaviour.", *Journal of Constructional Steel Research*, 60(9), pp. 1291-1318.

Gardner, L. and Nethercot, D. A. (2004)[2]. "Experiments on stainless steel hollow sections – Part 2: Member behaviour of columns and beams.",*Journal of Constructional Steel Research*, 60(9), pp. 1319-1332.

Grabovac, I., Bartholomeusz, R. A., and Baker, A. A. (1991). "Fibre composite reinforcement of metallic plates of varying thickness and contour.", *International Conference of Aircraft Damage Assessment and Repair*, Melbourne, Australia, August 26-28, pp. 231-238.

Harries et al. (2006). "Seismic Retrofit of Lap Splices in Non-ductile Columns Using CFRP Jackets." ACI Structural Journal.

Hollaway, L. C. and Cadei, J. (2002). "Progress in the technique of upgrading metallic structures with advanced polymer composites.", *Prog. Struct. Eng. Mater.*, 4(2), pp. 131-148.

Hashin, Z. (1980). "Failure criteria for unidirectional fiber composites.", *Journal of Applied Mechanics*, 47, pp. 329-334.

Hashin, Z. and Rotem, A. (1973). "A fatigue criterion for fiber-reinforced materials.", *Journal of Composite Materials*, 7, pp. 448-464

Illig, G. and White, D. (2010). "Using carbon fiber reinforced polymers (CFRP) to strengthen the sunshine skyway bridge.", *Structures Congress 2010*, 10.1061/41130(369)62, pp. 676-688.

Jama, H. H., Bambach, M. R., Nurick, G. N., Grzebieta, R. H. and Zhao, X. L. (2009). "Numerical modelling of square tubular steel beams subjected to transverse blast loads.", *Thin-Walled Structures*, 47(12), pp. 1523-1534.

Kabir, M. H., Fawzia, S., Chan, T. H. T., Gamage, J. C. P. H. and Bai, J. B. (2016). "Experimental and numerical investigation of the behaviour of CFRP strengthened CHS beams subjected to bending.", *Engineering Structures*, 113, pp. 160–173.

Kalavagunta, S., Naganathan, S. and Mustapha, K. N. B. (2014). "Axially loaded steel columns strengthened with CFRP.", *Jordan Journal of Civil Engineering*, 8(1), pp.58-69.

Karbhari, V. M. and Shulley, S. B. (1995). "Use of composites for rehabilitation of steel structures-Determination of bond durability.", *Journal of Materials in Civil Engineering*, ASCE, 7(4), pp. 239-245.

Law, K. H. and Gardner, L. (2013). "Buckling of elliptical hollow section members under combined compression and uniaxial bending.", *Journal of Constructional Steel Research*, 86, pp. 1-16.

Lapczyk, I. and Hurtado, J. A. (2007). "Progressive damage modeling in fiber-reinforced materials.", *Composite Part A-Applied Science and Manufacturing*, 38, pp. 2333-41.

Miller, T. C., Chajes, M. J., Mertz, D. R. and Hastings, J. N. (2001). "Strengthening of a steel bridge girder using CFRP plates.", *Journal of Bridge Engineering*, ASCE, 6(6), pp. 514-522.

NEES Project Warehouse, Retrieved from http: // nees.org/ warehouse/ experiment/ 1112/ project/ 605.

Narmashiri, K., Sulong, N. H. R. and Jumaat, M. Z. (2012). "Failure analysis and structural behaviour of CFRP strengthened steel I-beams.", *Contruction and Building Materials*, 30, pp. 1-9.

Narmashiri, K. and Jumaat, M. Z. (2011). "Reinforced steel I-beams: A comparison between 2D and 3D simulation.", *Simulation Modelling Practice and Theory*, 19(1), pp. 564-585.

Naghipour, P., Schneider, J., Bartsch, M., Hausmann, J. and Voggenreiter, H. (2009). "Fracture simulation of CFRP laminates in mixed mode bending.", *Eng. Fracture Mechanics*, 76, pp. 2821-33.

Oehlers, D. J. and Seracino, R. (2004). *Design of FRP and steel plated RC structures*, Elsevier Ltd.

Prince Engineering, PLC Experienced Civil Engineering. Retrieved from http://www.build-on-prince.com.

Peiris, A. and Harik, I. (2014). "Steel bridge girder strengthening using post installed shear connectors and UHM CFRP laminates.", *Journal of Performance of Constructed Facilities*, 10.1061/(ASCE)CF.1943-5509.0000625, 04014139.

Patton, M. L. and Singh, K. D. (2012). "Numerical modeling of lean duplex stainless steel hollow columns of square, L-, T- and +- shaped cross sections under pure axial compression.", *Thin-Walled Structures*, 53, pp. 1-8.

Raj, K. S. and Nirmalkumar, K. (2014). "Application of FRP wraps in arresting corrosion of steel structures.", *International Journal of Engineering Science Invention Research & Development*, 1(3).

Ritchie, A., Fam, A. and MacDougall, C. (2014). "Strengthening long steel columns of S-sections against global buckling around weak axis using CFRP plates of various moduli.", *Journal of Composites for Construction*, 10.1061/(ASCE)CC.1943-5614.0000534, 04014074.

Rui, X., Ekiert, D. C., Krause, J. C., Hai, R., Crowe, J. E. and Wilson, I. A. (2010). "Structural basis of preexisting immunity to the 2009 H1N1 pandemic influenza virus.", *Science* 328.5976, pp. 357-360.

Shi, Y., Swait, T. and Soutis, C. (2012). "Modelling damage evolution in composite laminates subjected to low velocity impact.", *Composite Structures*, 94, pp. 2902-13.

Sadeghian, P., Rahai, A. and Ehsani, M. (2010). "Experimental study of rectangular RC columns strengthened with CFRP composites under eccentric loading.", *Journal of Composites for Construction*, 14(4), pp. 443-450.

Shaat, A. and Fam, A. (2009). "Slender steel columns strengthened using high-modulus CFRP plates for buckling control.", *Journal of Structural Engineering*, ASCE, 13(1), pp. 2-12.

Schnerch, D. and Rizkalla, S. (2008). "Flexural strengthening of steel bridges with high modulus CFRP strips.", *Journal of Bridge Engineering*, 13(2), pp. 192-201.

Shaat, A. and Fam, A. (2008). "Repair of cracked steel girders connected to concrete slabs using carbon-fiber-reinforced polymer sheets.", *Journal of Composites for Construction*, 12(6), pp.650-659.

Shaat, A. and Fam, A. (2007). "Fiber-element model for slender HSS columns retrofitted with bonded high-modulus composites.", *Journal of Structural Engineering*, ASCE, 133(1), pp. 85-95.

Shaat, A. and Fam, A. (2006). "Axial loading tests on short and long hollow structural steel columns retrofitted using carbon fiber reinforced polymers.", *Canadian Journal of Civil Engineering*, 33 (4), pp. 458-470.

Shaat, A., Schnerch, D., Fam, A. and Rizkalla, S. (2004). "Retrofit of steel structures using fiber reinforced polymers (FRP): State-of-the-Art." *Transportation research board (TRB) annual meeting*, CD-ROM (04-4063).

Teng, J. G., Yu, T. and Fernando, D. (2012). "Strengthening of steel structures with fiber-reinforced polymer composites.", *Journal of Constructional Steel Research*, 78, pp. 131-143.

Teng, J. G. and Hu, Y. M. (2007). "Behaviour of FRP-jacketed circular steel tubes and cylindrical shells under axial compression.", *Construction and Building Materials*, 21(4), pp. 827-838.

Tavakkolizadeh, M. and Saadatmanesh, H. (2001). "Galvanic corrosion of carbon and steel in aggressive environments.", *Journal of Composites for Construction*, 5(3), pp. 200-210.

Wu, G., Dong, Z., Wu, Z. and Zhang, L. (2014). "Performance and parametric analysis of flexural strengthening for RC beams with NSM-CFRP bars.", *Journal of Composites for Construction*, 18(4), 04013051.

Zilch, K., Niedermeier, R. and Finckh, W. (2014*). Strengthening of concrete structures with adhesively bonded reinforcement*, Wilhelm Ernst &Sohn, Berlin, Germany.

Zhao, X. L. (2013). *FRP strengthened metallic structures*, Taylor & Francis, U.K.

Zhao, X. L. and Zhang, L. (2007). "State-of-the-art review on FRP strengthened steel structures.", *Engineering Structures*, 29 (8), pp. 1808-1823.

APPENDIX A

Table A-1: Dimensions and Properties of Square HSS Sections from AISC Manual.

Shape	Design Wall Thickness, t	Nominal Wt.	Area, A	b/t	h/t	I	S	r	Z	Worka-ble Flat	Torsion J	C	Surface Area	Compact/ Non-compact (for F_y=380 MPa)
	in.	lb/ft	in.^{2}			in.^{4}	in.^{3}	in.	in.^{3}	in.	in.^{4}	in.^{3}	ft^2/ft	
HSS16×16× ⅝	0.581	127.00	35.0	24.5	24.5	1370	171	6.25	200	13.19	2170	276	5.17	Compact
× ½	0.465	103.00	28.3	31.4	31.4	1130	141	6.31	164	13.75	1770	224	5.20	Compact
× ⅜	0.349	78.45	21.5	42.8	42.8	873	109	6.37	126	14.31	1350	171	5.23	Non-compact
× 5/16	0.291	65.82	18.1	52.0	52.0	739	92.3	6.39	106	14.63	1140	144	5.25	Non-compact
HSS14×14× ⅝	0.581	110.00	30.3	21.1	21.1	897	128	5.44	151	11.19	1430	208	4.50	Compact
× ½	0.465	89.55	24.6	27.1	27.1	743	106	5.49	124	11.75	1170	170	4.53	Compact
× ⅜	0.349	68.24	18.7	37.1	37.1	577	82.5	5.55	95.4	12.31	900	130	4.57	Non-compact
× 5/16	0.291	57.31	15.7	45.1	45.1	490	69.9	5.58	80.5	12.63	759	109	4.58	Non-compact
HSS12×12× ⅝	0.581	93.14	25.7	17.7	17.7	548	91.4	4.62	109	9.19	885	151	3.83	Compact
× ½	0.465	75.94	20.9	22.8	22.8	457	76.2	4.68	89.6	9.75	728	123	3.87	Compact
× ⅜	0.349	58.03	16.0	31.4	31.4	357	59.5	4.73	69.2	10.31	561	94.6	3.90	Compact

Table A-1: (Continued)

Shape	Design Wall Thickness, t	Nominal Wt.	Area, A	b/t	h/t	I	S	r	Z	Worka-ble Flat	Torsion J	C	Surface Area	Compact/ Non-compact (for F_y=380 MPa)
	in.	lb/ft	in.^{2}			in.^{4}	in.^{3}	in.	in.^{3}	in.	in.^{4}	in.^{3}	ft^2/ft	MPa)
× 5/16	0.291	48.81	13.4	38.2	38.2	304	50.7	4.76	58.6	10.63	474	79.7	3.92	Non-compact
× ¼	0.233	39.40	10.8	48.5	48.5	248	41.4	4.79	47.6	10.88	384	64.5	3.93	Non-compact
× 3/16	0.174	29.82	8.15	66.0	66.0	189	31.5	4.82	36.0	11.19	290	48.6	3.9	Non-compact
HSS10×10× ⅝	0.581	76.13	21.0	14.2	14.2	304	60.8	3.80	73.2	7.19	498	102	3.17	Compact
× ½	0.465	62.33	17.2	18.5	18.5	256	51.2	3.86	60.7	7.75	412	84.2	3.20	Compact
× ⅜	0.349	47.82	13.2	25.7	25.7	202	40.4	3.92	47.2	8.31	320	64.8	3.23	Compact
× 5/16	0.291	40.30	11.1	31.4	31.4	172	34.5	3.94	40.1	8.63	271	54.8	3.25	Compact
× ¼	0.233	32.60	8.96	39.9	39.9	141	28.3	3.97	32.7	8.88	220	44.4	3.27	Non-compact
× 3/16	0.174	24.72	6.76	54.5	54.5	108	21.6	4.00	24.8	9.19	167	33.6	3.28	Non-compact
HSS9×9× ⅝	0.581	67.62	18.7	12.5	12.5	216	47.9	3.40	58.1	6.19	356	81.6	2.83	Compact

Table A-1: (Continued)

Shape	Design Wall Thickness, t	Nominal Wt.	Area, A	b/t	h/t	I	S	r	Z	Worka-ble Flat	Torsion J	C	Surface Area	Compact/ Non-compact (for F_y=380 MPa)
	in.	lb/ft	in.^{2}			in.^{4}	in.^{3}	in.	in.^{3}	in.	in.^{4}	in.^{3}	ft^2/ft	
× ½	0.465	55.53	15.3	16.4	16.4	183	40.6	3.45	48.4	6.75	296	67.4	2.87	Compact
× ⅜	0.349	42.72	11.8	22.8	22.8	145	32.2	3.51	37.8	7.31	231	52.1	2.90	Compact
× 5/16	0.291	36.05	9.92	27.9	27.9	124	27.6	3.54	32.1	7.63	196	44.0	2.92	Compact
× ¼	0.233	29.19	8.03	35.6	35.6	102	22.7	3.56	26.2	7.88	159	35.8	2.93	Non-compact
× 3/16	0.174	22.16	6.06	48.7	48.7	78.2	17.4	3.59	20.0	8.19	121	27.1	2.95	Non-compact
× ⅛	0.116	14.95	4.09	74.6	74.6	53.5	11.9	3.62	13.6	8.44	82.0	18.3	2.97	Non-compact
HSS8×8× ⅝	0.581	59.11	16.4	10.8	10.8	146	36.5	2.99	44.7	5.19	244	63.2	2.50	Compact
× ½	0.465	48.72	13.5	14.2	14.2	125	31.2	3.40	37.5	5.75	204	52.4	2.53	Compact
× ⅜	0.349	37.61	104	19.9	19.9	100	24.9	3.10	29.4	6.31	160	40.7	2.57	Compact
× 5/16	0.291	31.79	8.76	24.5	24.5	85.6	21.4	3.13	25.1	6.63	136	34.5	2.58	Compact

Shape	Design Wall Thickness, t	Nominal Wt.	Area, A	b/t	h/t	I	S	r	Z	Worka-ble Flat	Torsion		Surface Area	Compact/ Non-compact (for F_y=380 MPa)
											J	C		
	in.	lb/ft	in.^{2}			in.^{4}	in.^{3}	in.	in.^{3}	in.	in.^{4}	in.^{3}	ft^2/ft	
× ¼	0.233	25.79	7.10	31.3	31.3	70.7	17.7	3.15	20.5	6.88	111	28.1	2.60	Compact
× 3/16	0.174	19.61	5.37	43.0	43.0	54.4	13.6	3.18	15.7	7.19	84.5	21.3	2.62	Non-compact
× ⅛	0.116	13.25	3.62	66.0	66.0	37.4	9.34	3.21	10.7	7.44	57.3	14.4	2.63	Non-compact
HSS7×7× ⅝	0.581	50.60	14.0	9.05	9.05	93.4	26.7	2.58	33.1	4.19	158	47.1	2.17	Compact
× ½	0.465	41.91	11.6	12.1	12.1	80.5	23.0	2.63	27.9	4.75	133	39.3	2.20	Compact
× ⅜	0.349	32.51	8.97	17.1	17.1	65.0	18.6	2.69	22.1	5.31	105	30.7	2.23	Compact
× 5/16	0.291	27.54	7.59	21.2	21.2	56.1	16.0	2.72	18.9	5.63	89.7	26.1	2.25	Compact
× ¼	0.233	22.39	6.17	27.0	27.0	46.5	13.3	2.75	15.5	5.88	73.5	21.3	2.27	Compact
× 3/16	0.174	17.06	4.67	37.2	37.2	36.0	10.3	2.77	11.9	6.19	56.1	16.2	2.28	Non-compact
× ⅛	0.116	11.55	3.16	57.3	57.3	24.8	7.09	2.80	8.13	6.44	38.2	11.0	2.30	Non-compact

Table A-1: (Continued)

Shape	Design Wall Thickness, t	Nominal Wt.	Area, A	b/t	h/t	I	S	r	Z	Worka-ble Flat	Torsion J	C	Surface Area	Compact/ Non-compact (for F_y=380 MPa)
	in.	lb/ft	in.^{2}			in.^{4}	in.^{3}	in.	in.^{3}	in.	in.^{4}	in.^{3}	ft^2/ft	
HSS6×6× ⅝	0.581	42.10	11.7	7.33	7.33	55.2	18.4	2.17	23.2	3.19	94.9	33.1	1.83	Compact
× ½	0.465	35.11	9.74	9.90	9.90	48.3	16.1	2.23	19.8	3.75	81.1	28.1	1.87	Compact
× ⅜	0.349	27.41	7.58	14.2	14.2	39.5	13.2	2.28	15.8	4.31	646	22.1	1.90	Compact
× 5/16	0.291	23.29	6.43	17.6	17.6	34.3	11.4	2.31	13.6	4.63	55.4	18.9	1.92	Compact
× ¼	0.233	18.99	5.24	22.8	22.8	28.6	9.54	2.34	11.2	4.88	45.6	15.4	1.93	Compact
× 3/16	0.174	14.51	3.98	31.5	31.5	22.3	7.42	2.37	8.63	5.19	35.0	11.8	1.95	Non-compact
× ⅛	0.116	9.85	2.70	48.7	48.7	15.5	5.15	2.39	5.92	5.44	23.9	8.03	1.97	Non-compact
HSS5½×5½ ×⅜	0.349	24.85	6.88	12.8	12.8	29.7	10.8	2.08	13.1	3.81	49.0	18.4	1.73	Compact
× 5/16	0.291	21.16	5.85	15.9	15.9	25.9	9.43	2.11	11.3	4.13	42.2	15.7	1.75	Compact
× ¼	0.233	17.28	4.77	20.6	20.6	21.7	7.90	2.13	9.32	4.38	34.8	12.9	1.77	Compact
× 3/16	0.174	13.23	3.63	28.6	28.6	17.0	6.17	2.16	7.19	4.69	26.7	9.85	1.78	Compact

Shape	Design Wall Thickness, t	Nominal Wt.	Area, A	b/t	h/t	I	S	r	Z	Worka-ble Flat	Torsion J	C	Surface Area	Compact/ Non-compact (for F_y=380 MPa)
	in.	lb/ft	in.^{2}			in.^{4}	in.^{3}	in.	in.^{3}	in.	in.^{4}	in.^{3}	ft^2/ft	MPa)
× ⅛	0.116	9.00	2.46	44.4	44.4	11.8	4.30	2.19	4.95	4.94	18.3	6.72	1.80	Non-compact
HSS5×5 × ½	0.465	28.30	7.88	7.75	7.75	26.0	10.4	1.82	13.1	2.75	44.6	18.7	1.53	Compact
× ⅜	0.349	22.30	6.18	11.3	11.3	21.7	8.68	1.87	10.3	3.31	36.1	14.9	1.57	Compact
× 5/16	0.291	19.03	5.26	14.2	14.2	19.3	762	1.90	9.16	3.63	31.2	12.8	1.58	Compact
× ¼	0.233	15.58	4.30	18.5	18.5	16.3	6.41	1.93	7.61	3.88	25.8	10.5	1.60	Compact
× 3/16	0.174	11.96	3.28	25.7	25.7	12.6	5.03	1.96	5.89	4.19	19.9	8.08	1.62	Compact
× ⅛	0.116	8.15	2.23	40.1	40.1	8.80	3.52	1.99	4.07	4.44	13.7	5.53	1.63	Non-compact
HSS4½×4½ ×½	0.465	24.90	6.95	6.68	6.68	18.1	8.03	1.61	10.2	2.25	31.3	14.8	1.37	Compact
× ⅜	0.349	19.75	5.48	9.89	9.89	15.3	6.79	1.67	8.36	2.81	25.7	11.9	1.40	Compact
× 5/16	0.291	16.91	4.68	12.5	12.5	13.5	6.00	1.70	7.27	3.13	22.3	10.2	1.42	Compact
× ¼	0.233	13.88	3.84	16.3	16.3	11.4	5.08	1.73	6.06	3.38	18.5	8.44	1.43	Compact

Shape	Design Wall Thickness, t	Nominal Wt.	Area, A	b/t	h/t	I	S	r	Z	Worka-ble Flat	Torsion J	C	Surface Area	Compact/ Non-compact (for F_y=380 MPa)
	in.	lb/ft	in.^{2}			in.^{4}	in.^{3}	in.	in.^{3}	in.	in.^{4}	in.^{3}	ft^2/ft	
× 3/16	0.174	10.68	2.93	22.9	22.9	9.02	4.01	1.75	4.71	3.69	14.4	.6.49	1.45	Compact
× ⅛	0.116	7.30	2.00	35.8	35.8	6.35	2.82	1.78	3.27	3.94	9.92	4.45	1.47	Non-compact
HSS4×4 ×½	0.465	21.50	6.02	5.60	5.60	11.9	5.97	1.41	7.70	−	21.0	11.2	1.20	Compact
× ⅜	0.349	17.20	4.78	8.46	8.46	10.3	5.13	1.47	6.39	2.31	17.5	9.14	1.23	Compact
× 5/16	0.291	14.78	4.10	10.7	10.7	9.14	4.57	1.49	5.59	2.63	15.3	7.91	1.25	Compact
× ¼	0.233	12.18	3.37	14.2	14.2	7.80	3.90	1.52	4.69	2.88	12.8	6.56	1.27	Compact
× 3/16	0.174	9.40	2.58	20.2	20.2	6.21	3.10	1.55	3.67	3.19	10.0	5.07	1.28	Compact
× ⅛	0.116	6.45	1.77	31.5	31.5	4.40	2.20	1.58	2.56	3.44	6.91	3.49	1.30	Non-compact
HSS3½×3½ ×⅜	0.349	14.65	4.09	7.03	7.03	6.49	3.71	1.26	4.69	−	11.2	6.77	107	Compact
× 5/16	0.291	12.65	3.52	9.03	9.03	5.84	3.34	1.29	4.14	2.13	9.89	5.90	1.08	Compact
× ¼	0.233	10.48	2.91	12.0	12.0	5.04	2.88	1.32	3.50	2.38	8.35	4.92	1.10	Compact

Table A-1: (Continued)

Shape	Design Wall Thickness, t	Nominal Wt.	Area, A	b/t	h/t	I	S	r	Z	Worka-ble Flat	Torsion J	Torsion C	Surface Area	Compact/ Non-compact (for F_y=380 MPa)
	in.	lb/ft	in.^{2}			in.^{4}	in.^{3}	in.	in.^{3}	in.	in.^{4}	in.^{3}	ft^2/ft	MPa)
× 3/16	0.174	8.13	2.24	17.1	17.1	4.05	2.31	1.35	2.76	2.69	6.56	3.83	1.12	Compact
× 1/8	0.116	5.60	1.54	27.2	27.2	2.90	1.66	1.37	1.93	2.94	4.58	2.65	1.13	Compact
HSS3×3 ×3/8	0.349	12.09	3.39	5.60	5.60	3.78	2.52	1.06	3.25	−	6.64	4.74	0.900	Compact
× 5/16	0.291	10.53	2.94	7.31	7.31	3.45	2.30	1.08	290	−	5.94	4.18	0.917	Compact
× 1/4	0.233	8.78	2.44	9.88	9.88	3.02	2.01	1.11	2.48	−	5.08	3.52	0.933	Compact
× 3/16	0.174	6.85	1.89	14.2	14.2	2.46	1.64	1.14	1.97	2.19	4.03	2.76	0.950	Compact
× 1/8	0.116	4.75	1.30	22.9	22.9	1.78	1.19	1.17	1.40	2.44	2.84	1.92	0.967	Compact
HSS2½×2½ ×5/16	0.291	8.40	2.35	5.59	5.59	1.82	1.46	0.88	1.88	−	3.20	2.74	0.750	Compact
× 1/4	0.233	7.08	1.97	7.73	7.73	1.63	1.30	0.91	1.63	−	2.79	2.35	0.767	Compact
× 3/16	0.174	5.57	1.54	11.4	11.4	1.35	1.08	0.94	1.32	−	2.25	1.86	0.784	Compact
× 1/8	0.116	3.90	1.07	18.6	18.6	0.998	0.799	0.97	0.95	−	1.61	1.31	0.800	Compact

Shape	Design Wall Thickness, t	Nominal Wt.	Area, A	b/t	h/t	I	S	r	Z	Worka-ble Flat	Torsion		Surface Area	Compact/ Non-compact (for F_y=380 MPa)
											J	C		
	in.	lb/ft	in.^{2}			in.^{4}	in.^{3}	in.	in.^{3}	in.	in.^{4}	in.^{3}	ft^2/ft	
HSS2¼×2¼	0.233	6.23	1.74	6.66	6.66	1.13	1.01	0.81	1.28	−	1.96	1.85	0.683	Compact
×¼	0.174	4.94	1.37	9.93	9.93	0.953	0.847	0.84	1.04	−	1.60	1.48	0.700	Compact
× 3/16	0.116	3.47	0.96	16.4	16.4	0.712	0.633	0.86	0.75	−	1.15	1.05	0.717	Compact
× ⅛														
HSS2×2 ×¼	0.233	5.38	1.51	5.58	5.58	0.747	0.747	0.70	0.96	−	1.31	1.41	0.600	Compact
× 3/16	0.174	4.30	1.19	8.49	8.49	0.641	0.641	0.73	0.80	−	1.09	1.14	0.617	Compact
× ⅛	0.116	3.04	0.84	14.2	14.2	0.488	0.486	0.76	0.58	−	0.79	0.82	0.633	Compact
− Flat depth or width is too small to establish a workable flat														

APPENDIX B

Table B-1a: Summary of the Parametric Study on selected AISC Square HSS Sections (For HSS 16×16×5/16).

Slenderness Ratio, KL/r	Specimen Identification	Maximum Load (Devi and Amanat, 2015)[1] (KN)	% gain	Maximum Load (Present Analysis) (KN)	% gain
0.25C_c	Control	3957.4	-	4046.63	-
	1L-2S	3997.2	1.01	4704.57	16.26
	3L-2S	4073.5	2.93	4895.96	21.0
	5L-2S	4294.8	8.53	5053.05	24.87
0.5C_c	Control	3928.1	-	4489.32	-
	1L-2S	3963.5	0.90	4599.73	2.46
	3L-2S	4043.1	2.93	4805.79	7.05
	5L-2S	4186.7	6.58	5047.23	12.43
0.75C_c	Control	3478.6	-	4329.89	-
	1L-2S	3569	2.60	4697.92	8.50
	3L-2S	3708.4	6.61	4559.5	5.30
	5L-2S	3909.7	12.39	4954.47	14.42
C_c	Control	2227.3	-	3597.86	-
	1L-2S	2362.4	6.07	4045.94	12.45
	3L-2S	2508.1	12.61	3713.68	3.22
	5L-2S	2587.6	16.18	4088.57	13.64
1.25C_c	Control	1468.4	-	2550.45	-
	1L-2S	1548.4	5.45	2699.67	5.85
	3L-2S	1608.7	9.55	2677.37	4.98
	5L-2S	1669.8	13.72	2837.91	11.27
1.5C_c	Control	1031.6	-	1847.71	-
	1L-2S	1081.7	4.86	1932.62	4.60
	3L-2S	1121.5	8.71	1953.96	5.75
	5L-2S	1159.1	12.36	2066.38	11.84

Table B-1b: Summary of the Parametric Study on selected AISC Square HSS Sections (For HSS 14×14×5/16).

Slenderness Ratio, *KL/r*	Specimen Identification	Maximum Load (Devi and Amanat, 2015)[1] (KN)	% gain	Maximum Load (Present Analysis) (KN)	% gain
0.25C_c	Control	4065.2	-	4086.99	-
	1L-2S	4238.6	4.27	4291.62	5.01
	3L-2S	4519.7	11.18	4282.56	4.79
	5L-2S	4795.3	17.96	4445.9	8.78
0.5C_c	Control	3876.7	-	4036.25	-
	1L-2S	4045.6	4.36	4283.01	6.11
	3L-2S	4336.1	11.85	4174.03	3.41
	5L-2S	4585.7	18.29	4412.04	9.31
0.75C_c	Control	3085.2	-	3823.43	-
	1L-2S	3262.5	5.75	4252.16	11.21
	3L-2S	3555.4	15.24	3930.56	2.80
	5L-2S	3843.4	24.58	4312.08	12.78
C_c	Control	1945.9	-	3042.22	-
	1L-2S	2065.2	6.13	3478.99	14.36
	3L-2S	2188.1	12.45	3184.84	4.69
	5L-2S	2262.7	16.28	3515.69	15.56
1.25C_c	Control	1280.8	-	2168.87	-
	1L-2S	1350.7	5.46	2327.67	7.32
	3L-2S	1400.5	9.35	2296.49	5.88
	5L-2S	1462.6	14.19	2443.36	12.66
1.5C_c	Control	900	-	1593.95	-
	1L-2S	943.6	4.84	1667.03	4.58
	3L-2S	976.3	8.48	1682.19	5.54
	5L-2S	1030.1	14.46	1781.31	11.75

Table B-1c: Summary of the Parametric Study on selected AISC Square HSS Sections (For HSS 12×12×3/16).

Slenderness Ratio, KL/r	Specimen Identification	Maximum Load (Devi and Amanat, 2015)[1] (KN)	% gain	Maximum Load (Present Analysis) (KN)	% gain
0.25C_c	Control	1228.2	-	1577.28	-
	1L-2S	1286	4.71	1709.52	8.38
	3L-2S	1441.6	17.38	1935.18	22.69
	5L-2S	1680.9	36.86	2052.47	30.13
0.5C_c	Control	1196.6	-	1513.02	-
	1L-2S	1249	4.38	1725.35	14.03
	3L-2S	1262	5.47	1905.41	25.93
	5L-2S	1510.4	26.22	2033.93	34.43
0.75C_c	Control	1094	-	1532.6	-
	1L-2S	1137.3	3.96	1705.17	11.26
	3L-2S	1261.3	15.29	1861.17	21.44
	5L-2S	1469.7	34.34	2006.02	30.89
C_c	Control	909.5	-	1125.41	-
	1L-2S	963.6	5.95	1634.83	45.27
	3L-2S	1097	20.62	1693.43	50.47
	5L-2S	1276.5	40.35	1860.08	65.28
1.25C_c	Control	639.5	-	1038.43	-
	1L-2S	695.4	8.74	1257.95	21.14
	3L-2S	752	17.59	1250.03	20.38
	5L-2S	925.6	44.74	1346.59	29.68
1.5C_c	Control	457.6	-	823.367	-
	1L-2S	496.3	8.46	898.678	9.15
	3L-2S	524.9	14.71	921.15	11.88
	5L-2S	672.2	46.90	1004.01	21.94

Table B-1d: Summary of the Parametric Study on selected AISC Square HSS Sections (For HSS 9×9×⅛).

Slenderness Ratio, KL/r	Specimen Identification	Maximum Load (Devi and Amanat, 2015)[1] (KN)	% gain	Maximum Load (Present Analysis) (KN)	% gain
0.25C_c	Control	553.9	-	683.553	-
	1L-2S	618.9	11.73	847.219	23.94
	3L-2S	798.5	44.16	909.224	33.01
	5L-2S	1049.8	89.53	1019.3	49.11
0.5C_c	Control	532.3	-	648.679	-
	1L-2S	589.9	10.82	847.721	30.68
	3L-2S	750.6	41.01	946.479	45.91
	5L-2S	995.5	87.02	1001.95	54.46
0.75C_c	Control	474.9	-	642.97	-
	1L-2S	521.4	9.79	847.039	31.74
	3L-2S	661	39.19	899.446	39.89
	5L-2S	900.1	89.53	995.068	54.76
C_c	Control	391.8	-	553.128	-
	1L-2S	436	11.28	799.262	44.50
	3L-2S	567.9	44.95	812.823	46.95
	5L-2S	773.1	97.32	898.583	62.45
1.25C_c	Control	303.5	-	438.794	-
	1L-2S	345.8	13.94	639.955	45.84
	3L-2S	439.4	44.78	638.372	45.48
	5L-2S	552.6	82.08	681.892	55.40
1.5C_c	Control	223.2	-	384.444	-
	1L-2S	255.1	14.29	462.215	20.23
	3L-2S	327	46.51	477.232	24.14
	5L-2S	404.7	81.32	540.569	40.61

Table B-1e: Summary of the Parametric Study on selected AISC Square HSS Sections (For HSS 7×7×⅛).

Slenderness Ratio, *KL/r*	Specimen Identification	Maximum Load (Devi and Amanat, 2015)[1] (KN)	% gain	Maximum Load (Present Analysis) (KN)	% gain
0.25C_c	Control	571.5	-	681.702	-
	1L-2S	633.8	10.90	755.515	10.83
	3L-2S	839.8	46.95	836.962	22.78
	5L-2S	1139.9	99.46	895.516	31.36
0.5C_c	Control	571.4	-	748.185	-
	1L-2S	627.1	9.75	784.005	4.79
	3L-2S	816.3	42.86	814.807	8.90
	5L-2S	1123.3	96.59	898.45	20.08
0.75C_c	Control	536.2	-	634.45	-
	1L-2S	590.2	10.07	806.924	27.18
	3L-2S	766.1	42.88	751.119	18.39
	5L-2S	994.1	85.40	857.644	35.18
C_c	Control	383.1	-	555.547	-
	1L-2S	437	14.07	711.861	28.13
	3L-2S	553.5	44.48	624.158	12.35
	5L-2S	661.5	72.67	699.335	25.88
1.25C_c	Control	256	-	424.539	-
	1L-2S	281.3	9.88	491.301	15.73
	3L-2S	307.4	20.08	477.115	12.38
	5L-2S	442.1	72.70	526.477	24.01
1.5C_c	Control	180.6	-	319.532	-
	1L-2S	196.1	8.58	352.633	10.36
	3L-2S	263.9	46.12	359.396	12.48
	5L-2S	314	73.86	408.105	27.72

Table B-1f: Summary of the Parametric Study on selected AISC Square HSS Sections (For HSS 5×5×⅛).

Slenderness Ratio, *KL/r*	Specimen Identification	Maximum Load (Devi and Amanat, 2015)[1] (KN)	% gain	Maximum Load (Present Analysis) (KN)	% gain
0.25*C$_c$*	Control	578.1	-	537.248	-
	1L-2S	654.7	13.25	600.976	11.86
	3L-2S	823.9	42.52	584.41	8.78
	5L-2S	958.3	65.77	647.829	20.58
0.5*C$_c$*	Control	550.9	-	514.967	-
	1L-2S	613.7	11.40	595.192	15.58
	3L-2S	733.1	33.07	546.398	6.10
	5L-2S	881.4	59.99	619.405	20.28
0.75*C$_c$*	Control	437.8	-	466.665	-
	1L-2S	499.9	14.18	580.78	24.45
	3L-2S	602.4	37.60	491.621	5.35
	5L-2S	698.9	59.64	581.127	24.53
C$_c$	Control	277.1	-	380.561	-
	1L-2S	309.5	11.69	473.681	24.47
	3L-2S	392.5	41.65	405.81	6.63
	5L-2S	465	67.81	465.121	22.22
1.25*C$_c$*	Control	182.3	-	277.855	-
	1L-2S	198.5	8.89	323.84	16.55
	3L-2S	260.7	43.01	311.871	12.24
	5L-2S	309	69.50	350.79	26.25
1.5*C$_c$*	Control	128.1	-	212.018	-
	1L-2S	138.3	7.96	235.783	11.21
	3L-2S	184.8	44.26	237.006	11.79
	5L-2S	219	70.96	270.564	27.61

Table B-1g: Summary of the Parametric Study on selected AISC Square HSS Sections (For HSS 3×3×⅛).

Slenderness Ratio, *KL/r*	Specimen Identification	Maximum Load (Devi and Amanat, 2015)[1] (KN)	% gain	Maximum Load (Present Analysis) (KN)	% gain
0.25C_c	Control	336.2	-	301.497	-
	1L-2S	385.7	14.72	349.963	16.08
	3L-2S	464.1	38.04	322	6.8
	5L-2S	563.1	67.49	362.204	20.14
0.5C_c	Control	320.2	-	280.137	-
	1L-2S	353.5	10.40	347.018	23.87
	3L-2S	415.8	29.86	297.608	6.24
	5L-2S	494.7	54.50	352.394	25.79
0.75C_c	Control	255.5	-	248.903	-
	1L-2S	289.3	13.23	331.806	33.31
	3L-2S	344	34.64	261.512	5.07
	5L-2S	395.5	54.79	321.726	29.26
C_c	Control	161.4	-	197.725	-
	1L-2S	179.3	11.09	267.903	35.49
	3L-2S	224.7	39.22	215.94	9.21
	5L-2S	264.1	63.63	260.758	31.88
1.25C_c	Control	106.4	-	153.056	-
	1L-2S	115	8.08	189.123	23.56
	3L-2S	148.9	39.94	169.981	11.06
	5L-2S	175.4	64.85	198.885	29.94
1.5C_c	Control	74.8	-	117.42	-
	1L-2S	80	6.95	137.579	17.17
	3L-2S	105.2	40.64	131.848	12.29
	5L-2S	123.9	65.64	151.408	28.95